

**A Combined Experimental and Computational Study of Ligand Effects on C-H  
Bond Activation by Palladium and Platinum Complexes**

Thesis by

Bo-Lin Lin

In Partial Fulfillment of the  
Requirements for the Degree of  
Doctor of Philosophy

California Institute of Technology  
Pasadena, CA

2009

(Defended March 18<sup>th</sup>, 2009)

© 2009

Bo-Lin Lin

All Rights Reserved

For my mother, my father, my brothers, and Lu

## Acknowledgment

More than half a decade has passed since I first came to Caltech. In these years, I have made many friends and received tremendous help from them. After looking back to all my days here, I have to say the decision to come to Caltech for my graduate study is undoubtedly right. In spite of the unavoidable bitterness due to occasional failures in my research adventures, my overall experience at Caltech is quite enjoyable because of all the wonderful people I have met here.

I would like to thank John and Jay for their great tutelage in the past several years at first. They taught me how to approach chemical problems rigorously and present research results precisely and elegantly. I admire their honest attitude towards science very much and highly appreciate the freedom they have given to me for the development of my own taste and interests in research. I am sure all I have learned here will benefit my research forever.

Bob, Harry, and Linda have been very nice and helpful to me. I feel really lucky to have such a fantastic committee to give me advice on my research and proposals and am very grateful for their help on my postdoctoral application.

I also want to thank my fellows in Bercaw group. Without all your kind help and encouragement, it would have been impossible for me to get through the whole journey here. George Chen, my good friend, is always a great person to discuss things inside and outside chemistry. Thank you for all your time in the proofreading of my manuscripts. Jon Owen taught me many fundamental Schlenck techniques. His encouragement helped me to overcome the barrier for my change from computational chemistry to experimental organometallic chemistry. Sara Klamo also gave me a lot of encouragement in my early

days here. Her help made my job as a TA of Ch 154a much easier. Dave Weinberg trained me on the green box and is always very friendly to me. I often have fun going out with him for food. Paul Elowe, my only classmate in the lab, is another great person to talk about all sorts of things. I found our conversation is a good way to alleviate my pressure from research. Koyel Bhattacharyya is a happy young lady and an excellent SURF student from MIT. Our collaboration is really enjoyable.

It is a great fortune for me to interact with and learn from all the talented peoples in Bercaw lab. Theo Agapie and Jeff Byers are role models for me in chemistry. Their working ethics are so admirable. Steve Baldwin's knowledge in chemistry and Alex Miller's synthetic skills are both impressive. Val Scott's gold chemistry and Ted Weintrob's iron chemistry bring fresh air into the lab. I can always feel their excitement and get energized when I talk to them about their chemistry. Ian Tonks and Suzanne Golisz carry on the torch of early transition metal chemistry and continue to amuse me with interesting new discoveries in this area. Chatting with Paul Oblad about Korean and Chinese languages is also enjoyable. Rachel Klet and Ross Fu are the new force in the lab. I look forward to your good news in research.

I also want to thank the postdoctoral scholars that I have met in Bercaw lab: Parisa Mehrkhodavandi, Reto Dorta, Tom Driver, Xingwei Li, Travis Williams, Aaron Wilson, Nilay Hazari, and Ned West. Their experience and diverse backgrounds in chemistry benefit me a lot. I want to say it is my great pleasure to work with all of you. I also need to thank Pat for all her help on John's schedules and kindness to chat with me.

Outside Bercaw group, I want to thank Scott Virgil for his help on high-throughput experiments, Larry Henling and Mike Day for their work on my crystals, Mona

Shahgholi for her help on MS analyses, Rich Gerhart for his help on glasswares, and Crystal Shih and Kyle Lancaster for their generosity in giving me their chemicals. I would also like to thank my other friends, Tao Liu, Yong Hao, Baiyang Li, Yao Sha, Yan Xia, Jigang Wu, Kechun Zhang, Tingwei Mu, Peigen Cao, Yu Liu, Yue Zou, Xiquan Cui, Morgan Cable, Gretchen Keller, Emily Tsui, and Sibio Lin, for all the fun we had together and all the kind support they have given to me.

I am greatly indebted to my mother, my father, my elder brother, my younger brother, and my beloved wife, Lu. My parents and my brothers have always been supportive in my way from China to USA. And Lu, you have suffered so much since we were together and not together. Without your support, I don't know how far I could have come in the past few years.

**Abstract**

Abnormally large kinetic hydrogen/deuterium isotope effects (KIEs,  $\sim 20$ ) are measured for the protonolysis of several dimethylpalladium(II) complexes with various bidentate ligands by trifluoroethanol (TFE) at room temperature. Analyses of semiclassical KIE theory suggest that the occurrence of hydrogen tunneling needs to be invoked in order to explain these KIE values, which is further supported by the KIE-temperature-dependence study for the protonolysis of (dppe)Pd(CH<sub>3</sub>)<sub>2</sub> by CF<sub>3</sub>CD<sub>2</sub>OD/CF<sub>3</sub>CH<sub>2</sub>OH.

Density functional theory (DFT) computation suggests that protonation at the M<sup>II</sup>-C bond is kinetically preferred over protonation at the metal center for the protonolysis of (COD)Pt(CH<sub>3</sub>)<sub>2</sub> by TFA and the dimethylpalladium(II) complexes by TFE in dichloroethane. The computation further indicates the significant contribution of hydrogen tunneling in the abnormally large KIEs observed experimentally.

The monomethylpalladium(II) complex, (COD)Pd(CH<sub>3</sub>)Cl (COD = 1,5-cyclooctadiene), undergoes both benzene C-H activation and migratory insertion of olefin, with the former faster than the latter, at room temperature under the assistance of an anionic  $\beta$ -diketiminato ligand, to yield  $\eta^3$ -(2-R-cyclooctenyl)palladium(II)  $\beta$ -diketiminato (R = methyl or phenyl).

DFT computation result suggests that bisindolide-type ligands and carbenearyl-type ligands are likely to lead to faster benzene C-H bond activation as well as lower relative

barrier heights of the C-H bond activation versus the insertion of olefins than those in monomethyl palladium(II) with  $\beta$ -diketiminates.

Several pyridine-like ligands were found to improve  $\text{Pd}(\text{OAc})_2$ -catalyzed allylic oxidation of allylbenzene to cinnamyl acetate by *p*-benzoquinone in acetic acid. The best ligand examined, bipyrimidine, was used to identify the catalyst precursor for this system,  $(\text{bipyrimidine})\text{Pd}(\text{OAc})_2$ , which was fully characterized. Mechanistic studies suggest the reaction takes place through disproportionation of  $(\text{bipyrimidine})\text{Pd}(\text{OAc})_2$  to form a bipyrimidine-bridged dimer, which reacts with olefin to form a  $\text{Pd}^{\text{II}}$ -olefin adduct, followed by allylic C-H activation to produce  $(\eta^3\text{-allyl})\text{Pd}^{\text{II}}$  species. The  $(\eta^3\text{-allyl})\text{Pd}^{\text{II}}$  intermediate undergoes a reversible acetate attack to generate a  $\text{Pd}^0$ -(allyl acetate) adduct, which subsequently reacts with *p*-benzoquinone to release allyl acetate and regenerate  $(\text{bipyrimidine})\text{Pd}(\text{OAc})_2$ . No KIE is observed for the competition experiment between allylbenzene- $d_0$  and allylbenzene- $d_5$  ( $\text{CD}_2=\text{CD}-\text{CD}_2-\text{C}_6\text{H}_5$ ), suggesting that allylic C-H activation is not rate determining. Catalytic allylic acetoxylation of other terminal olefins as well as cyclohexene were also effected by  $(\text{bipyrimidine})\text{Pd}(\text{OAc})_2$ .



## Table of Contents

<b>Acknowledgment .....</b>	<b>IV</b>
<b>Abstract.....</b>	<b>VII</b>
<b>Table of Contents.....</b>	<b>IX</b>
<b>List of Figures.....</b>	<b>XII</b>
<b>List of Schemes .....</b>	<b>XV</b>
<b>List of Tables .....</b>	<b>XVIII</b>
<b>Chapter 1. General Introduction .....</b>	<b>1</b>
References .....	8
<b>Chapter 2. Hydrogen Tunneling in the Protonolysis of Dimethylpalladium(II)</b>	
<b>Complexes .....</b>	<b>10</b>
Abstract .....	10
1. Introduction .....	11
2. Results and Discussions .....	11
3. Conclusions .....	31
Experimental Section.....	31
References.....	34
<b>Chapter 3. Mechanisms and Hydrogen Tunneling in Protonolysis of Platinum(II)</b>	
<b>and Palladium(II) Methyl Complexes: Computational Evidences .....</b>	<b>38</b>
Abstract .....	38
1. Introduction .....	39
2. Results and Discussion.....	40
3. Conclusions .....	48

Computational Methods.....	49
References .....	53
<b>Chapter 4. Competitive Benzene C-H Bond Activation versus Olefin Insertion in a Palladium(II) <math>\beta</math>-Diketiminato Complex.....</b>	<b>55</b>
Abstract .....	55
1. Introduction .....	56
2. Results and Discussion.....	57
3. Conclusions .....	64
Experimental Section.....	65
References .....	68
<b>Chapter 5. Computational Investigations of Competitive Benzene C-H Bond Activation versus Olefin Insertion in Palladium(II) with Various Anionic Ligands .....</b>	<b>72</b>
Abstract .....	72
1. Introduction .....	73
2. Results and Discussion.....	74
3. Conclusions .....	84
Computational Methodology.....	84
References .....	85
<b>Chapter 6. Mechanistic Investigations of Bipyrimidine-Promoted Palladium(II)- Catalyzed Allylic Acetoxylation of Olefins .....</b>	<b>87</b>
Abstract .....	87
1. Introduction .....	88

2. Results and Discussion.....	89
3. Conclusions .....	101
Experimental Section.....	101
References .....	112
<b>Appendix A. Mechanistic Study of the One-Pot Synthesis of Methyl Acetate from a CH<sub>3</sub>OH/CH<sub>3</sub>CN Mixture with a Ru<sup>II</sup>-Sn<sup>II</sup> Bimetallic Complex as the Catalyst.....</b>	<b>115</b>
Abstract .....	115
1. Introduction .....	116
2. Result and Discussion .....	118
3. Conclusions .....	120
Experimental Section.....	123
References .....	123
<b>Appendix B. X-Ray Crystallographic Data for Complex 2 (Chapter 2).....</b>	<b>124</b>
<b>Appendix C. X-Ray Crystallographic Data for Complex 3 (Chapter 4) .....</b>	<b>133</b>
<b>Appendix D. X-Ray Crystallographic Data for Complex 6 (Chapter 4) .....</b>	<b>143</b>
<b>Appendix E. X-Ray Crystallographic Data for Complex 1·H<sub>2</sub>O (Chapter 6) .....</b>	<b>154</b>

## List of Figures

### Chapter 2.

Figure 1. X-ray crystal structure of complex 2 (CCDC 263612).....	13
Figure 2. Wigner's tunneling correction.....	26
Figure 3. Full tunneling correction.....	27
Figure 3. Plot of $\ln(k_H/k_D)$ over $1/T$ .....	28

### Chapter 3.

Figure 1. Plot of LogKIE against $1/T$ .....	47
--	----

### Chapter 4.

Figure 1. X-ray crystal structure of compound 3 (CCDC 295981).....	58
Figure 2. X-ray crystal structure of compound 6 (CCDC 296075).....	62

### Chapter 5.

Figure 1.....	77
Figure 2.....	83

### Chapter 6.

Figure 1. X-ray crystallographic structure and the crystal packing of [(bipyrimidine)Pd(OAc) <sub>2</sub> ·H <sub>2</sub> O] (CCDC634014).....	91
Figure 2. Effect of BPM to Pd(OAc) <sub>2</sub> ratio on allylic oxidation of allylbenzene by benzoquinone, Pd(OAc) <sub>2</sub> fixed to be 5 mol% .....	95
Figure 3. Oxidation of ( $\eta^3$ -allyl)Pd <sup>II</sup> by benzoquinone is independent of the concentration of benzoquinone .....	96

Figure 4. No significant KIE is observed for competition reaction between allylbenzene- $d_0$ and allylbenzene- $d_5$ .....	100
---	-----

## Appendix A.

Figure 1. Mass spectrum of the methyl acetate from the reaction of $\text{CH}_3\text{OH} + \text{CD}_3\text{CN}$ ; $m/z$ : $[\text{CD}_3\text{COOCH}_3]^+$ 77, $[\text{COOCH}_3]^+$ 59, $[\text{CD}_3\text{C(O)}]^+$ 46.....	121
--	-----

Figure 2. Mass spectrum of methanol after the reaction indicates that there is no significant H/D exchange.....	121
---	-----

Figure 3. Mass spectrum of the methyl acetate from the reaction of $\text{CD}_3\text{OH} + \text{CH}_3\text{CN}$ ; $m/z$ : $[\text{CH}_3\text{COOCD}_3]^+$ 77, $[\text{COOCD}_3]^+$ 52, $[\text{CH}_3\text{C(O)}]^+$ 43.....	122
--	-----

Figure 4. Mass spectrum of acetonitrile after the reaction indicates that there is no significant H/D exchange.....	122
---	-----

## Appendix B.

Figure B.1 Minimum overlap view of 2 .....	128
--	-----

## Appendix C.

Figure C.1 Minimum overlap view of 3 .....	137
--	-----

Figure C.2 Crystal Packing of 3 .....	137
---------------------------------------	-----

Figure C.1 Unit cell contents of 3 .....	138
--	-----

## Appendix D.

Figure D.1 Minimum overlap view of 6.....	147
---	-----

Figure D.2 Crystal packing of 6.....	147
--------------------------------------	-----

Figure D.3 Unit cell contents of 6 .....	148
--	-----

## Appendix E.

Figure E.1 Minimum overlap view of $1 \cdot \text{H}_2\text{O}$ .....	158
---	-----

Figure E.2 Crystal packing of $1 \cdot \text{H}_2\text{O}$ .....	159
Figure E.3 Unit cell contents of $1 \cdot \text{H}_2\text{O}$ .....	160

## List of Schemes

### Chapter 1.

Scheme 1 .....	1
Scheme 2 .....	2
Scheme 3 .....	3
Scheme 4 .....	4
Scheme 5 .....	5

### Chapter 2.

Scheme 1 .....	12
Scheme 2 .....	12
Scheme 3 .....	13
Scheme 4 .....	14

### Chapter 3.

Scheme 1 .....	39
Scheme 2 .....	40
Scheme 3 .....	41
Scheme 4 .....	41
Scheme 5 .....	42
Scheme 6 .....	43
Scheme 7 .....	44
Scheme 8 .....	45
Scheme 9 .....	46

Scheme 10 .....	50
Scheme 11 .....	51

**Chapter 4.**

Scheme 1 .....	56
Scheme 2 .....	57
Scheme 3 .....	59
Scheme 4 .....	60
Scheme 5 .....	61
Scheme 6 .....	61
Scheme 7 .....	63

**Chapter 5.**

Scheme 1 .....	74
Scheme 2 .....	75
Scheme 3 .....	80

**Chapter 6.**

Scheme 1 .....	92
Scheme 2 .....	93
Scheme 3 .....	93
Scheme 4 .....	94
Scheme 5 .....	97
Scheme 6 .....	98
Scheme 7 .....	98
Scheme 8 .....	99



**Appendix A.**

Scheme 1 .....	117
Scheme 2 .....	119

## List of Tables

### Chapter 2.

Table 1. Semiclassical upper limits of KIEs at 298 K for proton transfer from various <i>X-H</i> bonds.....	21
Table 2. KIEs for the protonolysis/deuterolysis of complex 4 by TFE in DCE- <i>d</i> <sub>4</sub> at various temperatures.....	28

### Chapter 3.

Table 1. Comparisons of experimental and calculated KIEs (without tunneling correction) for the protonolysis of 3 by TFA.....	47
---	----

### Chapter 5.

Table 1. Selected key structural parameters for transition states of C-H activation .....	75
Table 2. Activation barriers of benzene C-H bond activation by monomethyl-palladium(II) complexes with ligand 1–9 .....	76
Table 3. Equilibrium between the ethylene adduct and the benzene adduct .....	78
Table 4. Overall activation barriers of benzene C-H bond activation for the reaction starting from the ethylene adduct .....	80
Table 5. Activation barriers and reaction energies of olefin insertions.....	81

### Chapter 6.

Table 1. Nitrogen ligand effects on Pd(OAc) <sub>2</sub> -catalyzed allylic acetoxylation of allylbenzene.....	89
Table 2. (Bipyrimidine)Pd(OAc) <sub>2</sub> -catalyzed allylic acetoxylation of olefins.....	90

Table 3. Oxidant effects.....	103
Table 4. Solvent effects at 80 °C .....	104
Table 5. Solvent effects at 100 °C .....	105
Table 6. Acid-base effects.....	106

## Appendix B.

Table B.1 Crystal data and structure refinement for 2 (CCDC 263612) .....	125
Table B.2 Atomic coordinates ( $\times 10^4$ ) and equivalent isotropic displacement parameters ( $\text{\AA}^2 \times 10^3$ ) for 2 (CCDC 263612).....	129
Table B.3 Selected bond lengths [ $\text{\AA}$ ] and angles [ $^\circ$ ] for 2 (CCDC 263612).....	130
Table B.4 Bond lengths [ $\text{\AA}$ ] and angles [ $^\circ$ ] for 2 (CCDC 263612) .....	131
Table B.5 Anisotropic displacement parameters ( $\text{\AA}^2 \times 10^4$ ) for 2 (CCDC 263612) .....	132

## Appendix C.

Table C.1 Crystal data and structure refinement for 3 (CCDC 295981) .....	134
Table C.2 Atomic coordinates ( $\times 10^4$ ) and equivalent isotropic displacement parameters ( $\text{\AA}^2 \times 10^3$ ) for 3 (CCDC 295981).....	139
Table C.3 Selected bond lengths [ $\text{\AA}$ ] and angles [ $^\circ$ ] for 3 (CCDC 295981).....	140
Table C.4 Bond lengths [ $\text{\AA}$ ] and angles [ $^\circ$ ] for 3 (CCDC 295981) .....	141
Table C.5 Anisotropic displacement parameters ( $\text{\AA}^2 \times 10^4$ ) for 3 (CCDC 295981) .....	142

## Appendix D.

Table D.1 Crystal data and structure refinement for 6 (CCDC 296075).....	144
--	-----

Table D.2 Atomic coordinates ( $\times 10^4$ ) and equivalent isotropic displacement parameters ( $\text{\AA}^2 \times 10^3$ ) for 6 (CCDC 296075).....	149
Table D.3 Selected bond lengths [ $\text{\AA}$ ] and angles [ $^\circ$ ] for 6 (CCDC 296075).....	150
Table D.4 Bond lengths [ $\text{\AA}$ ] and angles [ $^\circ$ ] for 6 (CCDC 296075).....	151
Table D.5 Anisotropic displacement parameters ( $\text{\AA}^2 \times 10^4$ ) for 6 (CCDC 296075).....	153

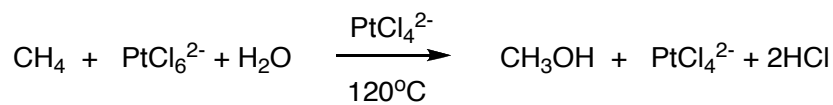
## Appendix E.

Table E.1 Crystal data and structure refinement for 1·H <sub>2</sub> O (CCDC634014).....	155
Table E.2 Atomic coordinates ( $\times 10^4$ ) and equivalent isotropic displacement parameters ( $\text{\AA}^2 \times 10^3$ ) for 1·H <sub>2</sub> O (CCDC634014).....	161
Table E.3 Selected bond lengths [ $\text{\AA}$ ] and angles [ $^\circ$ ] for 1·H <sub>2</sub> O (CCDC634014) .....	162
Table E.4 Bond lengths [ $\text{\AA}$ ] and angles [ $^\circ$ ] for 1·H <sub>2</sub> O (CCDC634014).....	163
Table E.5 Anisotropic displacement parameters ( $\text{\AA}^2 \times 10^4$ ) for 1·H <sub>2</sub> O (CCDC634014).....	165
Table E.6 Hydrogen coordinates ( $\times 10^4$ ) and isotropic displacement parameters ( $\text{\AA}^2 \times 10^3$ ) for 1·H <sub>2</sub> O (CCDC634014) .....	166
Table E.7 Hydrogen bonds for 1·H <sub>2</sub> O (CCDC634014) [ $\text{\AA}$ and $^\circ$ ].....	167

## Chapter 1. General Introduction

Selective transformations of C-H bonds to other functionalities are among the most fundamental challenges in chemistry. Selective aerobic oxidation of saturated hydrocarbons (methane, etc.) to alcohols (methanol, etc.) via C-H activation is of special importance because of its potential to solve the expected oil shortage in the near future. Although methods have already been reported for oxidations of hydrocarbons, few of them are potentially practical for reasons of selectivity—the unfavorable inherent relative reactivity of hydrocarbons and their partially oxidized derivatives. Among those methods, the selective oxidation of methane to methanol by chloroplatinates in water, originally reported by Shilov et al.,<sup>1</sup> is believed to be one of the most promising systems.

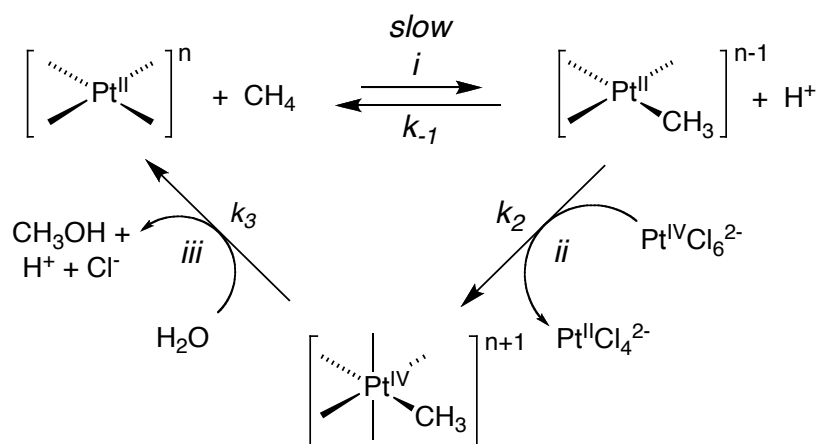
### Scheme 1.



Extensive investigations by our group<sup>2-4</sup> and others as well<sup>5-7</sup> suggest that there are three steps involved in the Shilov system: (i) electrophilic C-H bond activation to form a Pt(II)-C bond; (ii) oxidation of the Pt<sup>II</sup> intermediate to an octahedral Pt<sup>IV</sup> species by [PtCl<sub>6</sub>]<sup>2-</sup> via electron transfer; and (iii) nucleophilic attack by water at the carbon of Pt<sup>IV</sup>-C to regenerate the catalyst, [PtCl<sub>4</sub>]<sup>2-</sup>, and release the alcohol. The catalytic cycle composed of these three steps are known as the Shilov cycle (Scheme 2).

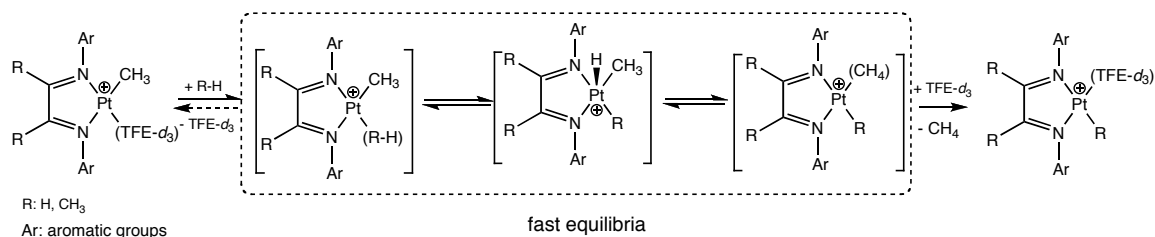
Investigations of competitive oxidation versus protonolysis of a Pt(II)-methyl species suggest that the rate of steps *ii* and *iii* are much faster than the reverse of step *i*.<sup>8, 9</sup> This kinetic feature ensures the efficiency of the catalytic cycle. Furthermore, the facile protonolysis on Pt(II)-hydrocarbyl to form the corresponding hydrocarbon indicates that the forward reaction of step *i* is uphill.<sup>10</sup> Based on these observations, it appears that electrophilic C-H bond activation is the rate-determining step of the whole catalytic cycle.

**Scheme 2.**



Because of the complicated nature of the original Shilov system, much of the mechanistic understanding of step *i* has been obtained from well-defined model systems, particularly ones based on complexes of the form  $[(N-N)Pt(CH_3)_2]$  (N-N are bidentate nitrogen-based ligands). According to the principle of microscopic reversibility, protonolysis of the Pt(II)-C bond shares the same mechanism as the reverse C-H bond activation process and thus serves as a model system for the mechanistic investigations of step *i* in the Shilov cycle.

Scheme 3.

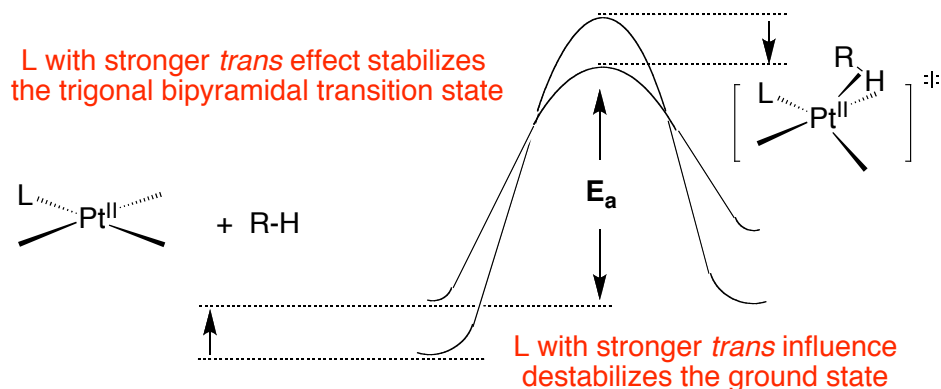


Detailed protonolysis studies on the model systems suggest that the following three steps are involved in the corresponding reverse process:<sup>10</sup> (*ia*) the replacement of a Pt(II)-solvento ligand by hydrocarbon, leading to the formation of a Pt(II)-hydrocarbon sigma adduct; (*ib*) oxidative cleavage of the C-H bond coordinated to Pt(II) to form a Pt(IV)-hydride intermediate; and (*ic*) deprotonation of the Pt(IV)-hydride intermediate to produce a Pt(II)-alkyl (Scheme 3). The irreversibility of the loss of methane in the protonolysis implies that the rate-determining step in the corresponding reverse process is the replacement of a Pt(II)-solvento ligand by the hydrocarbon C-H bond.

The dependence of CH<sub>4</sub>/CH<sub>3</sub>D ratio on the concentration of acetonitrile in the deuterolysis of [(diimine)Pt(CH<sub>3</sub>)<sub>2</sub>] implies an associative mechanism for methane displacement, the microscopic reverse process of methane coordination.<sup>11</sup> The negative activation volume measured for benzene C-H bond activation by Pt(II) further supports an associative mechanism.<sup>12</sup>

The observations upon the model systems implicate that the rate-determining step for the Shilov cycle is the substitution of a Pt(II)-solvento ligand by the C-H bond of the hydrocarbon to be activated via an associative mechanism. Therefore, promoting the rate of the C-H bond coordination is a key to improving the efficiency of the Shilov cycle.

Scheme 4.

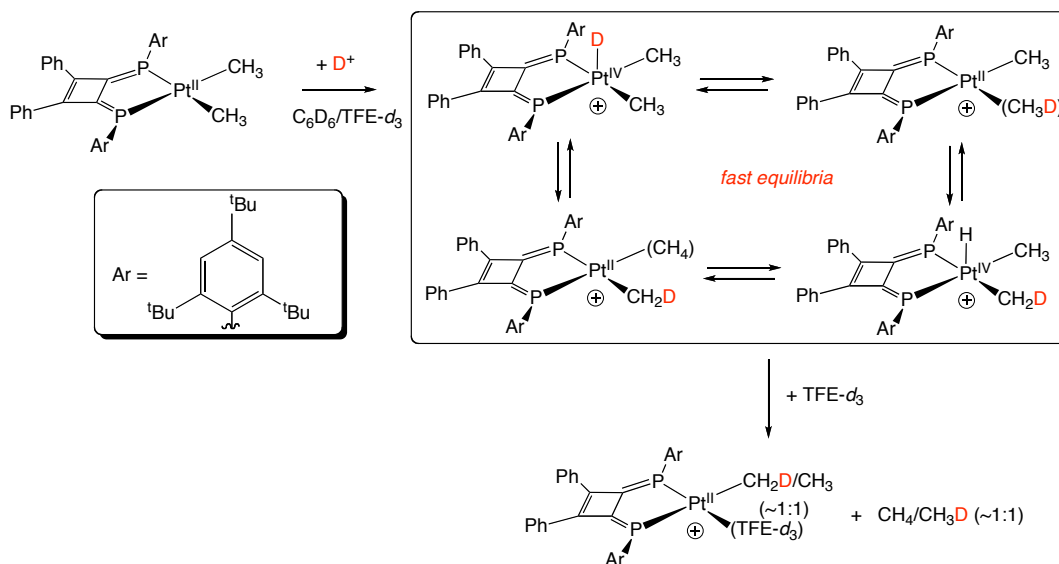


Ligands with both strong *trans* influence and  $\pi$ -accepting ability appear to be good candidates to serve for this purpose. As shown in Scheme 4, ligands with stronger *trans* influence weaken the bond between Pt and the *trans* ligand to be displaced and increase the energy of ground state accordingly; at the same time, their stronger  $\pi$ -accepting ability also stabilizes the trigonal-bipyramidal transition state. A combined effect of these two factors is thus expected to facilitate C-H bond coordination.

We decided to investigate the relevant chemistry of dimethylplatinum(II) complexes with bisphosphinidine-based ligands as a beginning point of the research described in this dissertation, because these ligands have both stronger *trans* influence and stronger  $\pi$ -accepting ability than nitrogen-based ligands. The deuterolysis of  $(\text{P-P})\text{PtMe}_2$  ( $\text{P-P}$  = bisphosphinidine)<sup>13</sup> in  $\text{C}_6\text{D}_6/\text{TFE-d}_3$  leads to results similar to those observed for its diimine counterparts (Scheme 5). However, the resultant monomethyl platinum(II) species shows no activity in term of benzene C-H bond activation, probably due to the inhibition of associative C-H bond coordination by the bulky *tert*-butyl group on the P-aryl substituent that overrides the electronic promotion effect of bisphosphinidine.



Scheme 5.



Therefore, we decided to use a different metal instead of ligand modification as an alternative strategy to enhance the rate of C-H bond activation. Studies on the chemistry of aromatic C-H bond activation by  $[(\text{diimine})\text{M}(\text{CH}_3)(\text{H}_2\text{O})]^+$  ( $\text{M} = \text{Pd}^{\text{II}}, \text{Pt}^{\text{II}}$ ) reveal that palladium(II) and electron-rich diimine ligands lead to faster C-H bond activation than their platinum(II) and electron-poor diimine counterparts, respectively.<sup>11,14</sup> To further explore the electronic effect of nitrogen-based ligand on C-H bond activation, diamine- and  $\beta$ -diketimide-monomethylpalladium(II) complexes were chosen as the target systems. Both ligands are expected to provide a more electron-rich palladium(II) center than diimine.

We first focused on the protonolysis chemistry. Deuterolysis of these dimethylpalladium(II) complexes does not lead to any significant deuterium scrambling, unlike that observed in the deuterolysis of  $[(\text{diimine})\text{Pt}(\text{CH}_3)_2]$ . Moreover, a surprisingly large amount of  $\text{CH}_4$  is formed with the expected  $\text{CH}_3\text{D}$ . Abnormally large KIE in the competitive protonolysis/deuterolysis is the most straightforward explanation, and the

involvement of hydrogen tunneling in such process was soon recognized. This part of the work is described in Chapter 2.

Later on, a similar phenomenon was observed in the deuterolysis of  $(\text{COD})\text{Pt}(\text{CH}_3)_2$ , which is still the only platinum example so far.<sup>15</sup> DFT computation suggests that the protonolysis of the dimethylpalladium(II) and of  $(\text{COD})\text{Pt}(\text{CH}_3)_2$  share a similar mechanism, wherein protonation of the  $\text{M}^{\text{II}}\text{-C}$  bond is kinetically preferred over protonation at the metal center. The computation further suggests that the occurrence of hydrogen tunneling should be invoked to explain the abnormally large KIEs observed experimentally. This part of the work is described in Chapter 3.

The protonolysis study also indicates that it is important to replace the ethylene linker of TMEDA in the TMEDA-ligated complex with a cyclohexylene linker in order to obtain a stable  $[(\text{diamine})\text{Pd}(\text{CH}_3)(\text{TFE-d}_3)]^+$  ( $\text{TFE-d}_3 = 2, 2, 2$  – trifluoroethanol- $\text{d}_3$ ) species, probably because of the fast decomposition of  $[(\text{TMEDA})\text{Pd}(\text{CH}_3)(\text{H}_2\text{O})]^+$  after the dechelation of the hemi-labile TMEDA ligand. However, even with the assistance of the cyclohexylene backbone, only a low yield of  $[(\text{diamine})\text{Pd}(\text{Ph})(\text{TFE-d}_3)]^+$ , the product of benzene C-H bond activation by  $[(\text{diamine})\text{PdCH}_3(\text{TFE-d}_3)]^+$ , is obtained.

One might argue that the results for  $[(\text{diamine})\text{PdCH}_3(\text{TFE-d}_3)]^+$  reflect the importance of  $\pi$ -accepting ability for the ligand to facilitate C-H coordination, which can presumably lead to higher yields of C-H bond activation product. Therefore,  $\beta$ -diketimide was chosen as the ligand to support monomethylpalladium(II) in subsequent studies. Then a monomethylpalladium(II) complex,  $(\text{COD})\text{Pd}(\text{CH}_3)\text{Cl}$  ( $\text{COD} = 1,5\text{-cyclooctadiene}$ ), is found to undergo both benzene C-H activation and migratory insertion of olefin, with the former faster than the latter, at room temperature under the assistance of an anionic

$\beta$ -diketiminate ligand, to yield  $\eta^3$ -(2-R-cyclooctenyl)palladium(II)  $\beta$ -diketiminate (R = methyl or phenyl). This part of the work is described in Chapter 4.

Faster aromatic C-H bond activation than the insertion of olefin at  $M^{II}$ -C bonds is an essential feature for catalytic olefin hydroarylation reactions.<sup>16</sup> We reason that modifying the system with electron-rich anionic ligands can enhance back donation from the metal center to the coordinated olefin by increasing the electron density on the metal center, which leads to the slower olefin insertion relative to the activation of benzene C-H bond. As a first step to find ligands that might lead to new Pd-based catalysts for olefin hydroarylation, we computationally screened the effects of 8 monoanionic ligands and 1 dianionic ligand on the competition between benzene C-H bond activation and ethylene insertion in their corresponding monomethylpalladium(II) complexes. This part of the work is described in Chapter 5.

In the last part of this dissertation, we turn our interest to the mechanism of another type of reactions, namely palladium-catalyzed dehydrogenative coupling involving C-H bond activation. In contrast to all reactions described earlier, a Pd(0)/Pd(II) redox cycle is involved in these reactions. Since catalysts of most of these reactions are not well defined,<sup>17</sup> we decided to develop our own catalysts that would allow in-depth mechanistic investigations. Supporting palladium with ligands is one obvious way toward this goal. However, it often turns out that the use of a ligand either shuts down or slows the reaction. And due to the poor knowledge about the mechanisms, it was not clear what type of ligands should be used at the beginning of this project. Therefore, we chose two ligands,  $\beta$ -diketiminate and bipyrimidine, to test if the reactions prefer electron-rich or electron-poor ligands. No catalytic reaction is achieved upon palladium systems with the

electron-rich  $\beta$ -diketiminate ligand, while bipyrimidine leads us to the first well-defined Pd catalyst for allylic oxidation of olefins, which allows us to probe the operational mechanism in great detail.<sup>18</sup> This part of the work is described in Chapter 6.

## References

- (1) Gol'dshleger, N. F.; Es'kova, V. V.; Shilov, A. E.; Shteinman, A. A. *Zh. Fiz. Khim.* **1972**, *46*, 1353–1354.
- (2) Labinger, J. A.; Herring, A. M.; Lyon, D. K.; Luinstra, G. A.; Bercaw, J. E.; Horvath, I. T.; Eller, K. *Organometallics* **1993**, *12*, 895–905.
- (3) Luinstra, G. A.; Wang, L.; Stahl, S. S.; Labinger, J. A.; Bercaw, J. E. *Organometallics* **1994**, *13*, 755–756.
- (4) Luinstra, G. A.; Wang, L.; Stahl, S. S.; Labinger, J. A.; Bercaw, J. E. *J. Organomet. Chem.* **1995**, *504*, 75–91.
- (5) Horvath, I. T.; Cook, R. A.; Millar, J. M.; Kiss, G. *Organometallics* **1993**, *12*, 8–10.
- (6) Hutson, A. C.; Lin, M. R.; Basicckes, N.; Sen, A. *J. Organomet. Chem.* **1995**, *504*, 69–74.
- (7) Kushch, L. A.; Lavrushko, V. V.; Misharin, Y. S.; Moravskii, A. P.; Shilov, A. E. *Nouv. J. Chim.* **1983**, *7*, 729–733.
- (8) Mitchenko, S. A.; Zamashchikov, V. V. *Kinet. Katal.* **1989**, *30*, 297.
- (9) Zamashchikov, V. V.; Popov, V. G.; Litvinenko, S. L. *Izv. Akad. Nauk., Ser. Khim.* **1993**, *42*, 389.
- (10) Stahl, S. S.; Labinger, J. A.; Bercaw, J. E. *J. Am. Chem. Soc.* **1996**, *118*, 5961–5976.

- (11) (a) Johansson, L.; Tilset, M. *J. Am. Chem. Soc.* **2001**, *123*, 739–740. (b) Zhong, H. A.; Labinger, J. A.; Bercaw, J. E. *J. Am. Chem. Soc.* **2002**, *124*, 1378–1399.
- (12) Procelewska, J.; Zahl, A.; van Eldik, R.; Zhong, H. A.; Labinger, J. A.; Bercaw, J. E. *Inorg. Chem.* **2002**, *41*, 2808–2810.
- (13) Synthesized according to a literature procedure: Ozawa, F.; Kawagishi, S.; Ishiyama, T.; Yoshifuji, M. *Organometallics* **2004**, *23*, 1325–1332.
- (14) Ackerman, L. J.; Sadighi, J. P.; Kurtz, D. M.; Labinger, J. A.; Bercaw, J. E. *Organometallics* **2003**, *22*, 3884–3890.
- (15) Bercaw, J. E.; Chen, G. S.; Labinger, J. A.; Lin, B. -L. *J. Am. Chem. Soc.* **2008**, *130*, 17654–17655.
- (16) Oxgaard, J.; Muller, R. P.; Goddard, W. A.; Periana, R. A. *J. Am. Chem. Soc.* **2004**, *126*, 352–363.
- (17) Dyker, G., Ed. *Handbook of C-H Transformations*; Wiley-VCH, Weinheim, Germany, **2005**.
- (18) Lin, B. -L.; Labinger, J. A.; Bercaw, J. E. *Can. J. Chem.* **2009**, *87*, 264–271.

## Chapter 2. Hydrogen Tunneling in the Protonolysis of Dimethylpalladium(II) Complexes

### Abstract

Abnormally large kinetic hydrogen/deuterium isotope effects (KIEs,  $\sim 20$ ) are measured for the protonolysis of several dimethylpalladium(II) complexes with various bidentate ligands by trifluoroethanol (TFE) at room temperature. This is the first time that KIEs greater than 10 at room temperature or higher are observed for the protonolysis of metal alkyls. Analyses of semiclassical KIE theory suggest that the occurrence of hydrogen tunneling needs to be invoked in order to explain these KIE values, which is further supported by the KIE-temperature-dependence study for the protonolysis of (dppe)Pd(CH<sub>3</sub>)<sub>2</sub> by CF<sub>3</sub>CD<sub>2</sub>OD/CF<sub>3</sub>CH<sub>2</sub>OH. It is also expected that proton loss from Pd<sup>II</sup> methane  $\sigma$  adduct, the microscopic reverse process of the protonolysis, should also involve hydrogen tunneling. Relevant phenomena for various types of C-H activations or the corresponding microscopic reverse in the literature are also briefly overviewed.

## 1. Introduction

The selective transformation of C-H bonds, especially partial oxidation of methane, represent an important area of current research.<sup>1</sup> Over the past several decades, numerous examples of C-H bond activation by transition metals have appeared in the literature.<sup>2</sup> Of particular significance is the development of a number of homogeneous catalytic systems based on late transition metals, especially platinum<sup>3</sup> and palladium.<sup>4</sup> The first of them, a Pt-based system discovered by Shilov and co-workers,<sup>3a</sup> has attracted the most research attention. Extensive mechanistic studies by our group and others on the Shilov system,<sup>5</sup> mainly through studies of alkylplatinum(II) model systems, suggest that C-H activation by Pt(II) is the first step in the oxidation, and is the rate- and selectivity-determining step. In sharp contrast, the mechanism for alkane C-H activation by Pd(II) is still largely unexplored, although the formation of alkylpalladium(II) intermediates via electrophilic C-H activation has also been proposed.<sup>4c,6</sup> We decided to investigate the mechanism of methane C-H bond activation by Pd(II) through the microscopic reverse, namely protonolysis of methylpalladium(II) (Scheme 1).<sup>7</sup> Herein, we report for the first time the observation of a new fundamental phenomenon, proton tunneling, in the protonolysis of several dimethylpalladium(II) model systems.

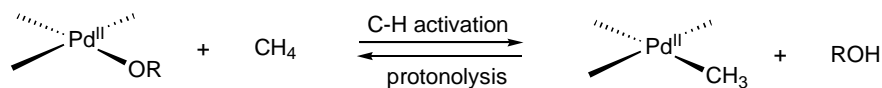
## 2. Results and Discussions

### 2.1 Abnormally Large KIEs in the Protonolysis of Palladium Methyl Complexes

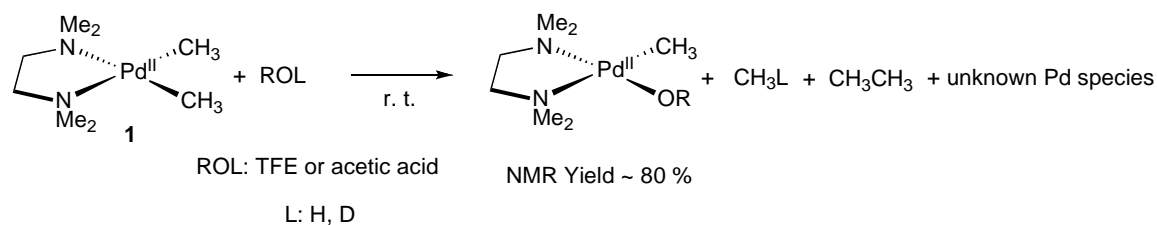
The first model system investigated is (tmeda)Pd(CH<sub>3</sub>)<sub>2</sub> (complex **1**, tmeda = (CH<sub>3</sub>)<sub>2</sub>NCH<sub>2</sub>CH<sub>2</sub>N(CH<sub>3</sub>)<sub>2</sub>). Gas bubbles are observed immediately after adding (tmeda)Pd(CH<sub>3</sub>)<sub>2</sub> to neat TFE-d<sub>3</sub> (TFE-d<sub>3</sub> = CF<sub>3</sub>CD<sub>2</sub>OD, D > 99% according to the

estimation by  $^1\text{H}$  NMR) at room temperature. The products observed by  $^1\text{H}$  NMR are mainly  $(\text{tmeda})\text{Pd}(\text{CH}_3)(\text{OCD}_2\text{CF}_3)$  and  $\text{CH}_3\text{D}$ .

**Scheme 1.**



**Scheme 2.**



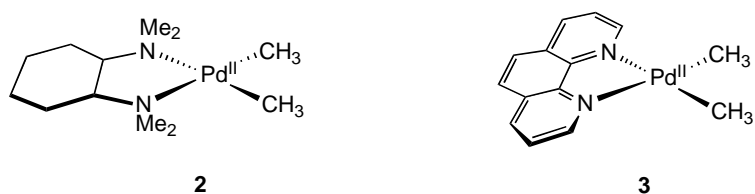
Surprisingly, a nonnegligible amount of  $\text{CH}_4$  is generated with  $\text{CH}_3\text{D}$ . Because no deuterium incorporation is observed in either the methyl or ligand  $^1\text{H}$  NMR signals of the product, residual  $\text{H}^+$  in the solvent is responsible for the  $\text{CH}_4$  formed. If a 20:1  $\text{TFE-}d_3$ : $\text{TFE-}d_0$  is used instead, the ratio of  $\text{CH}_4$ : $\text{CH}_3\text{D}$  increases to  $\sim 1$  (determined by integration of the two methane isotopologue signals in the  $^1\text{H}$  NMR), indicating abnormally large kinetic isotope effects ( $k_{\text{H}}/k_{\text{D}}$ ) are present in the competitive deuterolysis/protonolysis reactions for compound **1** (KIE  $\sim 20$  at room temperature). Unfortunately, a competing reaction involving reductive elimination of ethane, which is always observed through the screening of solvents (e.g., toluene, chloroform, and acetone) and H/D sources (TFE and acetic acid), complicates the precise determination of KIE values (Scheme 2).

The facile formation of ethane is somewhat unexpected because it is known that complex **1** is fairly stable even upon thermolysis at  $60\text{ }^\circ\text{C}$ .<sup>8</sup> This instability was first

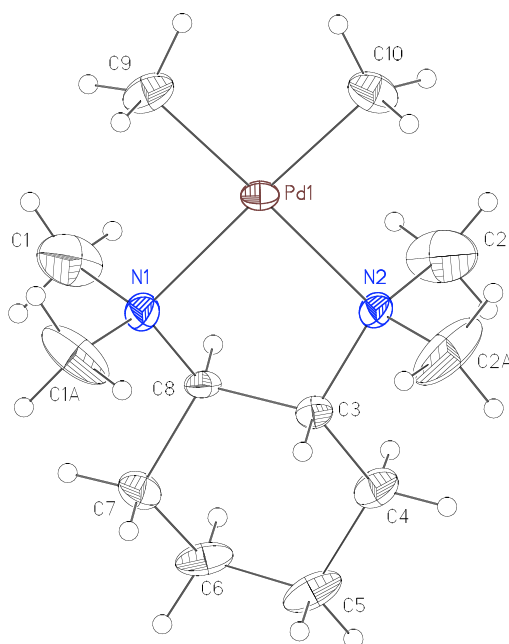


attributed to the hemilability of the tmeda ligand. Therefore, two rigid dinitrogen-based ligands are used in place of tmeda for the dimethylpalladium(II) complex (**2** and **3**, Scheme 3). (The crystal structure of complex **2** is shown in Figure 1.)<sup>9</sup> KIEs ~ 20 at room temperature are also observed for the protonolysis of both systems by TFE. However, the formation of a significant amount of ethane is still observed.

**Scheme 3.**



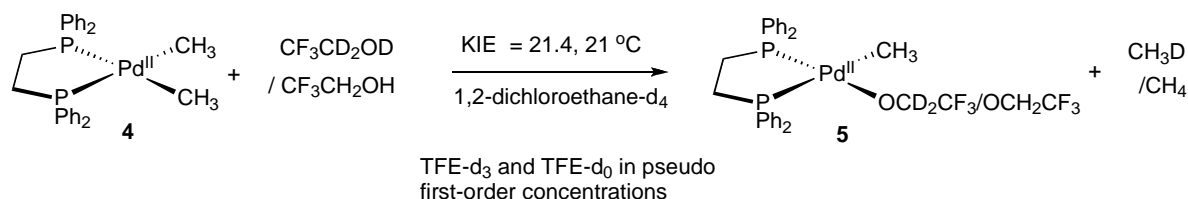
**Figure 1.** X-ray crystal structure of complex **2** (CCDC 263612)



In order to suppress the reductive elimination of ethane, we decided to use diphosphine ligands for the dimethylpalladium(II) complex instead of the dinitrogen ligands in

complexes **1**, **2**, and **3**. The softer phosphorus donor is expected to bind tighter with palladium(II) than its nitrogen counterparts and inhibit the reductive elimination. Indeed, this side reaction is virtually absent ( $< 1\%$ , estimated by  $^1\text{H}$  NMR) in the protonolysis of  $(\text{dppe})\text{Pd}(\text{CH}_3)_2$  (complex **4**,  $\text{dppe} = \text{Ph}_2\text{PCH}_2\text{CH}_2\text{PPh}_2$ ) by TFE in 1,2-dichloroethane (DCE) (Scheme 5). Similar to the deuterolysis of complex **1**, the resultant methane is a mixture of  $\text{CH}_4$  and  $\text{CH}_3\text{D}$ . No deuterium incorporation into the  $\text{Pd}-\text{CH}_3$  and the dppe ligand of complex **5** is observed. The measured  $k_{\text{H}}/k_{\text{D}}$  is  $21.4 \pm 0.7$  for the competitive protonolysis of **4** with a mixture of  $\text{TFE}-d_3$  and  $\text{TFE}-d_0$  in dichloroethane- $d_4$  to form **5** at  $21^\circ\text{C}$  (Scheme 4).

**Scheme 4.**



Based on these observations, abnormally large KIEs at room temperature appear to be fairly general for the protonolysis of dimethylpalladium(II) complexes. Surprisingly, no abnormally large KIE has been reported for the protonolysis of metal alkyls before this work.<sup>10</sup>

## 2.2 Semiclassical Limits of KIEs

It has been generally accepted that KIEs greater than 10 at room temperature or higher are out of the semiclassical upper limit of KIEs.<sup>11, 12</sup> However, the detailed reasons

leading to this argument are sporadic in the literature. Herein, derivations of this upper limit as well as the semiclassical limits of Arrhenius parameters for the temperature dependence of KIEs are given. These derivations are important for accurate interpretations of KIEs. For example, common understanding that KIEs are due to the change of zero-point vibrational energies is incomplete. And as we will see in the following derivations, other factors, such as isotope effect on the reaction activation entropy, also contribute to the magnitude of KIEs.

### 2.2.1 Semiclassical Expression of KIEs

Semiclassical Eyring's equation of absolute-rate constant can be expressed as

$$k = \frac{k_B T}{h} e^{S_a/R} e^{-H_a/RT} \quad \text{Equation (1)}$$

where  $k_B$ ,  $h$ ,  $S_a$ , and  $H_a$  are Boltzmann constant, Planck constant, activation entropy, and activation enthalpy, respectively,

$$\begin{aligned} S_a &= S_{t,a} + S_{r,a} + S_{v,a} \\ H_a &= E_a^{elec} + E_{t,a} + E_{r,a} + E_{v,a}. \end{aligned}$$

Because activation entropy is the sum of activation translational entropy ( $S_{t,a}$ ), rotational entropy ( $S_{r,a}$ ), and vibrational entropy ( $S_{v,a}$ ) and activation enthalpy is the sum of activation electronic energy ( $E_a^{elec}$ ), translational energy ( $E_{t,a}$ ), rotational energy ( $E_{r,a}$ ), and vibrational energy ( $E_{v,a}$ ), equation (1) can be further expressed as

$$k = \frac{k_B T}{h} e^{(TS_{t,a} - E_{t,a})/RT} e^{(TS_{r,a} - E_{r,a})/RT} e^{(TS_{v,a} - E_{v,a})/RT} e^{-E_a^{elec}/RT}.$$

According to statistical analysis of entropy, we have

$$\begin{aligned} Z_t &= e^{(TS_{t,a} - E_{t,a})/RT} \\ Z_r &= e^{(TS_{r,a} - E_{r,a})/RT} \\ Z_v &= e^{(TS_{v,a} - E_{v,a})/RT} \end{aligned}$$

where  $Z_t$ ,  $Z_r$ , and  $Z_v$  correspond to translational, rotational, and vibrational partition function, respectively.<sup>13</sup>

Therefore, Eyring's equation of absolute-rate constant can also be expressed as

$$k = \frac{k_B T}{h} Z_t Z_r Z_v e^{-E_a^{elec}/RT} \quad \text{Equation (2)}$$

where each  $Z$  is equal to corresponding partition function of the transition state divided by the product of partition functions of the reactants.

Because activation electronic energy ( $E_a^{elec}$ ) is isotope-insensitive, we obtain the following semiclassical expression for kinetic hydrogen/deuterium isotope effect (KIE).

$$\frac{k_H}{k_D} = \frac{Z_{t,H} Z_{r,H} Z_{v,H}}{Z_{t,D} Z_{r,D} Z_{v,D}} \quad \text{Equation (3)}$$

Translational partition function  $Z_t$  of a molecule is derived from one-dimensional box model and is given by

$$Z_t = \frac{(2\pi M k_B T)^{3/2}}{h}$$

where  $M$  is reduced mass of the molecule.<sup>13</sup>

Rotational partition function  $Z_r$  of a molecule is derived from rigid rotator model and is given by

$$Z_r = \frac{[\pi(8\pi^2 k_B T)^3 I_A I_B I_C]^{1/2}}{\sigma h^3}$$

where  $I_A$ ,  $I_B$ , and  $I_C$  are moments of inertia of the molecule along each coordinate axis and  $\sigma$  is the symmetry number.<sup>13</sup>

Vibrational partition function  $Z_v$  of a molecule is the sum of probability of vibronic states, which is equal to

$$Z_v = \prod_{i=1}^{3n-6} \frac{e^{-hv_i / 2k_B T}}{1 - e^{-hv_i / k_B T}}$$

where  $n$  is the number of atom in the molecule and  $v_i$  are vibrational frequencies. The number of vibrations is equal to  $3n-6$  for nonlinear molecules. For nonlinear transition states, there are  $3n-7$  vibrations and one imaginary vibration corresponding to the reaction coordinate.<sup>13</sup>

Vibrational partition function  $Z_v$  can be decomposed into two items,

$$Z_v = \prod_{i=1}^{3n-6} e^{-hv_i / 2k_B T} \prod_{i=1}^{3n-6} \frac{1}{1 - e^{-hv_i / k_B T}} = e^{-\sum_{i=1}^{3n-6} ZPE_i / k_B T} Z_v^{exc}$$

where the first item and the second item correspond to the sum of zero-point energies of all vibrations and the contribution of thermal excitations of vibronic states, respectively.

Based on the analysis above, the semiclassical expression for KIE can be expressed as

$$\frac{k_H}{k_D} = \frac{Z_{t,H} Z_{r,H} Z_{v,H}^{exc}}{Z_{t,D} Z_{r,D} Z_{v,D}^{exc}} e^{-\Delta\Delta ZPE / RT} \quad \text{Equation (4)}$$

where  $\Delta\Delta ZPE$  is the zero-point vibrational energy difference between the transition state and reactants with different isotopic contents.

Alternatively, KIE can be expressed based on Arrhenius equation, which gives

$$\frac{k_H}{k_D} = \frac{A_H}{A_D} e^{-(E_a^H - E_a^D) / RT} \quad \text{Equation (5)}$$

By correlating equation (4) and (5), we have the following expressions for the Arrhenius parameters of KIEs,

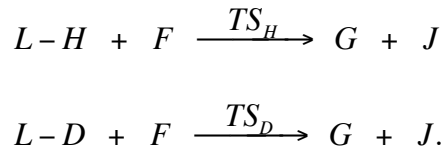
$$\frac{A_H}{A_D} = \frac{Z_{t,H} Z_{r,H} Z_{v,H}^{exc}}{Z_{t,D} Z_{r,D} Z_{v,D}^{exc}} \quad (E_a^H - E_a^D) = \Delta\Delta ZPE.$$

For large molecules, isotopic substitutions only have trivial effects on reduced mass and moments of inertia. Under this circumstance,  $Z_t$  and  $Z_r$  are nearly isotope insensitive.

Actually, the contribution of these two items to KIEs becomes important only when dihydrogen or other small molecules with multiple isotopic substitutions, such as CH<sub>4</sub> versus CD<sub>4</sub>, are involved. In general, we have

$$\frac{A_H}{A_D} \sim \frac{Z_{v,H}^{exc}}{Z_{v,D}^{exc}}.$$

Now let's consider KIE for the following biomolecular proton transfer reactions (all discussions below are based on the same reactions unless otherwise stated):



Based on the analysis above, the Arrhenius parameter  $A_H/A_D$  has the following expression

$$\frac{A_H}{A_D} = \left( \frac{M_H^{TS} M_{L-D}}{M_D^{TS} M_{L-H}} \right)^{3/2} \left( \frac{I_{A,H}^{TS} I_{B,H}^{TS} I_{C,H}^{TS} I_{A,L-D} I_{B,L-D} I_{C,L-D}}{I_{A,D}^{TS} I_{B,D}^{TS} I_{C,D}^{TS} I_{A,L-H} I_{B,L-H} I_{C,L-H}} \right)^{1/2} \prod_{i=1}^{3n'-7} \frac{1 - e^{-u_{D,i}^{TS}}}{1 - e^{-u_{H,i}^{TS}}} \prod_{i=1}^{3n-6} \frac{1 - e^{-u_{L-H,i}}}{1 - e^{-u_{L-D,i}}}$$

$$\frac{A_H}{A_D} = MMI \times EXC$$

where  $u_i = h\nu_i/k_B T$ . In the literature, *MMI* is generally used to stand for the reduced mass item and the moment of inertia item, while the excited vibronic states contribution is abbreviated as *EXC*. As discussed earlier, *MMI* is approximately equal to 1 for reactions only involving isotopic substitutions in large molecules.

### 2.2.2 The Semiclassical Lower Limit of $A_H/A_D$

In order to estimate the semiclassical lower limit of  $A_H/A_D$ , it is assumed that isotopic substitution of one atom in a reaction results in 3 isotope-sensitive vibrations because the

degree of freedom for the atom is 3.<sup>11</sup> Furthermore, one of the 3 vibrations is lost and becomes imaginary in the transition state. After canceling all isotope-insensitive vibrations, we have the following expression for  $A_H/A_D$  when  $MMI$  is  $\sim 1$ :

$$\frac{A_H}{A_D} \sim \prod_{i=1}^2 \frac{1 - e^{-u_{D,i}^{TS}}}{1 - e^{-u_{H,i}^{TS}}} \prod_{i=1}^3 \frac{1 - e^{-u_{L-H,i}}}{1 - e^{-u_{L-D,i}}} .$$

Because  $u_H$  is always greater than  $u_D$ , we have

$$\frac{1 - e^{-u_{L-H,i}}}{1 - e^{-u_{L-D,i}}} > 1 .$$

Consequently, we have

$$\frac{A_H}{A_D} > \prod_{i=1}^2 \frac{1 - e^{-u_{D,i}^{TS}}}{1 - e^{-u_{H,i}^{TS}}} .$$

The quotient in the right equation reaches minimum when its first-order derivative is zero, from which the following equation is obtained:

$$\frac{1 - e^{-u_{D,i}^{TS}}}{1 - e^{-u_{H,i}^{TS}}} = \frac{u_{D,i}^{TS}}{u_{H,i}^{TS}} e^{(u_{H,i}^{TS} - u_{D,i}^{TS})} .$$

Therefore, we have

$$\frac{1 - e^{-u_{D,i}^{TS}}}{1 - e^{-u_{H,i}^{TS}}} \geq \frac{u_{D,i}^{TS}}{u_{H,i}^{TS}} e^{(u_{H,i}^{TS} - u_{D,i}^{TS})} .$$

And because  $(u_{H,i}^{TS} - u_{D,i}^{TS})$  is always greater than 0, we have

$$\frac{1 - e^{-u_{D,i}^{TS}}}{1 - e^{-u_{H,i}^{TS}}} \geq \frac{u_{D,i}^{TS}}{u_{H,i}^{TS}} \geq \sqrt{\frac{1}{2}} .$$

Consequently, the semiclassical lower limit of  $A_H/A_D$  is estimated to be 0.5 for proton transfer reactions only involving isotopic substitutions in large molecules.

### 2.2.3 The Semiclassical Upper Limit of $A_H/A_D$

In order to estimate the semiclassical upper limit of  $A_H/A_D$ , an alternative expression of  $A_H/A_D$  based on Teller-Redlich product theorem (the following equation) needs to be invoked.<sup>14</sup>

$$MMI = \prod_{j=1}^n \frac{m_{H,j}}{m_{D,j}} \prod_{i=1}^{3n-6} \frac{v_{H,i}}{v_{D,i}}$$

Based on this theorem,  $A_H/A_D$  can also be expressed as

$$\frac{A_H}{A_D} = \frac{v_H^{TS,RC}}{v_D^{TS,RC}} \prod_{i=1}^{3n'-7} \frac{u_{H,i}^{TS} (1 - e^{-u_{D,i}^{TS}})}{u_{D,i}^{TS} (1 - e^{-u_{H,i}^{TS}})} \prod_{i=1}^{3n-6} \frac{u_{L-D,i} (1 - e^{-u_{L-H,i}})}{u_{L-H,i} (1 - e^{-u_{L-D,i}})}$$

where  $v^{TS,RC}$  is the imaginary frequency corresponding to the reaction coordinate in transition state.

At high temperatures,  $u$  approaches 0 and thus we have

$$1 - e^{-u} \sim 1 - (1 - u) = u.$$

Therefore,

$$\frac{u_{H,i}^{TS} (1 - e^{-u_{D,i}^{TS}})}{u_{D,i}^{TS} (1 - e^{-u_{H,i}^{TS}})} \sim 1$$

$$\frac{u_{L-D,i} (1 - e^{-u_{L-H,i}})}{u_{L-H,i} (1 - e^{-u_{L-D,i}})} \sim 1.$$

As a result, the high-temperature semiclassical limit of  $A_H/A_D$  is estimated to be  $\sim 1.4$  according to the following relations:

$$\left( \frac{A_H}{A_D} \right)_{HT} \sim \frac{v_H^{TS,RC}}{v_D^{TS,RC}} \leq \left( \frac{m_D}{m_H} \right)^{1/2} = \sqrt{2} \sim 1.4.$$

According to Bell's analysis,<sup>12</sup> the semiclassical upper limit of  $A_H/A_D$  is actually its high-temperature limit.



### 2.2.4 The Semiclassical Upper Limits of KIEs at 298 K

Based on the analysis above,  $A_H/A_D$  should be in the range of 0.5–1.4 if only the semiclassical factors are considered. Calculations on 5 model organic reactions with the temperature varying from 20 to 1000 K indicate that 0.7–1.2 are the practical semiclassical limits.<sup>15</sup> The upper limit of  $\Delta\Delta ZPE$  can be estimated from the circumstance where the  $X-H$  stretching vibration is completely lost in the transition state for a proton transfer reaction from such bond. Based on typical stretching frequencies of various  $X-H$  bonds, the maximum values of these  $\Delta\Delta ZPE$ s can thus be obtained, as shown in Table 1.

**Table 1.** Semiclassical upper limits of KIEs at 298 K for proton transfer from various  $X-H$  bonds

Bond	$\nu/\text{cm}^{-1}$	$\Delta\Delta ZPE/\text{cal mol}^{-1}$	$\text{Exp}(\Delta\Delta ZPE/RT)$	$\text{KIE}_{\text{max}}$
<i>C-H</i>	2900	1080	6.2	7.4
<i>N-H</i>	3100	1150	7.0	8.4
<i>O-H</i>	3300	1220	7.9	9.5
<i>S-H</i>	2500	930	4.8	5.8

Combining  $\Delta\Delta ZPE$  and the practical upper limits of  $A_H/A_D$ , we see that the semiclassical upper limit of KIEs at 298 K is  $\sim 10$ . Therefore, KIEs greater than 10 at room temperature cannot be solely explained by the aforementioned semiclassical theory and are generally attributed to the involvement of proton tunneling in the proton transfer reaction.

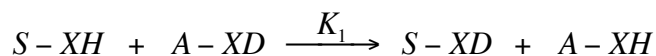
### 2.3 Composite KIEs

In case the observed KIEs are not solely due to single elementary step, composite KIEs are involved. In principle, abnormally large KIEs could be a combined result of multiple

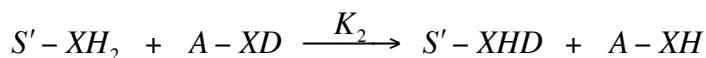
normal isotope effects, although well-characterized examples of this type are still rarely seen. In this section, postulations based on composite KIEs to explain abnormally large KIEs are discussed.

### 2.3.1 Fractionation Effect

If there is more than one protic chemical, either the solvent or the reactant, involved in the reaction, isotopic redistribution (or equilibrium) between these chemicals will affect the initial H/D ratio of the reactant as well as the observed values of KIEs. This is known as the fractionation effect. In contrast to kinetic isotope effects, no isotope-sensitive vibration is lost in the equilibrium. As a result, equilibrium isotope effects are generally approximately equal to the geometric mean, or in other words, determined by the statistical distribution of isotopes, if only one type of  $XH$  (e.g., OH) is involved<sup>14</sup> (see the following two examples).



$$K_1 = \frac{[S - XD][A - XH]}{[S - XH][A - XD]} \sim 1$$

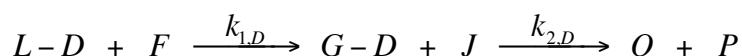
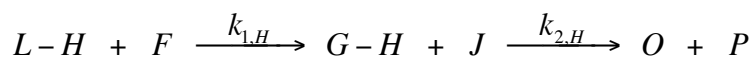


$$K_1 = \frac{[S - XHD][A - XH]}{[S - XH_2][A - XD]} \sim 2$$

Clearly, fractionation effect cannot explain the abnormally large KIEs observed here in the protonolysis of dimethylpalladium(II) complexes by TFE because only one protic solvent is involved.

### 2.3.2 Change of the Rate-Determining Step

For a multiple-step proton transfer reaction, the rate-determining step might change upon isotopic substitutions. Under this circumstance, more than one elementary step is involved in the observed KIEs. A close inspection, however, indicates that KIEs of this type should always be smaller than the KIEs of the rate-determining elementary step in the protium reaction. (The analysis of a two-step reaction is given below) Therefore, KIEs for this situation should also be smaller than the semiclassical upper limit if tunneling is not involved.



$$\text{if } k_{1,H} < k_{2,H} \ \& \ k_{1,D} > k_{2,D} \Rightarrow KIE \sim \frac{k_{1,H}}{k_{2,D}} < \frac{k_{1,H}}{k_{1,D}}$$

$$\text{if } k_{1,H} > k_{2,H} \ \& \ k_{1,D} < k_{2,D} \Rightarrow KIE \sim \frac{k_{2,H}}{k_{1,D}} < \frac{k_{2,H}}{k_{2,D}}$$

### 2.4 Hydrogen Tunneling and Bell's Model

Based on the discussions above, hydrogen tunneling appears to be the most reasonable explanation for the abnormally large KIEs observed. Bell's model<sup>10</sup> has been widely employed for the understanding of hydrogen tunneling. Approximations were made in the early literature for the calculation of hydrogen tunneling due to its complexity. To date, simplified tunneling calculations, such as Wigner's tunneling correction, are still widely used. However, the analysis in this section will show that such approximations are not valid under some circumstances.

In semiclassical kinetic theory, reactants pass over the reaction barrier to form the products only when their energies are higher than the activation energy. However, if the reactions involve the transfer of small particles, such as electron and protons, the wave particle duality starts to play an important role. According to the de Broglie relation  $(\lambda = h/p = h/[2mk_B T]^{1/2})$ , protons moving with thermal velocities at ordinary temperatures have wavelengths between 1 and 2 Å. Because the barriers of proton transfer reactions have a total width of a few Ångströms, we may expect to see that a percentage of protons involved in these reactions tunnel through the barrier even in case their energies are not enough to overcome the reaction barrier. As a result of proton tunneling, the semiclassical Eyring's equation for absolute rate constant of a proton transfer reaction ( $k_s$ ) should be corrected by a tunneling factor ( $Q_t$ ).

$$k_s = \frac{k_B T}{h} Z_t Z_r Z_v e^{-E_a^{elec}/RT}$$

$$k_t = Q_t k_s$$

$$k_t = \frac{k_B T}{h} Q_t Z_t Z_r Z_v e^{-E_a^{elec}/RT}$$

$Q_t$  is given by

$$Q_t = \int_0^\infty \frac{G(W)}{k_B T} e^{\frac{\varepsilon_a - W}{k_B T}} dW \quad \text{Equation (6)}$$

$$\varepsilon_a = \frac{E_a}{N_A} .$$

$N_A$  is Avogadro constant, and  $G(W)$  is the permeability of a particle with energy  $W$  passing through a barrier (barrier height,  $\varepsilon_a$ ), which is given by

$$G(W) = \frac{1}{1 + e^{\frac{2\pi(\epsilon_a - W)}{h\nu^{TS,RC}}}}.$$

Integration of equation (6) leads to the following expression:<sup>11</sup>

$$Q_t = \frac{\frac{1}{2}u^{TS,RC}}{\sin \frac{1}{2}u^{TS,RC}} - u^{TS,RC} e^{\frac{\epsilon_a}{k_B T}} \sum_{i=1}^{\infty} \frac{(-1)^{i+1} e^{-\frac{2i\pi\epsilon_a}{u^{TS,RC}k_B T}}}{2i\pi - u^{TS,RC}}.$$

The following expression of this equation is also seen in the literature,<sup>15</sup>

$$Q_t = \frac{\frac{1}{2}u^{TS,RC}}{\sin \frac{1}{2}u^{TS,RC}} - \sum_{i=1}^{\infty} \frac{(-1)^i e^{\frac{u^{TS,RC} - 2i\pi}{u^{TS,RC}}\alpha}}{\frac{u^{TS,RC}}{u^{TS,RC}} - 2i\pi} \quad \text{Equation (7)}$$

$$\alpha = \frac{\epsilon_a}{k_B T} = \frac{E_a}{RT} \quad (RT = 0.593 \text{ kcal/mol at } 298.15 \text{ K}).$$

In the early literature,<sup>11</sup> it is generally assumed that the second item is much smaller than 1, which leads to

$$Q_t \sim \frac{\frac{1}{2}u^{TS,RC}}{\sin \frac{1}{2}u^{TS,RC}}.$$

After Taylor expansion of the quotient on the right hand side, we have

$$Q_t \sim 1 + \frac{(u^{TS,RC})^2}{24} + \frac{7(u^{TS,RC})^4}{5760} + \dots \quad (u^{TS,RC} < 2\pi).$$

In general, all items after the second one can be ignored. Therefore, we have

$$Q_t \sim 1 + \frac{(u^{TS,RC})^2}{24} \quad (u^{TS,RC} < 2\pi).$$

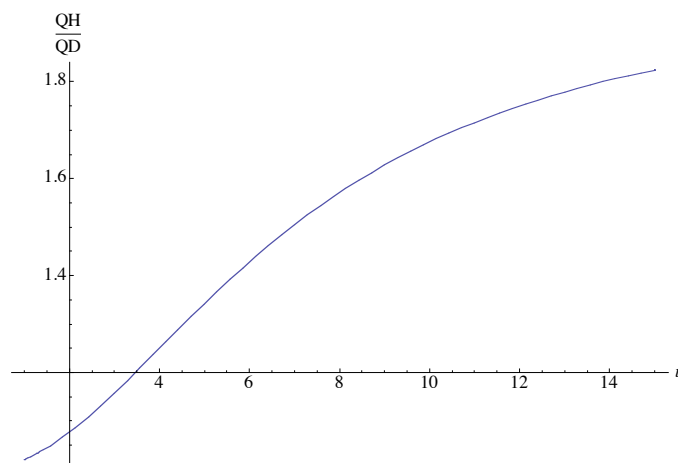
This expression is called Wigner's tunneling correction factor. Clearly,  $Q_t$  for proton is higher than that for deuterium because  $u^{TS,RC}$  for proton is always greater than that for the

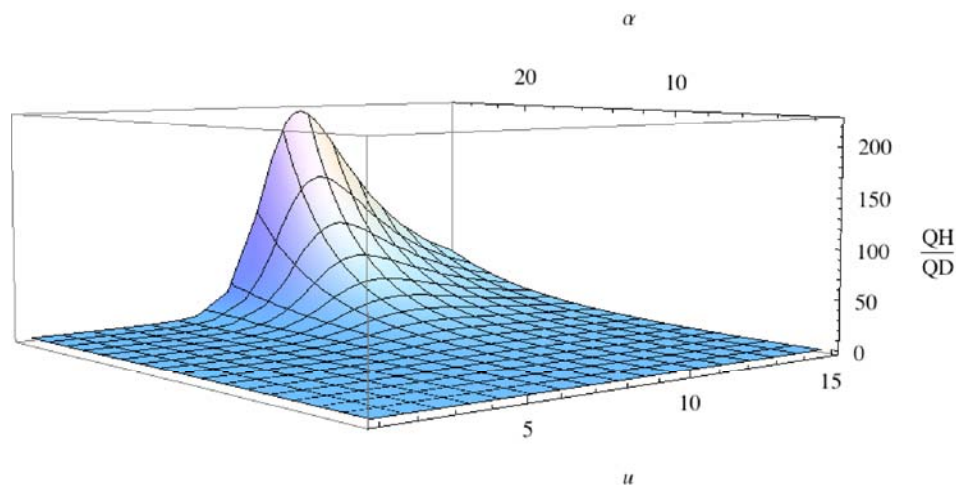
deuterium. As a result, the semiclassical expression of KIEs should also be corrected by a tunneling factor, which gives

$$\frac{k_{t,H}}{k_{t,D}} = \frac{Q_{t,H} Z_{t,H} Z_{r,H} Z_{v,H}^{exc}}{Q_{t,D} Z_{t,D} Z_{r,D} Z_{v,D}^{exc}} e^{-\Delta\Delta ZPE/RT}.$$

A graphical illustration for the dependence of  $Q_{t,H}/Q_{t,D}$  on  $u^{TS,RC}$ , using the highly simplified Wigner's tunneling correction and assuming  $u_H^{TS,RC} = 1.414 u_D^{TS,RC}$ , is shown in Figure 2 ( $u = 9.7$  at 298.15 K if  $\nu = 2000 \text{ cm}^{-1}$ ). According to Figure 2, the tunneling contribution to KIEs increases from 1 to  $\sim 1.8$  as  $u$  increases from 0 to 15. (It should be emphasized that Wigner's tunnel correction is generally thought to be valid only when  $u$  is smaller than  $2\pi$ . The unrealistic range of  $u$  in Figure 2 is just intended to show the trend.) Furthermore, Wigner's tunneling correction indicates that the KIEs for reactions with higher frequency for the vibrational normal mode corresponding to the reaction coordinate at or at lower temperatures have more tunneling contribution.

**Figure 2.** Wigner's tunneling correction



**Figure 3.** Full tunneling correction

However, if the full expression of the tunneling correction, with the first four items in the series of equation (7) (other items in the series are found to be trivial), is used instead, a much more complicated dependence of  $Q_{t,H}/Q_{t,D}$  on  $u^{TS,RC}$  is observed with the same  $u_H^{TS,RC} = 1.414 u_D^{TS,RC}$  assumption, as is shown in Figure 3. Several important observations can be made in comparisons between Figure 2 and Figure 3. First, Wigner's tunneling correction is no longer valid when both  $u$  and  $\alpha$  are large, or in other words, when the proton transfer reaction involved has high  $v^{TS,RC}$  or activation barrier, or the reaction takes place at low temperatures. The tunneling contribution to KIEs becomes much greater than that obtained by Wigner's tunneling correction. For example,  $Q_{t,H}/Q_{t,D}$  increases to  $\sim 5.9$  if  $u = 6$  and  $\alpha = 25$  ( $E_a = 14.8$  kcal/mol, 298.15 K), while Wigner's tunneling correction only gives  $Q_{t,H}/Q_{t,D} \sim 1.4$  for  $u = 6$ . Second, the tunneling contribution no longer increases monotonically as  $u$  increases if  $\alpha$  is sufficiently high. The maximum tunneling contribution is seen when  $u$  is approximately equal to 10 ( $v \sim 2000$  cm<sup>-1</sup> at 298.15 K). Third, the tunneling contribution increases as the activation

barrier increases, perhaps because the barrier is steeper, and thus more tunneling is involved.

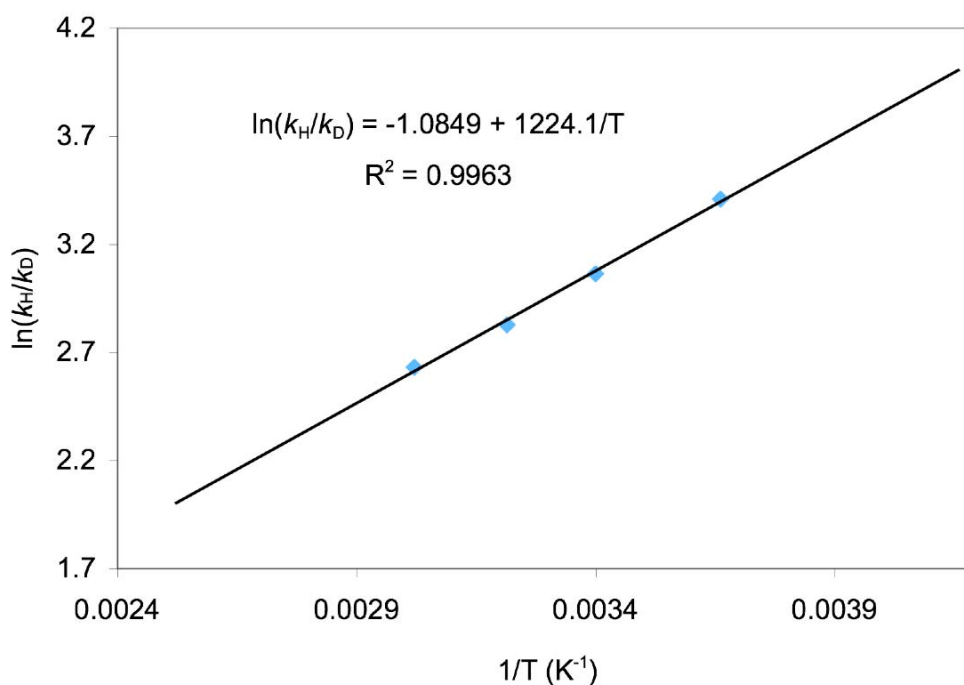
## 2.5 KIE Temperature Dependence for Protonolysis of Complex 4

**Table 2.** KIEs for the protonolysis/deuterolysis of complex 4 by TFE in DCE-d<sub>4</sub> at various temperatures

Temperature	273.15 K	294.15 K	311.15 K	331.15 K
KIE <sup>a</sup>	30.3 ± 1.0	21.4 ± 0.7	16.9 ± 0.4	13.9 ± 0.1
A <sup>H</sup> /A <sup>D</sup>	0.34 ± 0.06			
E <sub>a</sub> <sup>D</sup> – E <sub>a</sub> <sup>H</sup>	2.4 ± 0.1 kcal/mol			

<sup>a</sup> All KIEs are determined by the average of 3 runs for each temperature.

**Figure 4.** Plot of  $\ln(k_H/k_D)$  over  $1/T$



As discussed in Section 2.2, the presence of tunneling can also be characterized by examining the temperature dependence of the KIE. The limits for the Arrhenius



parameters associated with proton transfer reactions in the absence of tunneling have been illustrated earlier:  $0.7 < A_{\text{H}}/A_{\text{D}} < 1.2$  and  $(E_{\text{a}}^{\text{D}} - E_{\text{a}}^{\text{H}}) < 1.2$  kcal/mol (zero-point energy difference of OH stretching of the proton source). Proton transfer reactions with  $(E_{\text{a}}^{\text{D}} - E_{\text{a}}^{\text{H}})$  greater, and  $A_{\text{H}}/A_{\text{D}}$  smaller, than these predictions unambiguously demonstrate the involvement of tunneling. It should also be emphasized that Arrhenius parameters within the semiclassical ranges do not necessarily mean the absence of proton tunneling. In fact, proton tunneling should always exist if wave-particle duality is valid for hydrogen, although evidence(s) characterizing tunneling might not be obtained.

The temperature dependence of  $k_{\text{H}}/k_{\text{D}}$  for the protonolysis of **4** was investigated at four different temperatures (Table 2). Linear correlations between  $\ln(k_{\text{H}}/k_{\text{D}})$  and  $1/T$  are obtained for both systems (Figure 4), giving  $A_{\text{H}}/A_{\text{D}} = 0.34 \pm 0.06$  and  $(E_{\text{a}}^{\text{D}} - E_{\text{a}}^{\text{H}}) = 2.4 \pm 0.1$  kcal mol<sup>-1</sup> for **4**. These values are clearly indicative of a tunneling pathway for the protonolysis of the corresponding metal carbon bonds.

According to the principle of microscopic reversibility, proton tunneling is expected to be involved in the loss of proton from Pd<sup>II</sup> alkane  $\sigma$  adducts, either via oxidative C-H cleavage or an electrophilic C-H activation process, at room temperature or higher. Computational studies have demonstrated that proton tunneling is significant in oxidative addition of methane C-H bond to Pd<sup>0</sup> indicate at low temperatures.<sup>16</sup> However, the involvement of proton tunneling in C-H activation by Pd<sup>II</sup> via oxidative addition or electrophilic activation has not been demonstrated.

## 2.5 Other Types of C-H Activations or Corresponding Microscopic Reverse

Several general mechanisms for C-H activation by transition metal complexes have already been identified, including (1) electrophilic activation, (2) oxidative addition, (3)

$\sigma$ -bond metathesis, (4) 1,2-addition to metal-ligand multiple bonds, (5) H-atom abstraction by metal-oxo complexes, and (6) metalloradical activation.<sup>17</sup>

Systematic studies of the temperature dependence of  $k_{\text{H}}/k_{\text{D}}$  for C-H activations or the microscopic reverse are rarely found besides enzymatic C-H activations.<sup>18</sup> Schock et al. reported temperature-dependent KIEs typical of tunneling in the intramolecular aromatic C-H activation of  $\text{Cp}^*\text{ZrPh}_2$  via  $\sigma$ -bond metathesis.<sup>19</sup> A recent study on C-H activation by an oxoiron(IV) porphyrin radical cation led to a conclusion of the occurrence of hydrogen tunneling.<sup>20</sup> KIEs at two different temperatures have been measured for methane C-H activation by  $\text{Rh}^{\text{II}}$  porphyrin via the metalloradical mechanism, and the Arrhenius parameters obtained from the data indicate tunneling ( $k_{\text{H}}/k_{\text{D}} = 8.2$  at 296 K, 5.1 at 353 K,  $A_{\text{H}}/A_{\text{D}} = 0.43$ ,  $E_{\text{a}}^{\text{D}} - E_{\text{a}}^{\text{H}} = 1.7 \text{ kcal mol}^{-1}$ ).<sup>21</sup> KIEs at different temperatures for  $\alpha$ -hydrogen elimination, the microscopic reverse of 1,2-C-H-addition across  $\text{M}=\text{N}$  species, have not been measured. Therefore, mechanistically similar elimination KIEs observed for  $(^t\text{Bu}_3\text{SiNH})_3\text{TiCH}_3$  ( $k_{\text{H}}/k_{\text{D}} = 13.7$  at 297.95 K)<sup>22</sup> and  $(^t\text{Bu}_3\text{SiNH})_3\text{ZrCH}_3$  ( $k_{\text{H}}/k_{\text{D}} = 6.27$  at 369.85 K)<sup>23</sup> were used instead, which also suggests tunneling ( $A_{\text{H}}/A_{\text{D}} = 0.25$ ,  $E_{\text{a}}^{\text{D}} - E_{\text{a}}^{\text{H}} = 2.4 \text{ kcal mol}^{-1}$ ). (It should be admitted that this is a rough estimation.)

Slaughter et al. recently proposed, through partition function analysis of equilibrium isotope effects (EIEs) for 1,2-addition of C-H bonds across Ti-N multiple bonds, that it is not necessary to invoke tunneling to explain the abnormally large KIEs observed in these reactions.<sup>24</sup> This argument was used to explain the large KIEs in metalloradical C-H activation.<sup>21</sup> According to our above analysis, however, tunneling appears to be a more reasonable explanation.

### 3. Conclusions

In summary, our work indicates that tunneling can be observed experimentally at room temperature and higher in the protonolysis of several dimethylpalladium(II) complexes, which suggests that tunneling might also be involved in the microscopic reverse C-H activation processes. While tunneling at room temperature or higher has been observed in C-H activation by other transition metal complexes, no examples in which either an electrophilic or oxidative addition mechanism is involved has been reported previous to this work. Further studies regarding the mechanisms and hydrogen tunneling will be discussed in the following chapter.

### Experimental Section

**General Information:** All air and/or moisture sensitive compounds were manipulated using standard high-vacuum line, Schlenk, or cannula techniques, or in a glove box under a nitrogen atmosphere. TFE- $d_3$  was purchased from Cambridge Isotope Laboratories and dried over 3 Å molecular sieves for at least 5 days, then vacuum distilled onto B(C<sub>6</sub>F<sub>5</sub>)<sub>3</sub>, and shortly thereafter distilled into a Strauss flask. DCE- $d_4$  was purchased from Cambridge Isotope Laboratories and used immediately after the cap was opened. CD<sub>2</sub>Cl<sub>2</sub> and CDCl<sub>3</sub> were dried over Na<sub>2</sub>SO<sub>4</sub> just before use. A modified literature procedure was used for the synthesis of N,N,N',N'-tetramethyl-*trans*-cyclohexenediamine.<sup>25</sup> Compounds **1**, **2**, and **3** were synthesized according to literature procedures.<sup>8</sup> All other chemicals are commercially available and used as received without further purification. All NMR tubes were dried overnight in a 180 °C oven. Protonolysis studies were performed in a screw cap NMR tube with a PTFE/silicone septum. The error introduced

by residual protons from the glass surface of NMR tubes was found to be negligible by  $^1\text{H}$  NMR spectroscopy with internal standard (within  $^1\text{H}$  NMR error). All NMR spectra were recorded at room temperature using a Varian Mercury 300 spectrometer. NMR spectra were referenced to TMS using the residual impurities of the given solvent. Chemical shifts are reported using the standard  $\delta$  notation in parts per million (positive chemical shifts are to a higher frequency from TMS), and coupling constant are reported in Hz. Multiplicities are reported as follows: singlet (s), doublet (d), doublet of doublets (dd), doublet of triplets (dt), triplet (t), quartet (q), multiplet (m), broad resonance (br). The Caltech X-ray Crystallography Laboratory provided the X-ray analysis.

**Synthesis of Compound 2:** (TMEDA) $\text{Pd}(\text{CH}_3)_2$  (0.5 g, 2 mmol) and N,N,N',N'-tetramethyl-*trans*-cyclohexenediamine (3.4 g, 20 mmol) were added to a 20 ml vial. Benzene (10 mL) was added, and the reaction mixture was stirred for about 80 minutes, at which point colorless crystals were observed. The crystals were collected and washed with  $\text{Et}_2\text{O}$ . Recrystallization in  $\text{CH}_2\text{Cl}_2/\text{Et}_2\text{O}$  gave crystals suitable for X-ray diffraction analysis. Yield: 0.318 g, 55%.  $^1\text{H}$  NMR (300 MHz, acetone- $d_6$ )  $\delta$  2.6–2.7 (m, 2H), 2.49 (s, 6H), 2.36 (s, 6H), 1.6–1.8 (br m, 8H), -0.37 (s, 6H).

**Protonolysis of 1-3:** A stock solution of 20:1 TFE- $d_3$ /TFE- $d_0$  was prepared in the glove box and the ratio was confirmed by comparison of  $^1\text{H}$  NMR peaks using an internal standard. A known amount of **1-3** was dissolved in  $\text{CD}_2\text{Cl}_2$  or  $\text{CDCl}_3$  (0.7 mL) and transferred to a screw cap NMR tube sealed with a PTFE/silicone septum. A large excess amount of the 20:1 TFE- $d_3$ /TFE- $d_0$  solution was then slowly transferred into the NMR

tube by syringe. The NMR tube was then shaken manually to homogenize the mixture. The reactions of all three compounds were instantaneous and bubbles were observed upon mixing.  $^1\text{H}$  NMR spectroscopy was used to analyze the products and the  $\text{CH}_4/\text{CH}_3\text{D}$  ratios ( $\sim 1$  for all three cases).  $^1\text{H}$  NMR data of the (methyl)(trifluoroethoxy) $\text{Pd}^{\text{II}}$  complexes are similar to those previously reported.<sup>26</sup> The  $\text{Pd-OCH}_2\text{CF}_3$  signal is absent due to exchange with excess  $\text{TFE-}d_3$ . Ethane formation was also observed by  $^1\text{H}$  NMR spectroscopy, although the corresponding palladium products were not characterized. In all cases, no precipitates were observed. Protonolysis of **1** was also performed in neat  $\text{TFE-}d_3$ , giving a  $\sim 1:4$  mixture of  $\text{CH}_4/\text{CH}_3\text{D}$ .

**Protonolysis of 4:** Stock solutions of 20:1  $\text{TFE-}d_3/\text{TFE-}d_0$  and dimethylpalladium(II) **4** (15 mg) in  $\text{DCE-}d_4$  (2.3 mL) were prepared in the glove box in glass vials with PTFE/silicone septa. The vials with the stock solutions were then placed in an ice or oil bath with three screw cap NMR tubes sealed with PTFE/silicone septa at a constant temperature (273 K, 294 K, 311 K, 331 K). After the solutions were given a few minutes to equilibrate, the  $\text{TFE-}d_3/\text{TFE-}d_0$  mixture (0.2 mL) and **4**/ $\text{DCE-}d_4$  solution (0.7 mL) were slowly transferred into the NMR tubes by syringes. After quickly shaking the tubes outside the bath to homogenize the mixtures, the NMR tubes were inserted back into the bath. The solutions were kept in the bath for a few more minutes before taking out for NMR analysis. The average  $\text{CH}_4/\text{CH}_3\text{D}$  ratios of three runs at each temperature were used. NMR data for **5** are consistent with those reported for analogous systems.<sup>26</sup> The  $\text{Pd-OCH}_2\text{CF}_3$  signal is absent due to exchange with excess  $\text{TFE-}d_3$ .

## References

- (1) (a) Arndtsen, B. A.; Bergman, R. G.; Mobley, T. A.; Peterson, T. H. *Acc. Chem. Res.* **1995**, 28, 154–162. (b) Crabtree, R. H. *Chem. Rev.* **1995**, 95, 987–1007. (c) Bergman, R. G. *Nature* **2007**, 446, 391–391.
- (2) (a) Shilov, A. E.; Shul'pin, G. B. *Activation and Catalytic Reactions of Saturated Hydrocarbons in the Presence of Metal Complexes*; Kluwer Academic Publishers, The Netherlands, **2000**. (b) Dyker, G., Ed. *Handbook of C-H Transformations*; Wiley-VCH: Weinheim, Germany, **2005**.
- (3) Pt<sup>II</sup>: (a) Goldshlegger, N. F.; Tyabin, M. B.; Shilov, A. E.; Shteinman, A. A. *Zh. Fiz. Khim.* **1969**, 43, 2174–2175. (b) Goldshlegger, N. F.; Eskova, V. V.; Shilov, A. E.; Shteinman, A. A. *Zh. Fiz. Khim.* **1972**, 46, 1353–1354. (c) Shilov, A. E.; Shul'pin, G. B. *Chem. Rev.* **1997**, 97, 2879–2932. (d) Periana, R. A.; Taube, D. J.; Gamble, S.; Taube, H.; Satoh, T.; Fujii, H. *Science* **1998**, 280, 560–564. (e) Lersch, M.; Tilset, M. *Chem Rev.* **2005**, 105, 2471–2526.
- (4) Pd<sup>II</sup>: (a) Lin, M. R.; Shen, C. Y.; Garcia-Zayas, E. A.; Sen, A. *J. Am. Chem. Soc.* **2001**, 123, 1000–1001. (b) Kao, L. C.; Hutson, A. C.; Sen, A. *J. Am. Chem. Soc.* **1991**, 113, 700–701. (c) Periana, R. A.; Mironov, O.; Taube, D.; Bhalla, G.; Jones, C. J. *Science* **2003**, 301, 814–818. (d) An, Z. J.; Pan, X. L.; Liu, X. M.; Han, X. W.; Bao, X. H. *J. Am. Chem. Soc.* **2006**, 128, 16028–16029.
- (5) (a) Hill, G. S.; Rendina, L. M.; Puddephatt, R. J. *Organometallics* **1995**, 14, 4966–4968. (b) Stahl, S. S.; Labinger, J. A.; Bercaw, J. E. *J. Am. Chem. Soc.* **1995**, 117, 9371–9372. (c) Romeo, R.; Plutino, M. R.; Elding, L. I. *Inorg. Chem.* **1997**, 36, 5909–5916. (d) Bartlett, K. L.; Goldberg, K. I.; Borden, W. T. *J. Am. Chem. Soc.*

- 2000**, 122, 1456–1465. (e) Bartlett, K. L.; Goldberg, K. I.; Borden, W. T. *Organometallics* **2001**, 20, 2669–2678. (f) Wik, B. J.; Lersch, M.; Tilset, M. *J. Am. Chem. Soc.* **2002**, 124, 12116–12117.
- (6) Gretz, E.; Oliver, T. F.; Sen, A. *J. Am. Chem. Soc.* **1987**, 109, 8109–8111.
- (7) Protonolysis of dimethylpalladium(II) complexes by various alcohols has been previously reported: (a) Kim, Y. J.; Osakada, K.; Sugita, K.; Yamamoto, T.; Yamamoto, A. *Organometallics* **1988**, 7, 2182–2188. (b) Kim, Y. J.; Osakada, K.; Takenaka, A.; Yamamoto, A. *J. Am. Chem. Soc.* **1990**, 112, 1096–1104. (c) Kapteijn, G. M.; Dervisi, A.; Grove, D. M.; Kooijman, H.; Lakin, M. T.; Spek, A. L.; van Koten, G. *J. Am. Chem. Soc.* **1995**, 117, 10939–10949.
- (8) de Graaf, W.; Boersma, J.; Smeets, W. J. J.; Spek, A. L.; van Koten, G. *Organometallics* **1989**, 8, 2907.
- (9) The X-ray crystal structure of **2** (CCDC 263612) is included in SI. Crystallographic data have been deposited at the CCDC, 12 Union Road, Cambridge CB2 1EZ, UK, and copies can be obtained on request, free of charge, by quoting the publication citation and the deposition number 263612.
- (10) (a) Wiberg, K. B. *Chem. Rev.* **1955**, 55, 713–743. (b) Ryabov, A. D. *Chem. Rev.* **1990**, 90, 403–424. (c) Romeo, R.; D'Amico, G. *Organometallics* **2006**, 25, 3435–3446.
- (11) (a) Bell, R. P. *Chem. Soc. Rev.* **1974**, 4, 513–544. (b) Bell, R. P. *The Proton in Chemistry*; Cornell University Press, Ithaca, NY, **1973**. (c) Bell, R. P. *The Tunnel Effect in Chemistry*; Chapman and Hall, London, **1980**.

- (12) (a) Caldin, E. F. *Chem. Rev.* **1969**, 69, 135-156. (b) Kwart, H. *Acc. Chem. Res.* **1982**, 15, 401-408. (c) Limbach, H.; Lopez, J. M.; Kohen, A. *Phil. Trans. R. Soc. B* **2006**, 361, 1399-1415.
- (13) Moore, W. J. *Physical Chemistry*, 3<sup>rd</sup> Ed.; Prentice-Hall, Englewood Cliffs, NJ, **1962**.
- (14) Melander, L.; Saunders, W. H. *Reaction Rates of Isotopic Molecules*; Krieger: Malabar, FL, **1987**.
- (15) Schneider, M. E.; Stern, M. J. *J. Am. Chem. Soc.* **1972**, 95, 1517-1522.
- (16) Mamaev, V. M.; Glorlov, I. P.; Ishchenko, S. Y.; Simonyan, V. V.; Myshakin, E. M.; Prisyajnyuk, A. V.; Ustynyuk Y. A. *J. Chem. Soc. Faraday Trans.* **1995**, 91, 3779-3782.
- (17) Labinger, J. A.; Bercaw, J. E. *Nature* **2002**, 417, 507-514.
- (18) Kohen, A. in *Hydrogen-Transfer Reactions*, Hynes, J. T.; Klinman, J. P.; Limbach, H. H.; Schowen, R. L. Eds., Wiley-VCH, Weinheim, **2007**; Vol. 4, pp 1311-1340.
- (19) Schock, L. E.; Brock, C. P.; Marks, T. J. *Organometallics* **1987**, 6, 232-241.
- (20) Pan, Z.; Horner, J. H.; Newcomb, M. *J. Am. Chem. Soc.* **2008**, 130, 7776-7777.
- (21) Cui, W.; Wayland, B. B. *J. Am. Chem. Soc.* **2004**, 126, 8266-8274.
- (22) Bennett, J. L.; Wolczanski, P. T. *J. Am. Chem. Soc.* **1997**, 119, 10696-10719.
- (23) Schaller, C. P.; Cummins, C. C.; Wolczanski, P. T. *J. Am. Chem. Soc.* **1996**, 118, 591-611.
- (24) Slaughter, L. M.; Wolczanski, P. T.; Klinckman, T. R.; Cundari, T. R. *J. Am. Chem. Soc.* **2000**, 122, 7953-7975.
- (25) Chooi, S. Y.; Tan, M. K.; Leung, P.H.; Mok, K. F. *Inorg. Chem.* **1994**, 33, 3096.



- (26) Kapteijn, G. M.; Dervisi, A.; Grove, D. M.; Kooijman, H.; Lakin, M. T.; Spek, A. L.; van Koten, G. *J. Am. Chem. Soc.* **1995**, *117*, 10939–10949.
- (27) Kim, Y. J.; Osakada, K.; Sugita, K.; Yamamoto, T.; Yamamoto, A. *Organometallics* **1988**, *7*, 2182–2188.

### **Chapter 3. Mechanisms and Hydrogen Tunneling in Protonolysis of Platinum(II) and Palladium(II) Methyl Complexes: Computational Evidences**

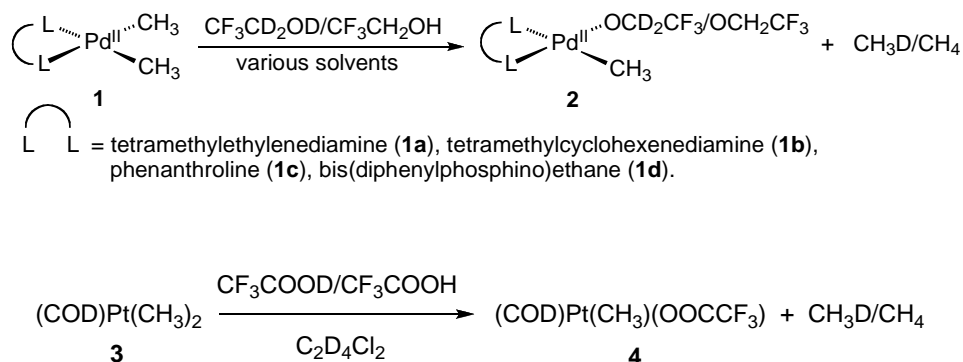
#### **Abstract**

Density functional theory computation suggests that protonation at the  $M^{II}-C$  bond is kinetically preferred over protonation at the metal center for the protonolysis of  $(COD)Pt(CH_3)_2$  by TFA and the dimethylpalladium(II) complexes by TFE in dichloroethane. Protonation at the  $M^{II}-C$  bond was found to be the rate-determining step in the protonolysis, which is consistent with experimental observations. KIEs calculated without tunneling correction for the protonolysis of  $(COD)Pt(CH_3)_2$  by TFA are much smaller than experimental KIEs at low temperatures. As the temperature increases, less hydrogen tunneling contribution is expected and thus theoretical and experimental KIEs gradually approach each other. These observations indicate the significant contribution of hydrogen tunneling in the abnormally large KIEs observed experimentally.

## 1. Introduction

Recently, we reported for the first time the observations of abnormally large KIEs at room temperature and higher in the protonolysis of several dimethylpalladium(II) complexes (**1a–d**) as well as (COD)Pt(CH<sub>3</sub>)<sub>2</sub> (**3**, COD, 1,5-cyclooctadiene)<sup>1</sup> (Scheme 1). The occurrence of proton tunneling was invoked to rationalize the abnormally large KIEs, which is supported by the temperature dependence of KIEs, with the corresponding Arrhenius parameters outside the theoretical semiclassical limits<sup>2</sup> ( $0.5 < A_{\text{H}}/A_{\text{D}} < 2^{1/2}$  and  $E_{\text{a}}^{\text{D}} - E_{\text{a}}^{\text{H}} < 1.2$  kcal/mol).

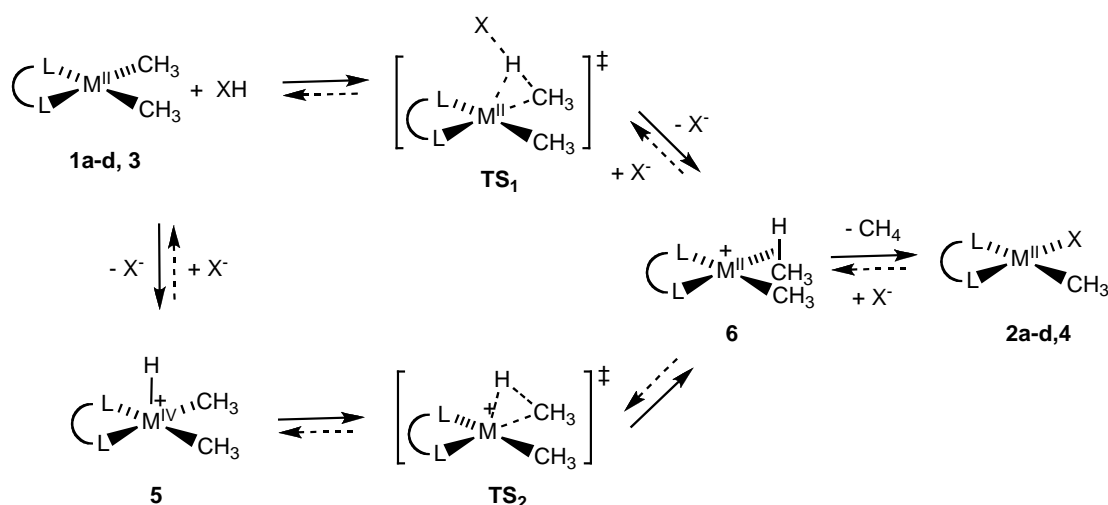
**Scheme 1.**



Two alternate routes have been proposed for the protonolysis of Pt<sup>II</sup>/Pd<sup>II</sup>-C bonds: (i) direct protonation of the M<sup>II</sup>-C bond (the microscopic reverse of electrophilic C-H activation) or (ii) protonation at M followed by reductive elimination (the microscopic reverse of oxidative C-H cleavage) (Scheme 2). Platinum(IV) hydride intermediates have been observed at low temperatures for the protonolysis of several diamine and diimine ligated platinum dimethyl systems, supporting the oxidative addition mechanism.<sup>3</sup> In contrast, no [Pt<sup>IV</sup>-H] is observed by <sup>1</sup>H NMR in the protonolysis of **3** at -80 °C in CD<sub>2</sub>Cl<sub>2</sub>;

one might expect the electron-withdrawing COD ligand to disfavor the formation of a platinum(IV) intermediate. Likewise, formation of  $[\text{Pd}^{\text{IV}}\text{-H}]$  should be relatively less favorable. Based on these considerations, a unifying mechanism with direct protonation of the  $\text{M}^{\text{II}}\text{-C}$  bond was proposed.<sup>1</sup> However, no direct evidence can be obtained experimentally to support this proposal. Herein, we report computational evidences to support the proposed direct protonation mechanism as well as the occurrence of proton tunneling in the reactions.

**Scheme 2.**



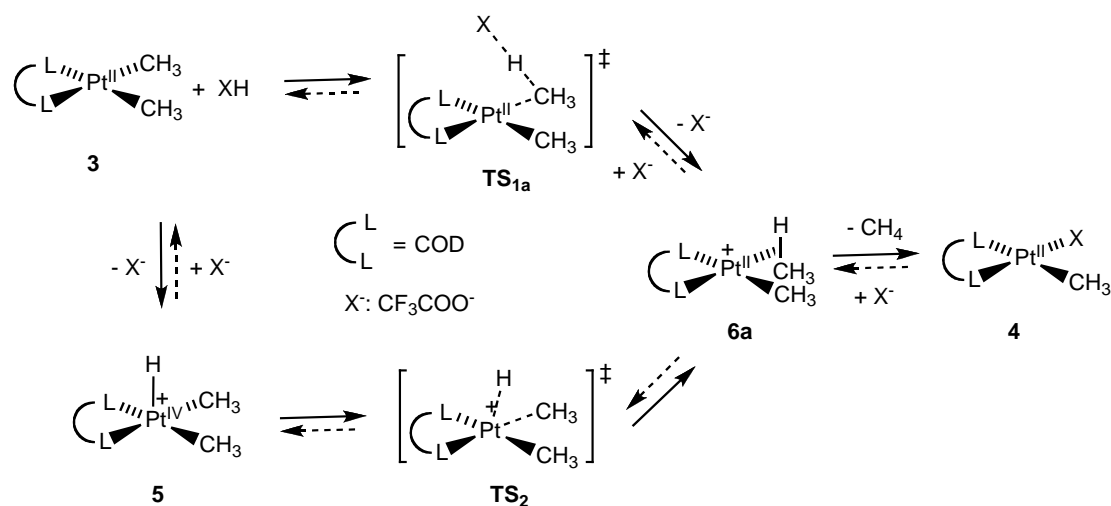
## 2. Results and Discussion

### 2.1 Protonolysis of $(\text{COD})\text{Pt}(\text{CH}_3)_2$ by Trifluoroacetic Acid (TFA)

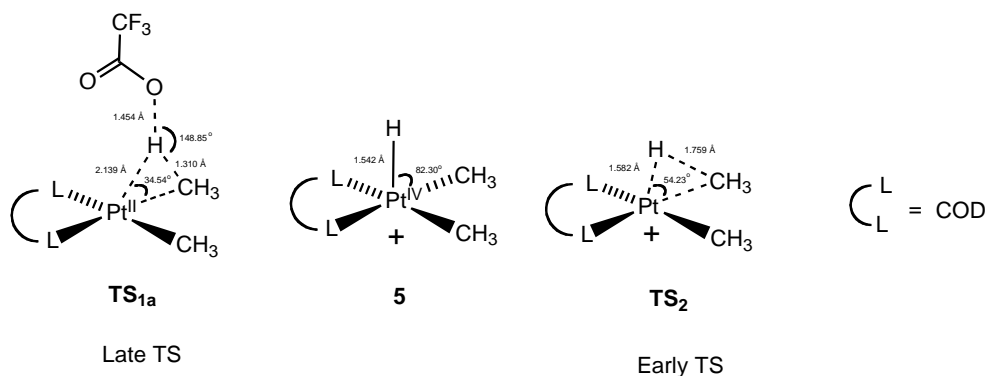
All complexes optimized in gas phase are shown in Scheme 3. No intermediate was located prior to the formation of **6a**, the  $\sigma$  complex, for the direct-protonation pathway. In contrast, a  $\text{Pt}^{\text{IV}}\text{-H}$  intermediate, **5**, was found for the oxidative addition/reductive

elimination pathway. A late transition state (**TS<sub>1a</sub>**) was located prior to the formation of **6a** for the direct-protonation route, while an early transition state (**TS<sub>2a</sub>**) was obtained for the reductive elimination from Pt<sup>IV</sup>-H (**5**) to form **6a** (Scheme 4). The much longer distance between Pt and the transferred hydrogen in **TS<sub>1a</sub>** (2.139 Å) relative to the Pt<sup>IV</sup>-H bond distance in **5** (1.542 Å) clearly indicates the proton nature of that hydrogen in **TS<sub>1a</sub>**, while a distance similar to that in **5** was found between Pt and the transferred hydrogen in **TS<sub>2</sub>** (1.582 Å), suggesting its platinum hydride nature.

**Scheme 3.**

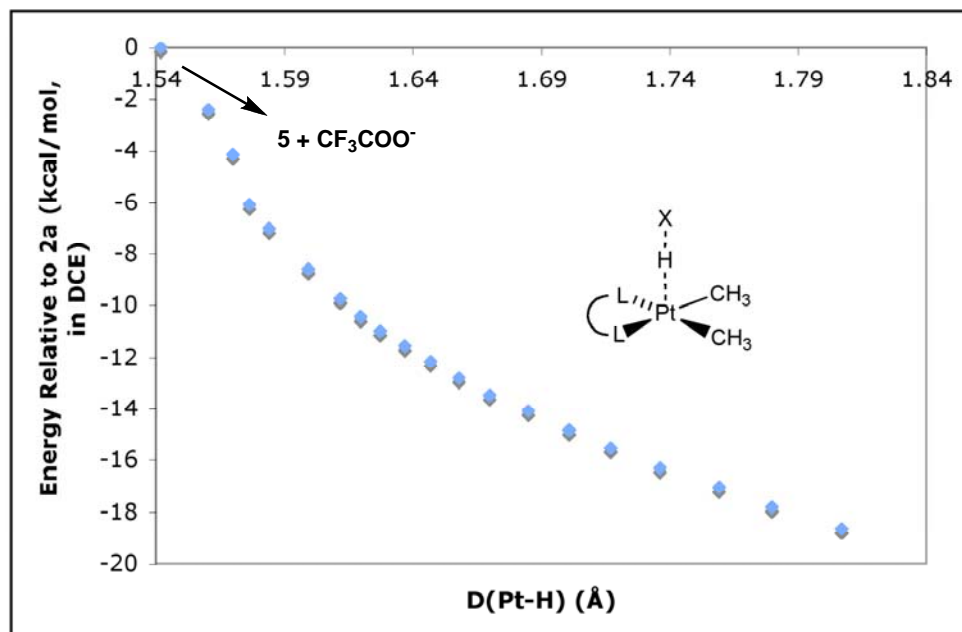
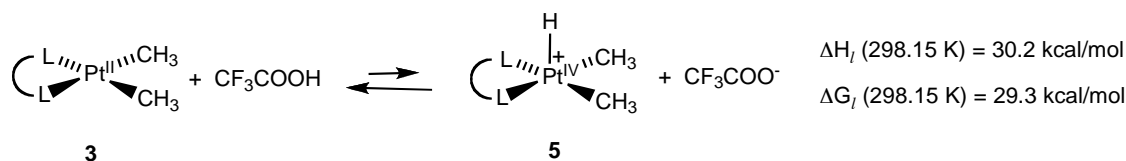


**Scheme 4.**



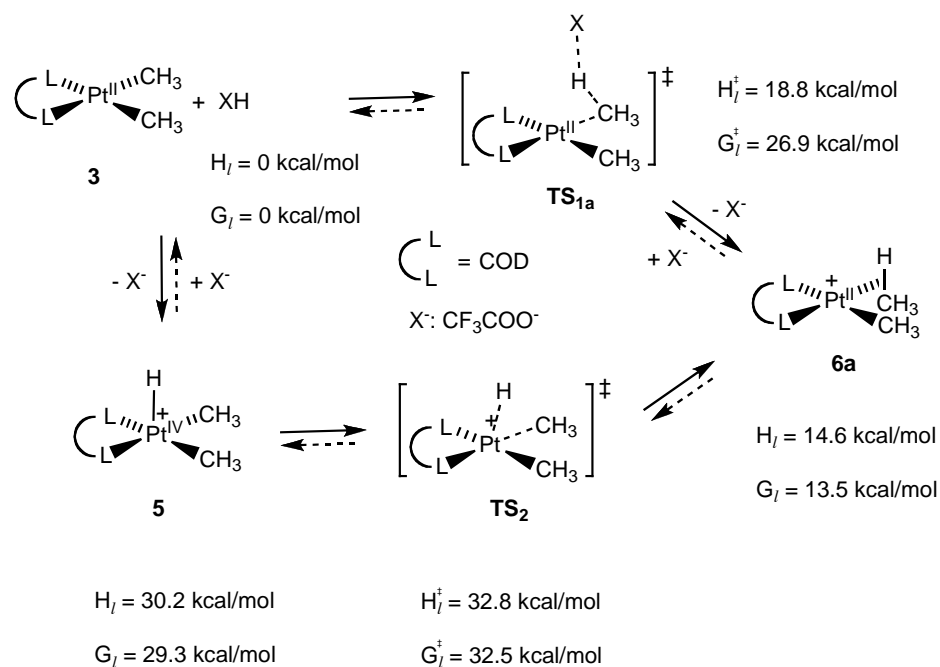
No transition state could be located for the proton transfer reaction from TFA to **3** to form **5**. The endothermic nature of this reaction suggests the involvement of a late transition state. However, a potential energy surface scan for the reverse process, deprotonation of **5** by trifluoroacetate to form **3**, shows that the energy (in dichloroethane) decreases monotonically as the platinum hydrogen distance increases. No maximum can be found along the potential surface. Based on these results, it appears that the activation barrier for the formation of **5** is approximately equal to the corresponding reaction energy. Therefore, **TS<sub>2</sub>** determines the overall barrier of the involved pathway (or at least the minimum of the barrier), whose activation enthalpy and free energy in dichloroethane were calculated to be 32.8 and 32.5 kcal/mol, respectively.

**Scheme 5.**



Much lower activation enthalpy (18.8 kcal/mol) and free energy (26.9 kcal/mol) for the formation of **6a** in DCE, on the other hand, were calculated for the direct protonation pathway (Scheme 6). Therefore, the computation suggests that protonation of the Pt<sup>II</sup>-C bond is the kinetically preferred over protonation of the Pt<sup>II</sup> center.

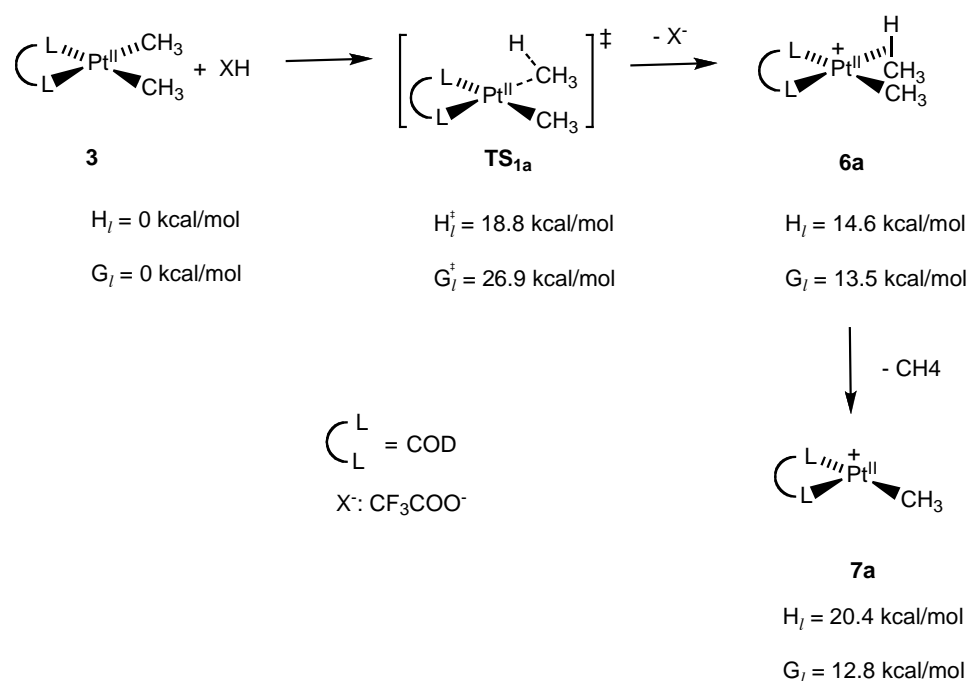
**Scheme 6.**



The dissociation of methane from **6a** can occur either through a dissociative or associative pathway. Although no transition state could be located for either mechanism, the activation barrier for the dissociation should be at least smaller than the barrier of the dissociative pathway, which is assumed to be approximately equal to the methane dissociation energy from **6a**. According to the computational result, the dissociation of methane in DCE is roughly a thermoneutral process and thus a small activation barrier is expected (Scheme 7). Therefore, protonation of the Pt<sup>II</sup>-C bond is calculated to be the

rate-determining step for the whole reaction, which is consistent with the experimentally observed abnormally large KIEs. Furthermore, the reverse process, deprotonation from **6a** to regenerate **3**, is also expected to be much slower than the loss of methane, which is consistent with the absence of deuterated methane isotopologues other than CH<sub>3</sub>D and the absence of deuterium incorporation into the resultant Pt-CH<sub>3</sub> of the product in the experiments reported earlier.<sup>1</sup>

**Scheme 7.**



## 2.2 Protonolysis of (dmpe)Pd(CH<sub>3</sub>)<sub>2</sub> (dmpe = Bis(dimethylphosphino)ethane) by Trifluoroethanol (TFE)

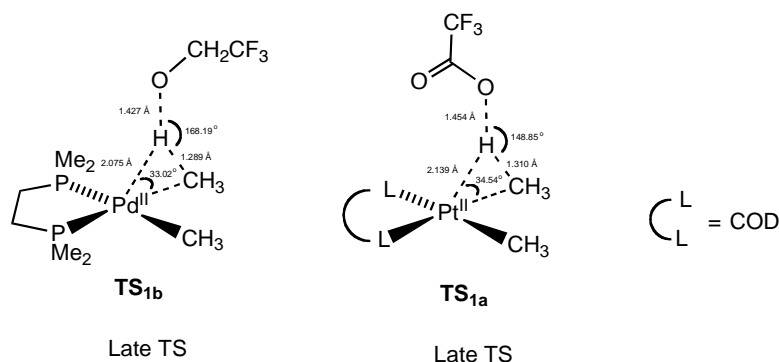
Due to the enormous computational cost for the calculation of the protonolysis of (dppe)Pd(CH<sub>3</sub>)<sub>2</sub> (**1d**) by TFE, wherein the competing reductive elimination of ethane is virtually absent, a smaller ligand, dmpe, is used instead of dppe. In contrast to



(COD)Pt(CH<sub>3</sub>)<sub>2</sub>, no Pd<sup>IV</sup>-H intermediate can be located for the oxidative addition/reductive elimination pathway in the protonolysis of (dmpe)Pd(CH<sub>3</sub>)<sub>2</sub> (**8**) by TFE, probably due to the instability of Pd<sup>IV</sup>-H as well as the unfavorable combination of the hard Pd<sup>IV</sup> center and the soft phosphorus donor.

The computational result appears to suggest that the direct protonation of the Pd<sup>II</sup>-C bond pathway is more viable than its alternative. For the direct-protonation pathway, a transition state (TS<sub>1b</sub>) analogous to TS<sub>1a</sub> was located prior to the formation of **6b**. The structural resemblance between TS<sub>1b</sub> and TS<sub>1a</sub> suggests a similar proton nature for the transferred hydrogen (Scheme 8).

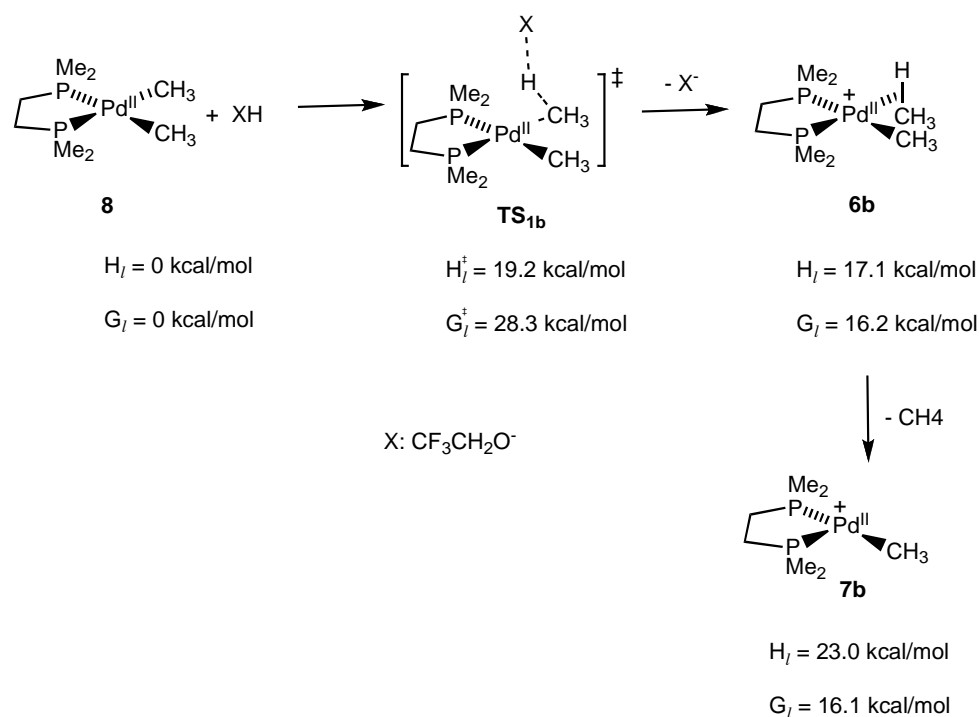
**Scheme 8.**



All complexes optimized are shown in Scheme 9. The activation enthalpy and free energy for the direct proton transfer from TFE to **8** to form **6b** in DCE were calculated to be 19.2 and 28.3 kcal/mol, respectively. These activation parameters are comparable to those in the protonolysis of (COD)Pt(CH<sub>3</sub>)<sub>2</sub>, which suggests that dimethylpalladium(II) complexes are more reactive in protonolysis than their platinum counterparts if the much weaker acidity of TFE relative to TFA is taken into consideration.

Analogous to the protonolysis of (COD)Pt(CH<sub>3</sub>)<sub>2</sub>, the dissociation of methane from **6b** in DCE is also estimated to be faster than the reverse deprotonation process, which is consistent with all experimental observations, including abnormally large KIEs, the absence of both deuterated methane isotopologues other than CH<sub>3</sub>D, and the absence of deuterium incorporation into Pd<sup>II</sup>-CH<sub>3</sub> of the product.<sup>1</sup>

**Scheme 9.**



### 2.3 KIEs Calculated Without Tunneling Correction for the Protonolysis of (COD)Pt(CH<sub>3</sub>)<sub>2</sub> by TFA

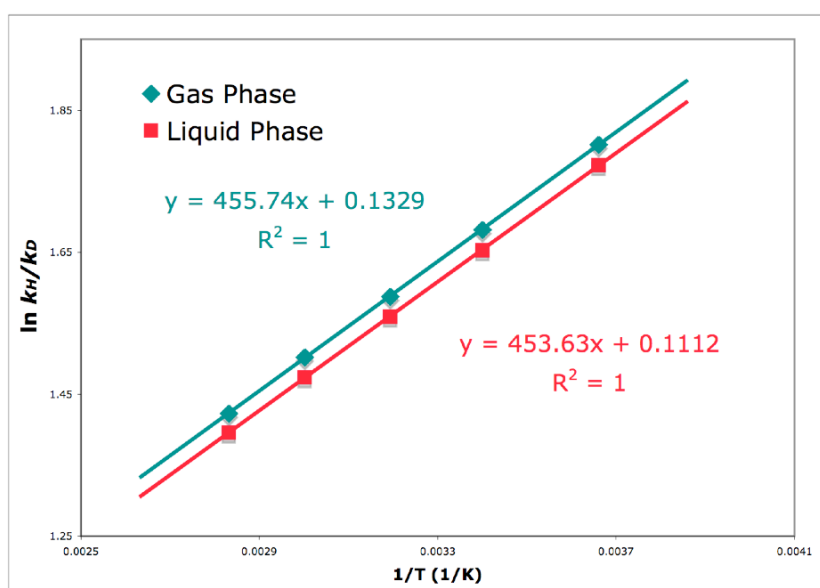
Based on partition-function analysis of equilibrium isotope effects for 1,2-addition of methane C-H bond across metal ligand multiple bonds of several simplified model systems or the corresponding microscopic reverse, it has been proposed that isotope-sensitive low-frequency vibrations of organometallic complexes might lead to

semiclassical KIEs larger than those expected for organic molecules and it is not necessary to invoke tunneling for the explanation of the abnormally large KIEs observed.<sup>4</sup> To test the validity of this theory for our systems, KIEs without tunneling correction were calculated for the protonolysis of (COD)Pt(CH<sub>3</sub>)<sub>2</sub> by TFA at various temperatures upon frequency analysis of the optimized complexes.

**Table 1.** Comparisons of experimental and calculated KIEs (without tunneling correction) for the protonolysis of **3** by TFA

3			
Temp	KIE <sup>expl</sup>	KIE <sub>g</sub> <sup>calc'd</sup>	KIE <sub>l</sub> <sup>calc'd</sup>
273 K	25.9 ± 0.3	6.1	5.9
294 K	17.5 ± 0.3	5.4	5.2
313 K	12.1 ± 0.3	4.9	4.8
333 K	9.2 ± 0.3	4.5	4.4
353 K	6.9 ± 0.3	4.2	4.0
A <sub>H</sub> /A <sub>D</sub>	0.075 ± 0.007	1.142	1.118
E <sub>a</sub> <sup>D</sup> - E <sub>a</sub> <sup>H</sup> (kcal/mol)	3.2 ± 0.1	0.91	0.90

**Figure 1.** Plot of lnKIE<sup>calc'd</sup> against 1/T



The calculated KIEs are shown in Table 1. KIEs in gas phase are similar to those in DCE, probably because the main difference between these two, the loss of part of the translational partition function, is nearly isotope-insensitive. All calculated KIEs are much smaller than the experimental KIEs at low temperatures. As the temperature increases, less hydrogen tunneling contribution to KIE is expected and thus the calculated and experimental KIEs gradually approach each other. Linear correlations between logarithms of the calculated KIEs and the inverse of temperature afford Arrhenius parameters within the theoretical semiclassical limits (Figure 1). Based on all these observations, it is clear that hydrogen tunneling plays an important role in the abnormally large KIEs as well as their experimentally observed temperature dependence.

### 3. Conclusions

In summary, computation suggests that protonation at the  $M^{II}$ -C bond is kinetically preferred over protonation at the metal center for the protonolysis of  $(COD)Pt(CH_3)_2$  by TFA and the dimethylpalladium(II) complexes by TFE in dichloroethane. Protonation at the  $M^{II}$ -C bond was found to be the rate-determining step in the protonolysis, which is consistent with all current experimental observations. Calculated KIEs without tunneling correction for the protonolysis of  $(COD)Pt(CH_3)_2$  by TFA indicates the significant contribution of hydrogen tunneling in the abnormally large KIEs observed experimentally. Given the importance of C-H activation by  $Pd^{II}$  and  $Pt^{II}$  and the mechanistic relevance of the protonolysis, more studies are currently underway to further investigate the factors that influence the mechanisms and hydrogen tunneling.

## Computational Methods

All computation was performed by Gaussian03 software package unless otherwise stated.<sup>5</sup> All species were treated as singlets. Geometries were optimized by density functional theory method (BP86) with a hybrid basis set (Pd and Pt: LANL2TZ(*f*),<sup>6, 7</sup> consisting of Wadt and Hay relativistic effective core potentials (RECPs),<sup>6a</sup> valence triple- $\zeta$  contraction functions, and an *f*-orbital polarization function; all other elements: 6-31+G(*d*), an all-electron basis set developed by Pople et al.<sup>8</sup>). Harmonic oscillator model was used for vibration frequency analysis of the optimized structures. All frequencies of the minima are positive, while transition states have one and only one negative frequency. The vibration mode of the negative frequency in transition states was confirmed to be the one that corresponds to the reaction coordinate.

Gas phase enthalpies (with *PV* term) and entropies (pressure = 1 atm, 298.15 K) of all species were obtained via frequency calculations with appropriate isotopic contents at various temperatures. No scaling factor was used for the calculated frequencies. An implicit solvation model, the CPCM polarizable continuum model, was then employed for the calculation of solvation energies. The sum of the gas phase enthalpies and the solvation energies was used directly as the enthalpies in DCE. For reactions wherein different numbers of reactants and transition states (the difference designated as *n*) are involved, an *nPV* error is introduced due to the absence of *PV* term in the liquid state, which underestimates the activation barrier of a biomolecular reaction by an  $\sim 0.6$  kcal/mol error at room temperature. Such a small error is generally ignored in the literature and is not essential as far as comparisons between reaction pathways with the

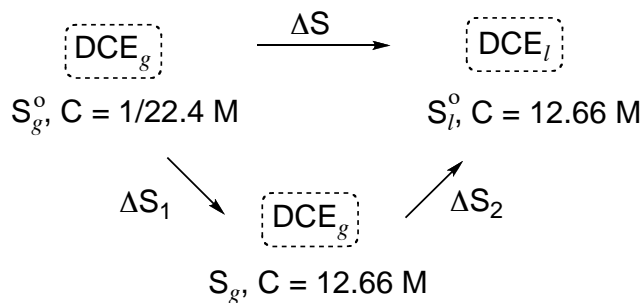
same  $n$  are concerned. Finally, the gas phase entropies were converted to corresponding entropies (1 M in DCE) according to Wertz's method.<sup>9</sup>

Geometries for the potential energy surface scan were optimized by density function theory B3LYP method as implemented in the Jaguar 6.5 program package.<sup>10</sup> The Pt hydride distance was fixed at a certain value, while all other structural parameters were fully optimized, during the optimization of each point of the potential energy surface. The Pt was treated by LACVP\*\*, a basis set consisting of the Wadt and Hay<sup>6a</sup> relativistic effective core potentials (RECPs) and valence double- $\zeta$  contraction functions. A modified variant of Pople's all-electron basis set,<sup>8</sup> 6-31G\*\*, where the six d functions have been reduced to five, was used for all other elements. Single-point energy and CPCM solvation energy (in dichloroethane) calculations were then performed for the optimized geometries by Gaussian03 software package with BP86 method and the same hybrid basis described earlier for optimizations by Gaussian03. Electronic energies plus the corresponding solvation energies were used to calculate the energies of each point of the potential energy surface.

### Wertz's method

Wertz's method is essentially composed of two steps.<sup>9</sup> Two thermodynamic cycles are constructed. In the first step, the entropy change from gas state (standard state,  $S_g^\circ = 0.308 \text{ kJ mol}^{-1} \text{ K}^{-1}$ ) to liquid state ( $S_l^\circ = 0.208 \text{ kJ mol}^{-1} \text{ K}^{-1}$ ) DCE consists of two steps: (i) adiabatic compression of ideal DCE gas in standard state to a hypothetical ideal gas state with the concentration equal to that of the liquid state (12.66 M); and (ii) conversion of the hypothetical state to the final liquid state (Scheme 10).

Scheme 10.



The entropy change of the first step can be estimated according to Maxwell's relations, while that of the second step can be derived from the thermodynamic cycle. The fraction of entropy lost in second step is defined as a coefficient,  $\alpha$ , which was calculated to be 0.202.

$$dG = -SdT + VdP = VdP \quad (dT = 0) \quad \text{Maxwell Relation}$$

$$\Delta G = \int_{P_1}^{P_2} VdP = \int_{P_1}^{P_2} \frac{RT}{P} dP = RT \ln \frac{P_2}{P_1} = -T\Delta S$$

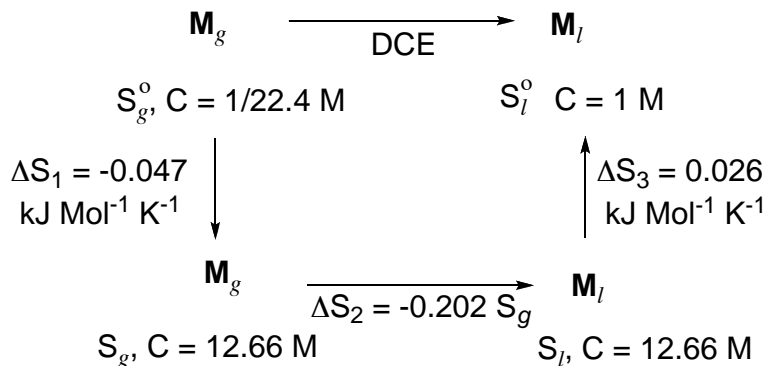
$$\Delta S_1 = -R \ln \frac{P_2}{P_1} = -0.047 \text{ kJ Mol}^{-1} \text{ K}^{-1}$$

$$\alpha = \frac{\Delta S_2}{S_g} = \frac{S_g - S_l^o}{S_g} = \frac{S_g^o + \Delta S_1 - S_l^o}{S_g} = 0.202$$

$$\Delta S_2 = 0.202 S_g$$

In the second step, the entropy change from the gas state of any given molecule, **M**, in standard state to its 1M state in DCE is decomposed to three steps: (i) adiabatic compression of ideal **M** gas in standard state to a hypothetical ideal gas state with the concentration equal to that of the liquid state (12.66 M); (ii) conversion of the hypothetical ideal gas state to a hypothetical liquid state; and (iii) expansion of the hypothetical liquid state to the 1M state in DCE (Scheme 11).

Scheme 11.



The entropy change of the first and the third step can be estimated according to Maxwell's relations. The fraction of entropy loss in the second step is assumed to be equal to  $\alpha$ . The calculated gas phase entropy of  $\mathbf{M}$  in standard state is then converted to the corresponding entropy in its 1M state in DCE according to the following equation and used for the calculations of free energies in DCE.

$$S_l^o = S_g^o + \Delta S_1 + \Delta S_2 + \Delta S_3 = 0.798 \times S_g^o - 0.012 \text{ kJ Mol}^{-1} \text{ K}^{-1}$$

The definition of the concentration of the final state in DCE is arbitrary. Different concentrations will lead to different thermodynamic parameters and thus different reaction rate constants. However, as demonstrated below using unimolecular reaction as the example, the calculated reaction rates of any given two concentrations are actually equal to each other. Numerically, the reaction rate is equal to the rate constant of the 1 M state ( $C_0$ ) in DCE.

$$\begin{aligned}
 \text{rate} &= k_c \times C_M = k_c \times \frac{P_C}{P_0} \times C_0 = \frac{k_B T}{h} e^{-\frac{\Delta G_a^C - RT \ln \frac{P_C}{P_0}}{RT}} \times C_0 = \frac{k_B T}{h} e^{-\frac{\Delta G_a^0}{RT}} \times C_0 = k_0 \times C_0 \\
 &\quad (C_0 = 1M)
 \end{aligned}$$



## References

- (1) Bercaw, J. E.; Chen, G. S.; Labinger, J. A.; Lin, B. -L. *J. Am. Chem. Soc.* **2008**, *130*, 17654–17655.
- (2) (a) Bell, R. P. *Chem. Soc. Rev.* **1974**, *4*, 513–544. (b) Bell, R. P. *The Proton in Chemistry*; Cornell University Press, Ithaca, NY, **1973**. (c) Bell, R. P. *The Tunnel Effect in Chemistry*; Chapman and Hall, London, **1980**.
- (3) (a) Stahl, S. S.; Labinger, J. A.; Bercaw, J. E. *J. Am. Chem. Soc.* **1995**, *117*, 9371–9372. (b) Wik, B. J.; Lersch, M.; Tilset, M. *J. Am. Chem. Soc.* **2002**, *124*, 12116–12117.
- (4) Slaughter, L. M.; Wolczanski, P. T.; Klinckman, T. R.; Cundari, T. R. *J. Am. Chem. Soc.* **2000**, *122*, 7953–7975.
- (5) Gaussian 03, Revision D.01, Frisch, M. J.; Trucks, G. W.; Schlegel, H. B.; Scuseria, G. E.; Robb, M. A.; Cheeseman, J. R.; Montgomery, J. A.; Vreven, T.; Kudin, K. N.; Burant, J. C.; Millam, J. M.; Iyengar, S. S.; Tomasi, J.; Barone, V.; Mennucci, B.; Cossi, M.; Scalmani, G.; Rega, N.; Petersson, G. A.; Nakatsuji, H.; Hada, M.; Ehara, M.; Toyota, K.; Fukuda, R.; Hasegawa, J.; Ishida, M.; Nakajima, T.; Honda, Y.; Kitao, O.; Nakai, H.; Klene, M.; Li, X.; Knox, J. E.; Hratchian, H. P.; Cross, J. B.; Bakken, V.; Adamo, C.; Jaramillo, J.; Gomperts, R.; Stratmann, R. E.; Yazyev, O.; Austin, A. J.; Cammi, R.; Pomelli, C.; Ochterski, J. W.; Ayala, P. Y.; Morokuma, K.; Voth, G. A.; Salvador, P.; Dannenberg, J. J.; Zakrzewski, V. G.; Dapprich, S.; Daniels, A. D.; Strain, M. C.; Farkas, O.; Malick, D. K.; Rabuck, A. D.; Raghavachari, K.; Foresman, J. B.; Ortiz, J. V.; Cui, Q.; Baboul, A. G.; Clifford, S.; Cioslowski, J.; Stefanov, B. B.; Liu, G.; Liashenko, A.; Piskorz, P.; Komaromi, I.; Martin, R. L.; Fox, D. J.; Keith, T.; Al-Laham, M. A.; Peng, C. Y.; Nanayakkara, A.; Challacombe, M.; Gill, P. M. W.; Johnson, B.;

Chen, W.; Wong, M. W.; Gonzalez, C.; Pople, J. A. Gaussian, Inc., Wallingford CT, **2004**.

(6) (a) Hay, P. J.; Wadt, W. R. *J. Chem. Phys.* **1985**, 82, 299–310. (b) Ehlers, A.W.; Bohme, M.; Dapprich, S.; Gobbi, A.; Hollwarth, A.; Jonas, V.; Kohler, K. F.; Stegmann, R.; Veldkamp, A.; Frenking, G. *Chem. Phys. Lett.* **1993**, 208, 111–114. (c) Roy, L.E.; Hay, P. J.; Martin, R. L. *J. Chem. Theory Comput.* **2008**, 4, 1029–1031.

(7) (a) Feller, D. *J. Comp. Chem.* **1996**, 17, 1571–1586. (b) Schuchardt, K. L.; Didier, B. T.; Elsethagen, T.; Sun, L.; Gurumoorthi, V.; Chase, J.; Li, J.; Windus, T. L. *J. Chem. Inf. Model.* **2007**, 47, 1045–1052.

(8) (a) Hariharan, P. C.; Pople, J. A. *Chem. Phys. Lett.* **1972**, 16, 217–219. (b) Franel, M. M.; Pietro, W. J.; Hehre, W. J.; Binkley, J. S.; Gordon, M. S.; DeFrees, D. J.; Pople, J. A. *J. Chem. Phys.* **1982**, 77, 3654–3665.

(9) Wertz, D. H. *J. Am. Chem. Soc.* **1980**, 102, 5316–5322.

(10) Jaguar, version 6.5; Schrodinger, LLC, New York, **2005**.

## Chapter 4. Competitive Benzene C-H Bond Activation versus Olefin Insertion in a Palladium(II) $\beta$ -Diketimate Complex

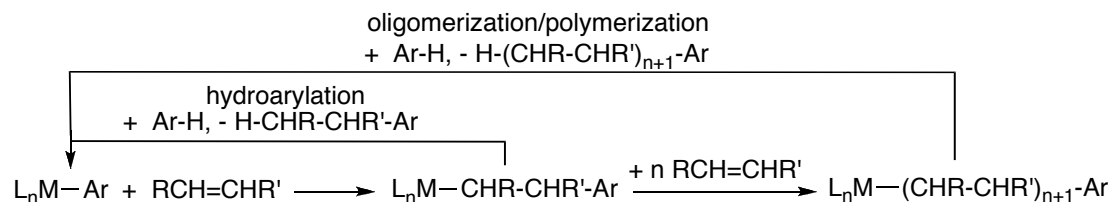
### Abstract

The monomethylpalladium(II) complex,  $(\text{COD})\text{Pd}(\text{CH}_3)\text{Cl}$  (COD = 1,5-cyclooctadiene), undergoes both benzene C-H activation and migratory insertion of olefin, with the former faster than the latter, at room temperature under the assistance of an anionic  $\beta$ -diketimate ligand, to yield  $\eta^3$ -(2-R-cyclooctenyl)palladium(II)  $\beta$ -diketimate (R = methyl or phenyl). Kinetic isotope effect suggests that the cleavage of benzene C-H bond is the rate-determining step for benzene C-H activation. Density functional theory<sup>1</sup> computation supports an  $\sigma$ -bond metathesis mechanism for the cleavage of benzene C-H bond.

## 1. Introduction

Coupling of arenes and olefins via aromatic C-H activation by transition metal complexes provides an efficient and atom-economic way to construct C-C bonds.<sup>1</sup> Most arene-olefin coupling reactions are limited to activated olefins and arenes with chelation assistance;<sup>2</sup> however, there have been several recent reports of hydroarylation involving simple arenes (e.g., benzene and toluene) and nonactivated olefins at elevated temperatures, using catalysts based on Ir, Ru, and Pt.<sup>3</sup> In general, these reactions proceed by aromatic C-H activation followed by migratory insertion of olefin into the resulting metal-aryl bond, to generate a  $\sigma$ -aryl-alkyl complex; this key intermediate can undergo aromatic C-H activation to liberate the C-C coupled product and regenerate the aryl complex.<sup>4</sup> However, it can also undergo additional olefin insertions, so that olefin oligomerization/polymerization can be a competing side reaction (Scheme 1). Understanding the factors controlling the relative rates of these two reactions, which determine the selectivity for olefin hydroarylation,<sup>3,4</sup> is essential for rational design of improved catalysts.

**Scheme 1.**



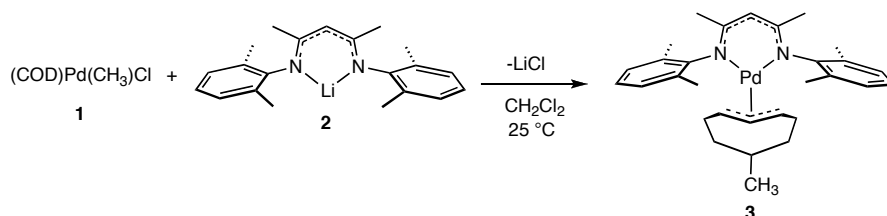
The results for platinum suggest that palladium might also be a promising metal for catalyzing olefin hydroarylation, and indeed C-H activation of simple arenes by

monomethylpalladium(II) has been demonstrated.<sup>5</sup> However, related monomethylpalladium(II) complexes often are highly active for olefin oligomerization/polymerization,<sup>6</sup> so the competition of Scheme 1 may well be unfavorable in many cases. Herein, we report a monomethylpalladium(II) system for which benzene C-H activation and migratory insertion of olefins are competitive, with the former faster at room temperature, along with experimental and computational findings relevant to the mechanism.

## 2. Results and Discussion

### 2.1 Experimental Observations

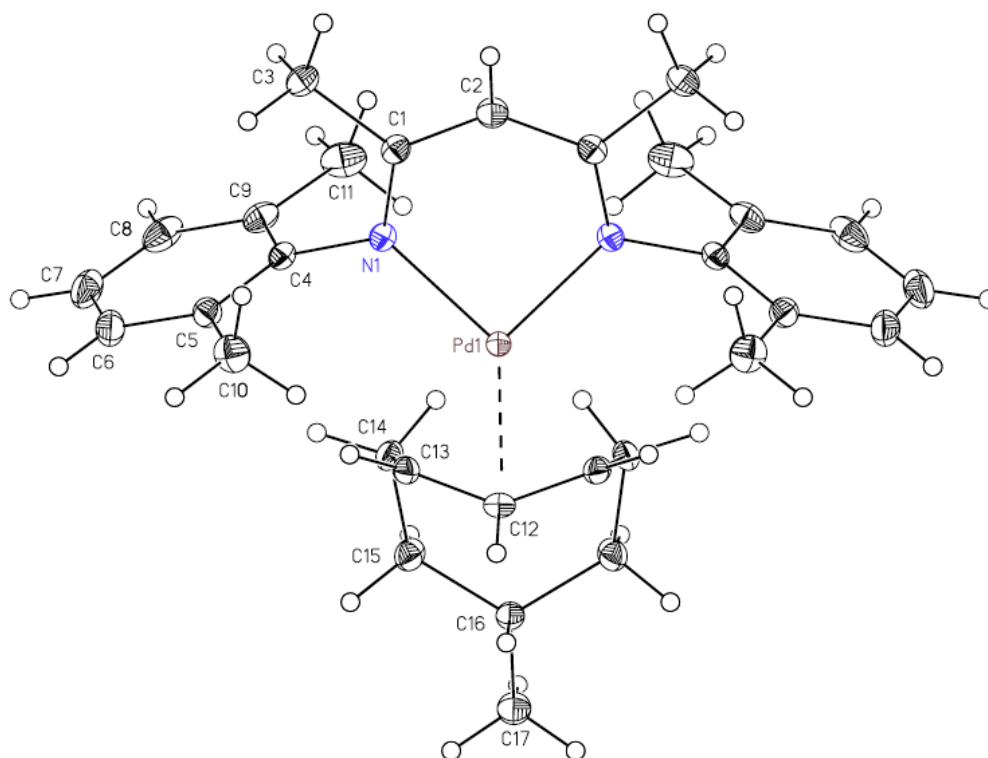
**Scheme 2.**



Addition of lithium β-diketiminate **2** to a CD<sub>2</sub>Cl<sub>2</sub> solution containing 1 equivalent of (COD)Pd(CH<sub>3</sub>)Cl (**1**, COD = 1, 5-cyclooctadiene), at room temperature under nitrogen, results in a yellow solution with some black precipitate. Crystals obtained from solution were identified by <sup>1</sup>H NMR and X-ray crystallography as η<sup>3</sup>-(2-methylcyclooctenyl)palladium(II) β-diketiminate (**3**, Scheme 2). The <sup>1</sup>H NMR spectrum, particularly the characteristic triplet, singlet, and doublet at δ<sub>H</sub> = 5.03 ppm (the proton at the central carbon of the η<sup>3</sup>-allyl fragment), 4.53 ppm (the proton at the central carbon of the

$\beta$ -diketiminate backbone), and 0.43 ppm (the proton of the methyl group on the cyclooctenyl moiety), respectively,<sup>7</sup> indicates that the complex is symmetrical about the plane bisecting the diketiminate ligand, while the crystal structure (Figure 1) shows that the methyl group on the cyclooctenyl moiety is *cis* to Pd.

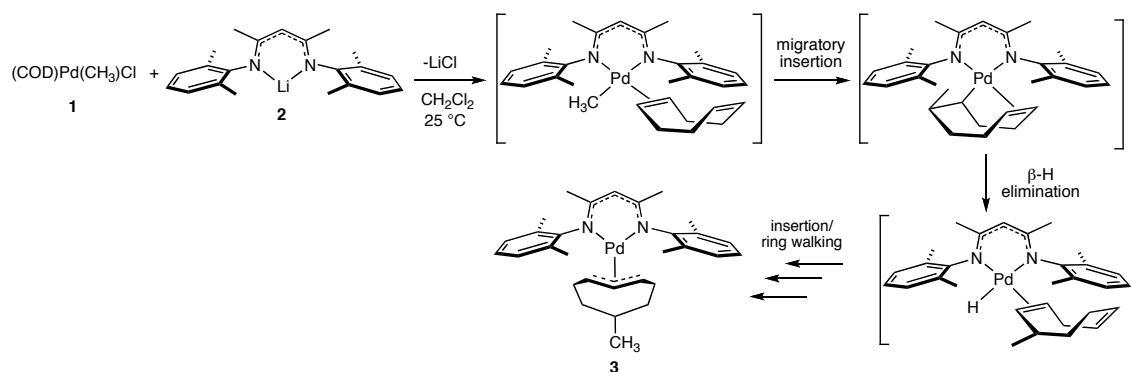
**Figure 1.** X-ray crystal structure of compound **3** (CCDC 295981). Selected bond distances (Å) and angles (deg): Pd(1)-N(1), 2.0708(10); Pd(1)-C(12), 2.0932(16); Pd(1)-C(13), 2.1696(11); C(12)-Pd(1)-C(13), 38.70(4); N(1)-Pd(1)-C(12), 133.35(3); N(1)-Pd(1)-C(13), 100.22(4)



A mechanism for the formation of **3** is proposed in Scheme 3. Salt metathesis between (COD)Pd(CH<sub>3</sub>)Cl and lithium  $\beta$ -diketiminate affords COD-coordinated

monomethylpalladium(II)  $\beta$ -diketiminate (**4**). Migratory insertion of COD into the Pd-CH<sub>3</sub> bond leads to  $\eta^1$ -methyl-cyclooctenylpalladium(II), which further undergoes a series of  $\beta$ -hydride eliminations and migratory insertions to form the  $\eta^3$ -allyl species **3**, presumably thermodynamically preferred among all the isomers in the ring-walking process. The *cis* conformation of **3** suggests that dissociation of coordinated olefins from the Pd(olefin)(H) intermediates does not occur.

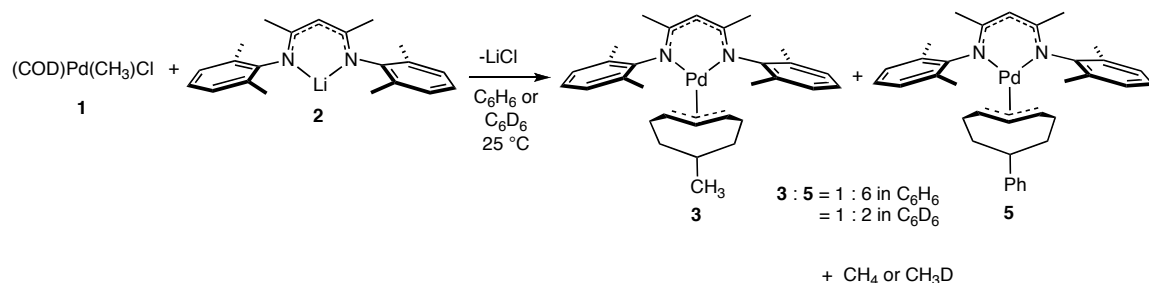
**Scheme 3.**



When the reaction is carried out in benzene (C<sub>6</sub>H<sub>6</sub>) instead of CD<sub>2</sub>Cl<sub>2</sub>, some **3** still forms, but the <sup>1</sup>H NMR indicates the presence of a new species **5** as well. The new <sup>1</sup>H NMR signals assigned to **5** (in CD<sub>2</sub>Cl<sub>2</sub>) are similar to those of **1**, with a triplet at  $\delta_{\text{H}}$  5.42 ppm and a singlet at  $\delta_{\text{H}}$  4.76 ppm; there are also several new signals in the aromatic region. If the same reaction is carried out in a closed NMR tube using C<sub>6</sub>D<sub>6</sub> as the solvent, formation of CH<sub>3</sub>D was observed, indicating benzene C-D bond activation by monomethylpalladium(II); and the new aromatic signals are absent. These findings strongly suggest that **5** is the phenyl analog of **3**,  $\eta^3$ -(2-phenylcyclooctenyl)palladium(II)  $\beta$ -diketiminate (Scheme 4). The assignment is further supported by high-resolution FAB+

mass spectroscopy, which gives signals corresponding to the molecular cation and the cation of molecule minus the phenyl-cyclooctenyl moiety.

**Scheme 4.**



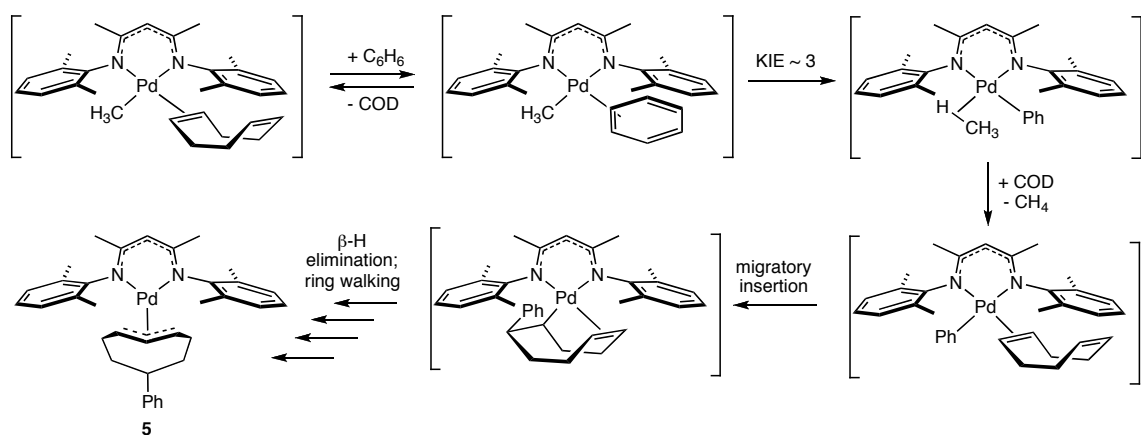
Because sharp  $^1\text{H}$  NMR signals are observed for N-aryl methyl groups of both **3** and **5**, rotation of the allyl moiety appears to be slow on the NMR time scale, which is in sharp contrast to many other  $(\eta^3\text{-allyl})\text{palladium}(\text{II})$  systems.<sup>8</sup> Slow apparent rotation has also been recently noted for  $(\eta^3\text{-propenyl})\text{palladium}(\text{II})$   $\beta$ -diketiminates.<sup>7</sup> The lack of apparent rotation might be a combined result of the tight binding between  $\beta$ -diketiminates and  $\text{Pd}^{\text{II}}$ , the absence of any potentially strongly coordinating counteranion, and the weak *trans* influence of  $\beta$ -diketiminates due to their anionic hard donor nature.

The ratio of products **3** and **5**, by NMR, is approximately 1:6 for the reaction in  $\text{C}_6\text{H}_6$  and 1:2 in  $\text{C}_6\text{D}_6$ . Since these ratios reflect the relative rates of benzene C-H/C-D activation by monomethylpalladium(II) and insertion of COD into the  $\text{Pd-CH}_3$  bond, and because the latter is isotope insensitive, the ratio ( $\sim 3$ ) reflects the kinetic isotope effect (KIE) for benzene C-H activation. This suggests that the breaking of C-H bond is the rate-determining step in the formation of **5**. Scheme 5 shows the proposed mechanism: after formation of intermediate **4**, displacement of COD by benzene takes place, followed

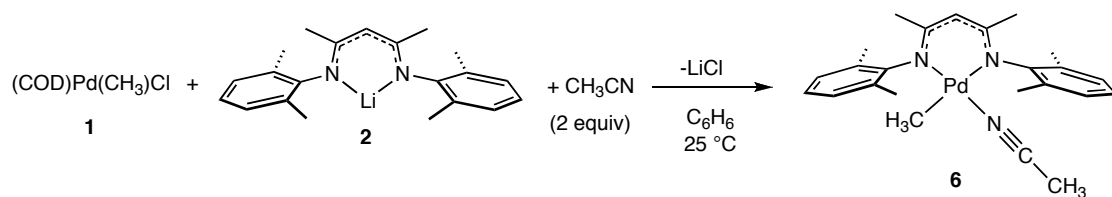


by C-H activation to form phenylpalladium(II) and release methane. The resultant phenylpalladium(II) then undergoes migratory insertion with COD and forms an  $\eta^1$ -(phenylcyclooctenyl)palladium(II); the ring-walking process discussed above leads to the  $\eta^3$ -allyl species **5**.

**Scheme 5.**



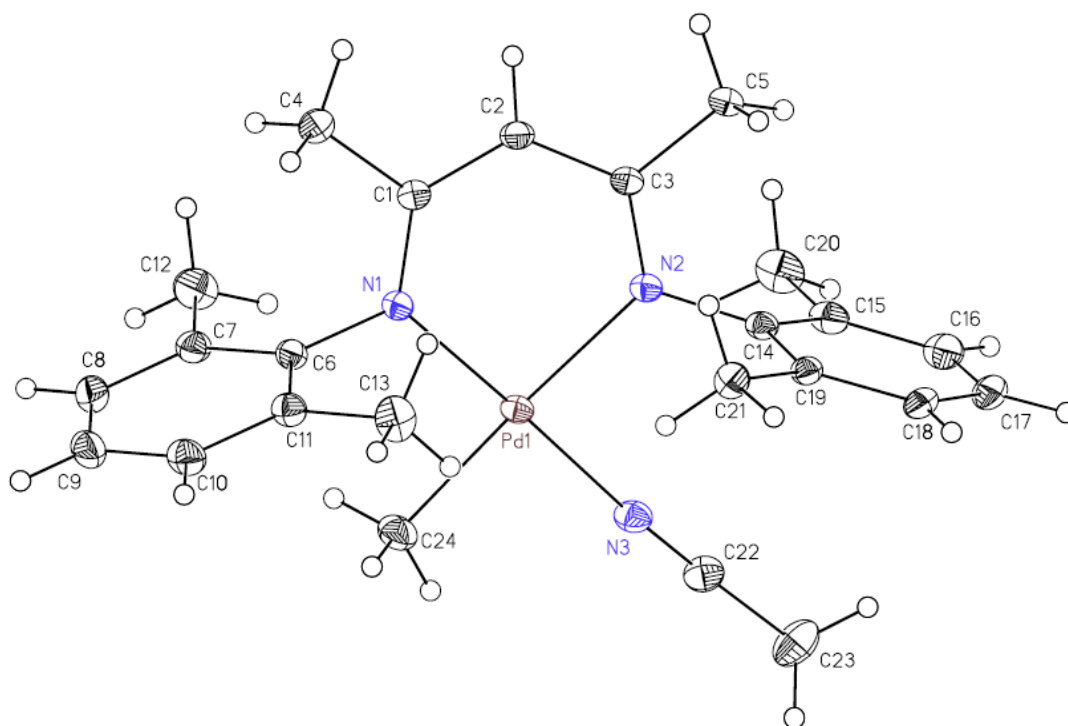
**Scheme 6.**



If two equivalents of acetonitrile are added to the reaction mixture containing **1** and **2** in benzene, neither **3** nor **5** is formed; instead monomethylpalladium(II)(acetonitrile) complex **6** is obtained quantitatively (Scheme 6). The crystal structure of **6** (Figure 2) shows that (in contrast to **3** and **5**) the coordination plane is a plane of symmetry,

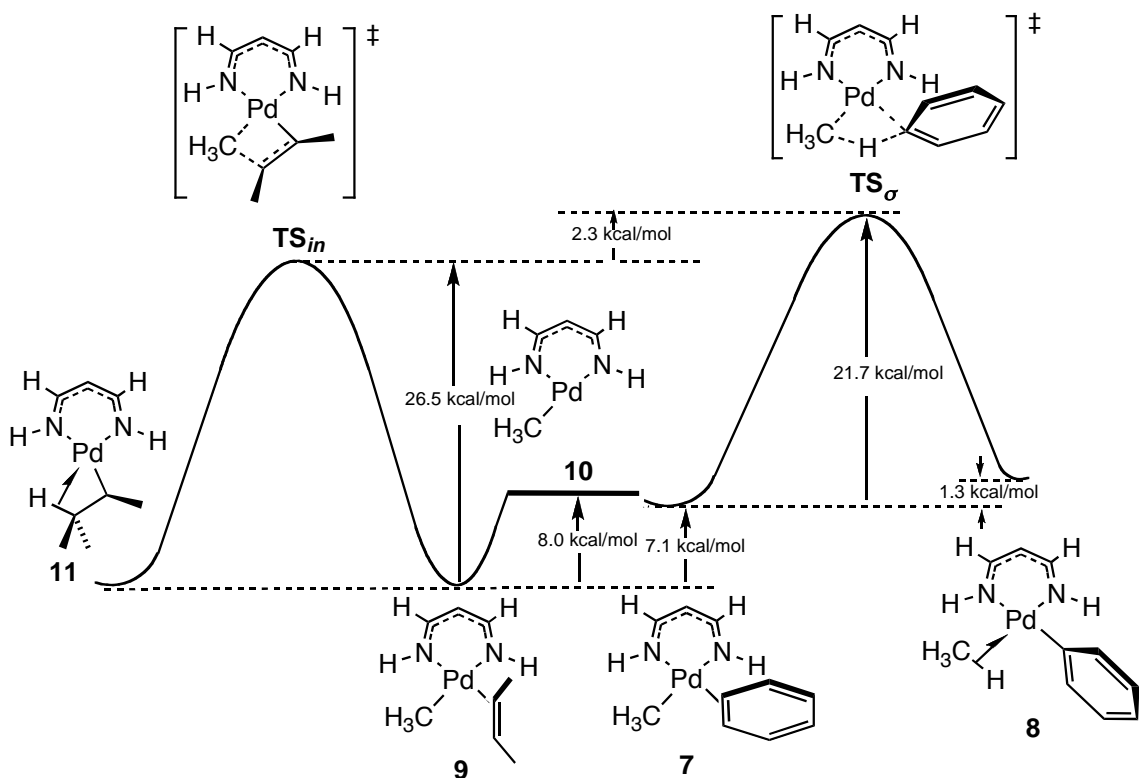
consistent with the  $^1\text{H}$  NMR spectrum. Related monomethylpalladium(II)  $\beta$ -diketimines have been previously reported.<sup>7,9</sup> Although **6** is fairly stable in  $\text{C}_6\text{D}_6$  at room temperature, it decomposes to a mixture of uncharacterized products at 80 °C with the formation of a significant amount of  $\text{CH}_3\text{D}$ , indicative of the activation of a benzene C-D bond. This is in sharp contrast to the platinum analog of **6**, which is stable in refluxing benzene.<sup>10</sup>

**Figure 2.** X-ray crystal structure of compound **6** (CCDC 296075). Selected bond distances (Å) and angles (deg): Pd(1)-N(3), 2.0135(9); Pd(1)-N(1), 2.0262(8); Pd(1)-C(24), 2.0526(9); Pd(1)-N(2), 2.1113(7); N(3)-Pd(1)-N(1), 178.19(3); N(3)-Pd(1)-C(24), 87.01(4); N(1)-Pd(1)-C(24), 91.41(4); N(3)-Pd(1)-N(2), 90.54(3); N(1)-Pd(1)-N(2), 91.03(3); C(24)-Pd(1)-N(2), 177.45(4).



## 2.1 DFT Computation

Scheme 7.



The mechanism for benzene C-H activation could involve either  $\sigma$ -bond metathesis or oxidative addition followed by reductive elimination.  $Pd^{IV}-H$  is generally considered to be a high-energy intermediate, which might argue against the latter, but it cannot be firmly excluded. To compare these two mechanisms, density function theory (DFT) calculations at the level of rB3LYP/LACVP\*\*<sup>11</sup> were performed on a model system with a simplified  $\beta$ -diketiminate ligand. The computational results (Scheme 7) suggest that  $\sigma$ -bond metathesis is indeed preferred over oxidative addition for the conversion of **7** to **8**, with the activation free energy of the former (21.7 kcal/mol) lower than that of the

latter by 9.6 kcal/mol, and the product, methane adduct **8**, is slightly less stable (by 1.3 kcal/mol) than benzene adduct **7**.

The competition between benzene C-H activation via  $\sigma$ -bond metathesis ( $TS_s$ ) and migratory insertion ( $TS_{in}$ ) was subsequently investigated by DFT for the same system, using *cis*-2-butene as a simplified model for COD. Coordination of benzene is calculated to be 7.1 kcal/mol weaker than that of *cis*-2-butene (**9** + C<sub>6</sub>H<sub>6</sub> to **7** + *cis*-2-butene, Scheme 7). Although a transition state for associative displacement of *cis*-2-butene by benzene (a mechanism tentatively suggested by experimental observations<sup>12</sup>) was not located, the activation barrier for the dissociative mechanism, which should be approximately equal to the dissociation free energy of coordinated *cis*-2-butene from **7**, 8.0 kcal/mol, can be taken as an upper limit. Hence displacement of olefin by benzene should be fast compared to breaking the benzene C-H bond, which is consistent with the experimentally observed KIE of about 3.

Further calculations indicate that migratory insertion of *cis*-2-butene into Pd-CH<sub>3</sub> (**9** to **11**, Scheme 7) is nearly thermoneutral and has a 26.5 kcal/mol activation free energy, lower than that of  $TS_s$  by 2.3 kcal/mol. This small difference appears consistent with the experimental observation of competitive C-H activation versus migratory insertion, given the imprecision of DFT calculations as well as the simplified model system.

### 3. Conclusions

In summary, we have demonstrated that our monomethylpalladium(II)  $\beta$ -diketiminate can undergo both benzene C-H activation and migratory insertion of olefin at room temperature. The simultaneous observation of these two reactions for metal alkyls has

previously only been demonstrated in the catalytic hydroarylation of olefins at elevated temperatures.<sup>3</sup> In addition, unlike other monomethylpalladium(II) systems, where olefin oligomerizations and polymerizations dominate, benzene C-H activation is somewhat favored in our system. DFT calculations on a simplified model system suggest that the C-H activation occurs through an  $\sigma$ -bond metathesis mechanism. Further work is underway to investigate effects of various anionic ligands on the competition between benzene C-H activation and migratory insertion at monomethylpalladium(II), with the goal of gaining insights leading to the design of Pd(II)-based catalysts for hydroarylation of olefins.

## Experimental Section

**General Information.** All air and/or moisture sensitive compounds were manipulated by using standard Schlenk techniques, or in a glove box under a nitrogen atmosphere. All starting materials are commercially available and used as received without further purification. Solvents were dried with appropriate methods before use and stored under nitrogen. (COD)Pd(CH<sub>3</sub>)Cl was synthesized according to the literature procedure.<sup>13</sup> A modified literature procedure was used for the synthesis of lithium  $\beta$ -diketiminates.<sup>14</sup> All NMR spectra were recorded at room temperature using a Varian Mercury 300 spectrometer. NMR spectra were referenced to TMS using the residual impurities of the given solvent. Chemical shifts are reported using the standard  $\delta$  notation in parts per million; positive chemical shifts are to a higher frequency from TMS, and coupling

constant are reported in hertz (Hz). Multiplicities are reported as follows: singlet (s), doublet (d), doublet of doublets (dd), doublet of triplets (dt), triplet (t), quartet (q), multiplet (m), broad resonance (br). The Caltech X-ray Crystallography Laboratory provided the X-ray analysis. High-resolution mass spectra were obtained at Caltech Mass Spectrometry Laboratory.

**Preparation of Compound 3.** Lithium *N,N'*-2,6-dimethylphenyl-substituted  $\beta$ -diketiminate **2** (11.8 mg, 0.0374mmol) and (COD)Pd(CH<sub>3</sub>)Cl (10 mg, 0.0377mmol) was mixed with 0.7 mL CD<sub>2</sub>Cl<sub>2</sub> at room temperature under nitrogen in a J-Young tube. The solution turned yellow immediately upon mixing with slow precipitation of black solid. The reaction was complete after 24 hours, with **3** as the major product (NMR yield: 90%). After removal of the precipitate, crystals suitable for X-ray structural analysis were obtained by thermal diffusion of petroleum ether into the filtrate in the refrigerator. <sup>1</sup>H NMR (300 MHz, CD<sub>2</sub>Cl<sub>2</sub>)  $\delta$  6.85–6.80 (m, 4H), 6.69–6.63 (m, 2H), 5.03 (t, *J* = 7.9, 1H), 4.53 (s, 1H), 2.40 (q, *J* = 8.0, 2H), 2.02 (s, 6H), 1.95 (s, 6H), 1.34 (s, 6H), 0.97–0.49 (m, 9H), 0.43 (d, *J* = 6.6, 3H). <sup>13</sup>C NMR (75 MHz, CH<sub>2</sub>Cl<sub>2</sub>)  $\delta$  158.30, 131.26, 129.67, 127.81, 127.75, 127.72, 123.23, 109.13, 93.99, 73.65, 34.64, 29.19, 28.14, 27.78, 22.13, 21.96, 18.66, 18.41. HRMS (FAB+) *m/z* calcd for C<sub>30</sub>H<sub>40</sub>N<sub>2</sub>Pd 534.2227, found 534.2207.

**Preparation of Compound 5.** Lithium *N,N'*-2,6-dimethylphenyl-substituted  $\beta$ -diketiminate **2** (11.8 mg, 0.0374mmol) and (COD)Pd(CH<sub>3</sub>)Cl (10 mg, 0.0377mmol) were dissolved in 0.5 mL C<sub>6</sub>H<sub>6</sub> and stirred overnight at room temperature under nitrogen. The solution turned yellow immediately upon mixing with slow precipitation of black solid. After the removal of the precipitate and the solvent, a yellow solid was obtained. The <sup>1</sup>H NMR spectrum of the solid in CD<sub>2</sub>Cl<sub>2</sub> shows that compound **5** is the major

product (NMR yield: 81%), which was further characterized by high-resolution mass spectroscopy.  $^1\text{H}$  NMR (300 MHz,  $\text{CD}_2\text{Cl}_2$ )  $\delta$  7.20–6.81 (m, 11H), 5.42 (t,  $J = 7.9$ , 1H), 4.76 (s, 1H), 2.79 (tt,  $J = 2.8$ , 12, 1H), 2.66 (q,  $J = 8.0$ , 2H), 2.27 (s, 6H), 2.19 (s, 6H), 1.57 (s, 6H), 1.39–0.98 (m, 8H). HRMS (FAB+)  $m/z$  calcd for  $\text{C}_{35}\text{H}_{42}\text{N}_2\text{Pd}$  596.2383, found 596.2424;  $[\text{M}-\eta^3\text{-phenyl-cyclooctenyl}]^+$  calcd for  $\text{C}_{21}\text{H}_{28}\text{N}_2\text{Pd}$  414.13, found 411.1061.

**Preparation of Compound 6.** Lithium  $N,N'$ -2,6-dimethylphenyl-substituted  $\beta$ -diketiminate **2** (11.8 mg, 0.0374 mmol), (COD)Pd( $\text{CH}_3$ )Cl (10 mg, 0.0377 mmol) and  $\sim 2$  eq. acetonitrile were dissolved in 0.7 mL  $\text{C}_6\text{H}_6$  and stirred overnight at room temperature under nitrogen. The solution turned yellow immediately upon mixing with slow precipitation of black solid. After 24 hours, the solution was filtered to remove the precipitate and volatiles removed under vacuum. A yellow solid was obtained, consisting entirely ( $^1\text{H}$  NMR,  $\text{CDCl}_3$ ) of **6**. Crystals suitable for X-ray structural analysis were obtained by thermal diffusion of petroleum ether into the filtrate in refrigerator (isolated yield > 95%).  $^1\text{H}$  NMR (300 MHz,  $\text{CDCl}_3$ )  $\delta$  7.04 (d,  $J = 7.4$ , 4H), 6.97–6.78 (m, 2H), 4.72 (s, 1H), 2.32 (s, 6H), 2.22 (s, 6H), 1.57 (s, 3H), 1.53 (s, 3H), 1.53 (s, 3H), -0.57 (s, 3H).  $^{13}\text{C}$  NMR (75 MHz,  $\text{CDCl}_3$ )  $\delta$  160.53, 159.91, 154.56, 147.69, 134.99, 134.77, 131.57, 130.14, 129.90, 126.21, 125.70, 96.08, 27.27, 25.47, 21.45, 21.28, 4.69, 0.63. HRMS (FAB+)  $m/z$  calcd for  $\text{C}_{24}\text{H}_{31}\text{N}_3\text{Pd}$  467.1553, found 467.1571.

**Computational Methodology.** All the structures were fully optimized by using restricted hybrid density function theory B3LYP method as implemented in the Jaguar 6.5 program package.<sup>11</sup> The Pd was described by LACVP\*\*, a basis set consisting of the Wadt and Hay<sup>15</sup> relativistic effective core potentials (RECPs) and valence double-z

contraction functions. A modified variant of Pople's<sup>16</sup> all-electron basis set, 6-31G\*\*, where the six d functions have been reduced to five, was used for all other atoms. It should be noted that the computation method used in this study is commonly more reliable in studying trends than providing absolute numbers for the reactions, although model calculations with similar methods have been demonstrated to afford remarkably accurate figures in absolute terms for migratory insertions.<sup>17</sup>

All species were treated as singlets. Harmonic vibrational frequencies were calculated with the B3LYP method for the optimized geometries. Zero-point vibrational energy corrections and thermodynamic corrections were obtained by using unscaled frequencies. Free energies were calculated for each species at 298 K and 1 atmosphere in gas phase. All transition structures possess one and only one imaginary frequency and were further confirmed by following the corresponding normal mode toward each product and reactant.

## References

- (1) Dyker, G., Ed. *Handbook of C-H Transformations*; Wiley-VCH, Weinheim, Germany, **2005**.
- (2) See the following reviews and references therein: (a) Jia, C. G.; Kitamura, T.; Fujiwara, Y. *Acc. Chem. Res.* **2001**, *34*, 633–639. (b) Kakiuchi, F.; Murai, S. *Acc. Chem. Res.* **2002**, *35*, 826–834. (c) Beccalli, E. M.; Broggini, G.; Martinelli, M.; Sottocornola, S. *Chem. Rev.* **2007**, *107*, 5318–5365.



(3) Ir: (a) Matsumoto, T.; Taube, D. J.; Periana, R. A.; Taube, H.; Yoshida, H. *J. Am. Chem. Soc.* **2000**, *122*, 7414–7415. (b) Matsumoto, T.; Periana, R. A.; Taube, D. J.; Yoshida, H. *J. Mol. Catal. A—Chem.* **2002**, *180*, 1–18. Ru: (c) Lail, M.; Arrowood, B. N.; Gunnoe, T. B. *J. Am. Chem. Soc.* **2003**, *125*, 7506–7507. (d) Foley, N. A.; Lail, M.; Lee, J. P.; Gunnoe, T. B.; Cundari, T. R.; Petersen, J. L. *J. Am. Chem. Soc.* **2007**, *129*, 6765–6781. (e) Foley, N. A.; Ke, Z. F.; Gunnoe, T. B.; Cundari, T. R.; Petersen, J. L. *Organometallics* **2008**, *27*, 3007–3017. Pt: (f) Karshtedt, D.; McBee, J. L.; Bell, A. T.; Tilley, T. D. *Organometallics* **2006**, *25*, 1801–1811. (g) McKeown, B. A.; Foley, N. A.; Lee, J. P.; Gunnoe, T. B. *Organometallics* **2008**, *27*, 4031–4033. (h) Leudtke, A. T.; Goldberg, K. I. *Angew. Chem. Int. Ed.* **2008**, *120*, 7808–7810.

(4) (a) Oxgaard, J.; Muller, R. P.; Goddard, W. A.; Periana, R. A. *J. Am. Chem. Soc.* **2004**, *126*, 352–363. (b) Oxgaard, J.; Periana, R. A.; Goddard, W. A. *J. Am. Chem. Soc.* **2004**, *126*, 11658–11665.

(5) Ackerman, L. J.; Sadighi, J. P.; Kurtz, D. M.; Labinger, J. A.; Bercaw, J. E. *Organometallics* **2003**, *22*, 3884–3890.

(6) For a reviewing article, see (a) Ittel, S. D.; Johnson, L. K.; Brookhart, M. *Chem. Rev.* **2000**, *100*, 1169–1203. For several recent examples, see (b) Kochi, T.; Nakamura, A.; Ida, H.; Nozaki, K. *J. Am. Chem. Soc.* **2007**, *129*, 7770–7771. (c) Luo, S.; Vela, J.; Lief, G. R.; Jordan, R. F. *J. Am. Chem. Soc.* **2007**, *129*, 8946–8947. (d) Kochi, T.; Noda, S.; Yoshimura, K.; Nozaki, K. *J. Am. Chem. Soc.* **2007**, *129*, 8948–8949. (e) Weng, W.; Shen, Z.; Jordan, R. F. *J. Am. Chem. Soc.* **2007**, *129*, 15450–15451.

(7) Synthesis of ( $\eta^3$ -propenyl)palladium(II)  $\beta$ -diketimines has recently been reported: Tian, X.; Goddard, R.; Porschke, K. R. *Organometallics* **2006**, *25*, 5854–5862.

- (8) For a review involving discussions of apparent rotation in ( $\eta^3$ -allyl)palladium(II) systems and its mechanisms, see: Trost, B. M.; Van Vranken, D. L. *Chem. Rev.* **1996**, *96*, 395–422.
- (9) Kang, M.; Sen, A. *Organometallics* **2005**, *24*, 3508–3515.
- (10) Iverson, C. N.; Carter, C. A. G.; Baker, R. T.; Scollard, J. D.; Labinger, J. A.; Bercaw, J. E. *J. Am. Chem. Soc.* **2003**, *125*, 12674–12675.
- (11) Jaguar, version 6.5; Schrodinger, LLC, New York, **2005**.
- (12) Use of the sterically bulkier N,N'-2,6-diisopropylphenyl-substituted  $\beta$ -diketiminato instead of **2** for the reaction in C<sub>6</sub>D<sub>6</sub> gives only a trace amount of CH<sub>3</sub>D, indicating that the activation of benzene C-D bond is significantly suppressed. This suggests that the displacement of COD by benzene in Scheme 5 is associative; however, in the absence of any well-characterized products from this reaction, no firm conclusion can be drawn.
- (13) Salo, E. V.; Guan, Z. B. *Organometallics* **2003**, *22*, 5033–5046.
- (14) Budzelaar, P. H. M.; de Gelder, R.; Gal, A. W. *Organometallics* **1998**, *17*, 4121–4123.
- (15) Hay, P. J.; Wadt, W. R. *J. Chem. Phys.* **1985**, *82*, 299–310.
- (16) (a) Hariharan, P. C.; Pople, J. A. *Chem. Phys. Lett.* **1972**, *16*, 217–219. (b) Franel, M. M.; Pietro, W. J.; Hehre, W. J.; Binkley, J. S.; Gordon, M. S.; DeFrees, D. J.; Pople, J. A. *J. Chem. Phys.* **1982**, *77*, 3654–3665.
- (17) (a) Musaev, D. G.; Svensson, M.; Morokuma, S.; Stromberg, S.; Zetterberg, K.; Siegbahn, P. E. M. *Organometallics* **1997**, *16*, 1933–1945. (b) Deng, L.; Woo, T. K.; Cavallo, L.; Margl, P. M.; Ziegler, T. *J. Am. Chem. Soc.* **1997**, *119*, 6177–6186. (c) Albert, K.; Gisdakis, P.; Rösch, N. *Organometallics* **1998**, *17*, 1608–1616. (d) Michalak,

A.; Ziegler, T. *J. Am. Chem. Soc.* **2001**, *123*, 12266–12278. (e) Lin, B.-L.; Liu, L.; Fu, Y.; Luo, S.-W.; Chen, Q.; Guo, Q.-X. *Organometallics* **2004**, *23*, 2114–2123.

## **Chapter 5. Computational Investigations of Competitive Benzene C-H Bond Activation versus Olefin Insertion in Palladium(II) with Various Anionic Ligands**

### **Abstract**

We computationally investigate the effects of nine ligands (8 monoanionic and 1 dianionic) on the competition between benzene C-H bond activation and olefin insertion in their corresponding monomethyl palladium(II) complexes. The computation result suggests that bisindolide-type ligands (**7**) and carbenearyl-type ligands (**9**) are likely to lead to faster benzene C-H bond activation as well as lower relative barrier heights of the C-H bond activation versus the insertion of olefins than those in monomethyl palladium(II) with  $\beta$ -diketiminate. All systems prefer  $\sigma$ -bond metathesis over oxidative addition for the mechanism of C-H bond activation except the one with bisindolide (**7**). The system with bisindolide (**7**) is also the only one that results in a lower barrier of benzene C-H bond activation relative to the insertion of ethylene.

## 1. Introduction

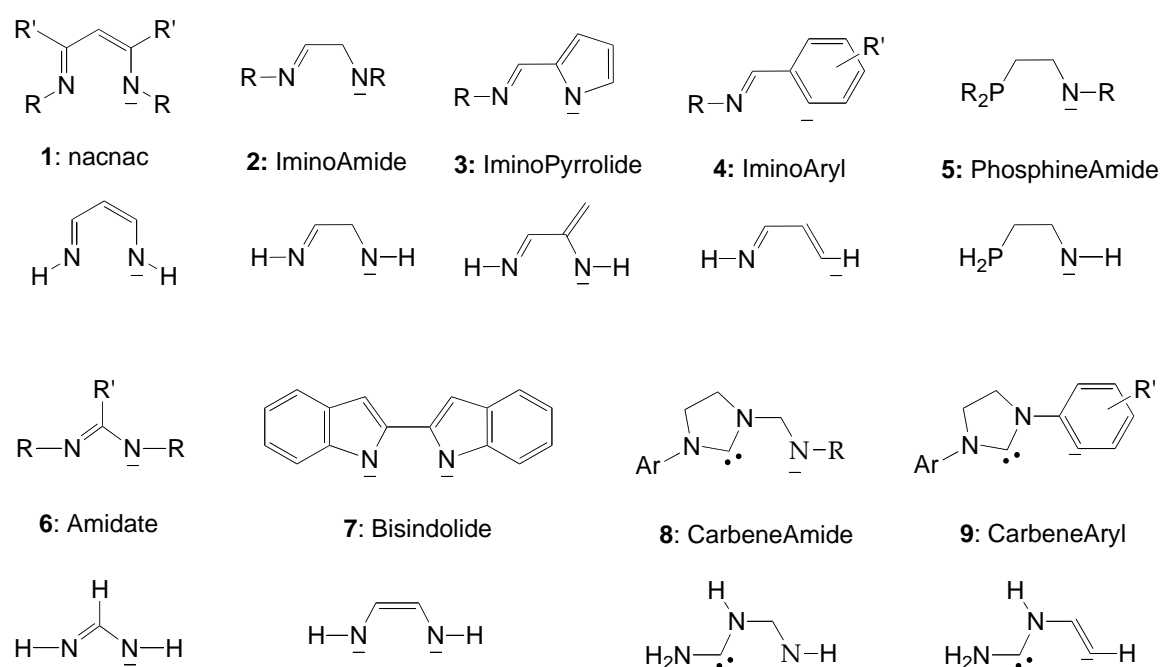
Investigations of C-H bond activation by metal alkyls have led to tremendous understanding for its mechanisms.<sup>1</sup> In general, a stoichiometric amount of metal-alkyl is sacrificed in the C-H bond activation, which provides the driving force for the reaction. Migratory insertion of olefin into the new metal-carbon bond followed by another C-H bond activation, or namely olefin hydroarylation, represents one of the rare examples that utilize metal alkyls as the catalysts.<sup>2</sup>

One major side reaction of olefin hydroarylation is the insertion of multiple equivalents of olefins into metal-carbon bonds prior to the C-H bond activation.<sup>2i, j</sup> Therefore, faster aromatic C-H bond activation than the olefin insertion in the corresponding metal alkyl intermediate is an important feature for a successful catalytic system of olefin hydroarylation. We have demonstrated a slightly faster benzene C-H bond activation relative to olefin (1,5-cyclooctadiene) insertion in a monomethyl palladium(II)  $\beta$ -diketiminate complex at room temperature.<sup>3</sup>

We reason that the electron-rich anionic  $\beta$ -diketiminate ligand is an important factor to account for the slower olefin insertion relative to C-H bond activation because of its ability to enhance back donation from the metal center to the coordinated olefins. Therefore, similar kinetic situations between these two competitive reactions are also expected to exist for other systems with anionic ligands. Herein, we report the computational result of the competition in a few simplified model systems with either a monoanionic (**1–6**, **8**, **9**, Scheme 1) or a dianionic bidentate ligand (**7**, Scheme 1). A similar computational method has been applied in investigations of a model system with a simplified  $\beta$ -diketiminate ligand and affords result consistent with relevant

experimental observations.<sup>3</sup> It should be noted that the computation method used in this study is commonly more reliable in studying trends than providing absolute numbers for the reactions, although model calculations with similar methods have been demonstrated to afford remarkably accurate figures in absolute terms for migratory insertions.<sup>4</sup>

**Scheme 1.**



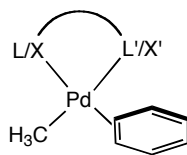
## 2. Results and Discussion

### 2.1 $\sigma$ -Bond Metathesis versus Oxidative Addition

Two possible mechanisms for the cleavage of benzene C-H bond by the palladium complexes,  $\sigma$ -bond metathesis versus oxidative addition, were compared at first. The geometrical isomer with the Pd-methyl *cis* to the donor with greater *trans* influence in the simplified ligand was investigated (e.g., the benzene adduct in Scheme 2). Transition

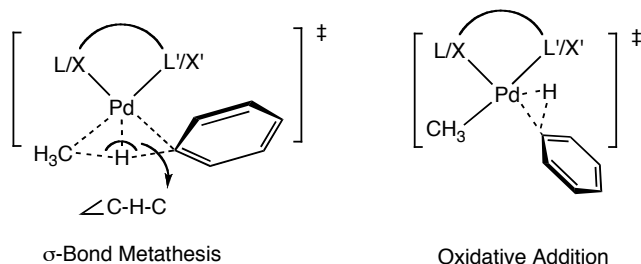
states for both mechanisms were located for all systems except the one corresponding to oxidative addition in the palladium complex with ligand **3** (iminopyrrolide).

**Scheme 2.**



L/X has greater *trans* influence than L'/X'.

**Table 1.** Selected key structural parameters for transition states of C-H activation



Ligand	$\sigma$ -Bond Metathesis		Oxidative Addition
	D(Pd-H) (Å)	$\angle$ C-H-C (°)	D(Pd-H) (Å)
<b>1</b>	1.69665	173.716	1.51084
<b>2</b>	1.68791	174.517	1.52193
<b>3</b>	1.6849	173.221	- <sup>a</sup>
<b>4</b>	1.70419	175.2	1.50126
<b>5</b>	1.72915	176.426	1.52298
<b>6</b>	1.68356	172.665	1.50244
<b>7</b>	1.70575	175.697	1.59585
<b>8</b>	1.71318	176.065	1.51693
<b>9</b>	1.72812	176.781	1.50395

<sup>a</sup> The transition state is not located.

Regardless of the ligand used, typical kite-shape (or 4-membered ring) and 3-membered ring structures were observed for transition states corresponding to  $\sigma$ -bond metathesis and oxidative addition, respectively. The 4-membered rings in the former are

nearly planar and coplanar with the coordination plane of the Pd complex. The C-H-C angles of these rings are close to 180 ° for all cases. In contrast, the hydrogen of the activated C-H bond in transition states of oxidative addition is out of the coordination plane. A schematic illustration of structures of these transition states and selected key structural parameters are shown in Table 1.

Pd hydrogen distances in transition states of  $\sigma$ -bond metathesis are all  $\sim 1.7$  Å, significantly longer than those in transition states of oxidative addition, which are generally  $\sim 1.5$  Å except that of the system with **7** (1.59585 Å), the dianionic bisindolide ligand. Clearly, interactions between hydrogen of the activated C-H bond and palladium in transition states of  $\sigma$ -bond metathesis are much weaker than those in transition states of oxidative addition.

**Table 2.** Activation barriers<sup>a</sup> of benzene C-H bond activation by monomethyl-palladium(II) complexes with ligand 1–9

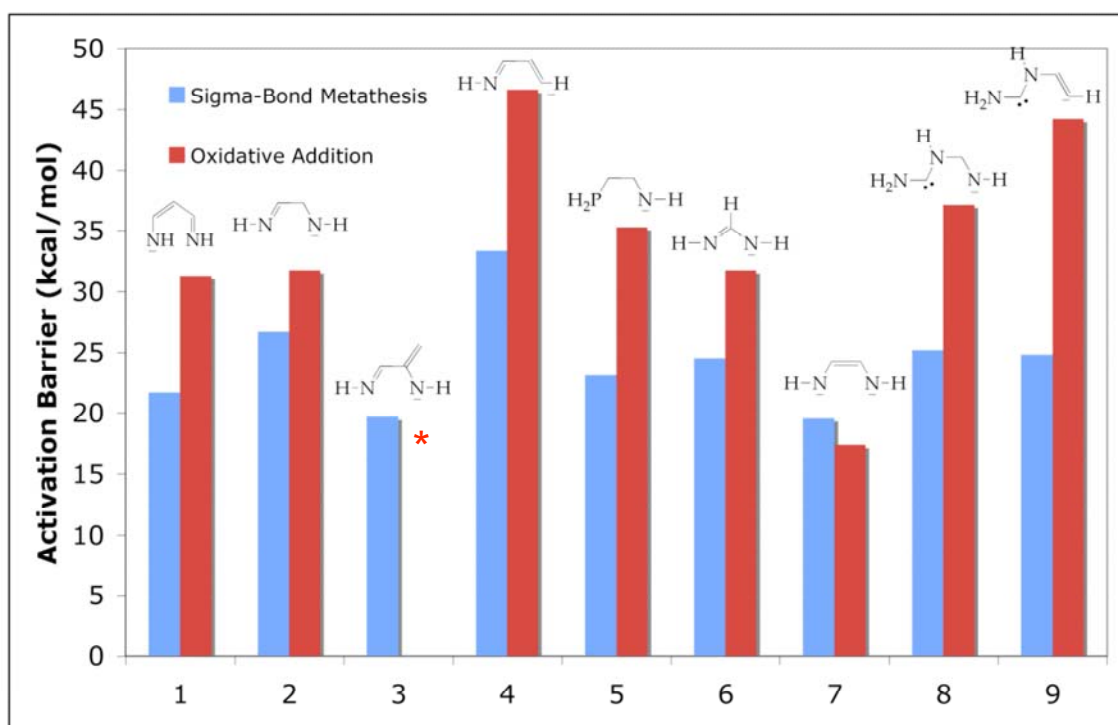
Ligand	$\sigma$ -bond metathesis (kcal/mol)	Oxidative Addition (kcal/mol)
<b>1</b>	21.7	31.3
<b>2</b>	26.7	31.7
<b>3</b>	19.7	- <sup>b</sup>
<b>4</b>	33.3	46.6
<b>5</b>	23.2	35.3
<b>6</b>	24.5	31.7
<b>7</b>	19.6	17.4
<b>8</b>	25.2	37.1
<b>9</b>	24.8	44.2

<sup>a</sup> Activation barriers relative to the benzene adduct; <sup>b</sup> the transition state is not located.



As shown in Table 2 and Figure 1, the activation barrier of the  $\sigma$ -bond metathesis pathway is generally much lower than that of the oxidative cleavage of C-H bond for all systems with monoanionic ligands. On the contrary, a 2.2 kcal/mol lower activation barrier is found for the oxidative addition pathway relative to that of the  $\sigma$ -bond metathesis pathway for the dianionic bisindolide ligand (**7**), revealing the mechanistic dependence of C-H bond activation on electronic properties of the palladium complex. (The subsequent reductive elimination does not increase the overall barrier.)

**Figure 1.**



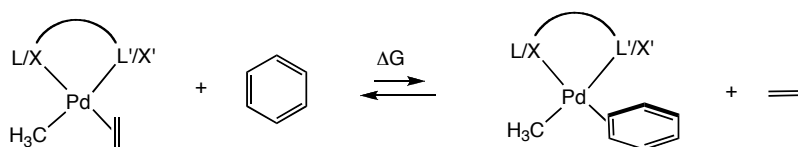
\* transition state of oxidative addition not located

## 2.2 Competitive Olefin Coordination versus Benzene Coordination

The C=C bond of the coordinated olefins in the olefin adducts is nearly perpendicular to the coordination plane for all systems studied here. In general, less-substituted olefins are

expected to bind more strongly with palladium than more-substituted olefins due to the steric factor. Our computational result indicates that the coordination of ethylene onto palladium(II) supported by ligand **1** ( $\beta$ -diketiminate) is stronger than that of *cis*-2-butene by 4.5 kcal/mol (Table 3). As a result, the ethylene adduct is more favorable in its equilibrium with the benzene adduct than in the corresponding equilibrium involving *cis*-2-butene. Therefore, a stronger inhibition effect on the C-H bond activation is expected for less-substituted olefins than for more-substituted olefins.

**Table 3.** Equilibrium between the ethylene adduct and the benzene adduct



Ligand	$\Delta G$ (kcal/mol)
<b>1</b> <sup>a</sup>	7.1
<b>1</b>	11.7
<b>2</b>	10.1
<b>3</b>	16.7
<b>4</b>	4.8
<b>5</b>	8.7
<b>6</b>	10.9
<b>7</b>	12.5
<b>8</b>	8.9
<b>9</b>	4.1

<sup>a</sup> Results of *cis*-2-butene

Comparable equilibrium free energies (difference within 3 kcal/mol) between the ethylene adduct and the benzene adduct are obtained if ligand **1** ( $\beta$ -diketiminate) is replaced by ligand **2** (iminoamide), **5** (phosphineamide), **6** (amidate), **7** (bisindolide), or **8**

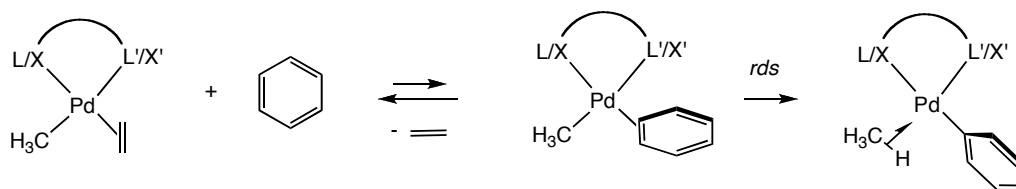
(carbeneamide). In case of ligand **4** (iminoaryl) and **9** (carbenearyl), the equilibrium dramatically shifts towards the benzene adduct. **3** (iminopyrrolide) is the only ligand that significantly shifts the equilibrium towards the ethylene adduct. Factors affecting the relative magnitude of these equilibrium free energies are still unclear.

Due to the stronger affinity between ethylene and palladium relative to that between benzene and palladium, high concentrations of olefins are expected to inhibit the C-H bond activation.

### **2.3 Benzene C-H Bond Activation from the Ethylene Adduct**

According to the calculated equilibrium free energies, the dominant species in the equilibrium is the ethylene adduct in high ethylene concentrations. Therefore, a displacement of olefin by benzene is expected to occur before the C-H bond activation under similar conditions. The upper limit for the displacement barrier can be estimated by the binding energy of ethylene. Based on this estimation, the C-H bond activation step is predicted to be rate determining in the reaction starting from the ethylene adduct (Scheme 3) for all systems investigated here.

Consequently, the overall barrier for the C-H bond activation is equal to the sum of the equilibrium energy and the activation energy of the C-H bond cleavage. As shown in Table 4, a lower overall barrier for benzene C-H bond activation relative to that in the system with ligand **1** ( $\beta$ -diketiminate) is found in those with ligand **5** (phosphineamide, by 1.5 kcal/mol), **7** (bisindolide, by 3.5 kcal/mol), and **9** (carbenearyl, by 4.5 kcal/mol), while all other ligands lead to higher barriers. Therefore, the systems with ligand **5**, **7**, and **9** are expected to undergo faster benzene C-H bond activation in the presence of olefins than the one with ligand **1**.

**Scheme 3.**

**Table 4.** Overall activation barriers<sup>a</sup> of benzene C-H bond activation for the reaction starting from the ethylene adduct

Ligand	Overall Barrier (kcal/mol)
<b>1</b>	33.4
<b>2</b>	36.8
<b>3</b>	36.4
<b>4</b>	38.1
<b>5</b>	31.9
<b>6</b>	35.4
<b>7</b>	29.9 <sup>a</sup>
<b>8</b>	34.1
<b>9</b>	28.9

<sup>a</sup> The activation barrier of the oxidative addition mechanism is used.

It should be pointed out that electronic effect on the preequilibrium between the water-coordinated species and TFE-coordinated species prior to the step of C-H bond cleavage has been successfully used to rationalize ligand effect on the rate of benzene C-H bond activation by cationic monomethyl platinum(II) species with diimine ligands.<sup>1a</sup> However, no similar correlation can be seen for the systems in this work. For example, although the equilibrium free energies between the ethylene adduct and the benzene adduct are similar for the systems with ligand **4** and **9** (the second lowest and the lowest, respectively), the overall barrier of C-H bond activation is the highest for the system with ligand **4** while

the one with ligand **9** is the lowest. Therefore, the ligand effect on overall barriers of C-H bond activation studied here cannot be solely attributed to ground state effect.

### 2.3 Migratory Insertion of Ethylene

**Table 5.** Activation barriers and reaction energies of olefin insertions

Ligand	Activation Barrier (kcal/mol)	Reaction Energy (kcal/mol)
<b>1</b> <sup>a</sup>	26.2	0.0
<b>1</b>	23.7	-2.6
<b>2</b>	29.8	4.7
<b>3</b>	28.0	2.8
<b>4</b>	32.1	-8.2
<b>5</b>	20.8	-8.9
<b>6</b>	23.7	-2.0
<b>7</b>	30.3	-6.3
<b>8</b>	25.9	-1.2
<b>9</b>	23.0	-3.8

<sup>a</sup> Results of *cis*-2-butene

For all systems in this study, the coordinated olefin is coplanar with the coordination plane in the transition state of the insertion, revealing an olefin-rotation process occurring prior to the insertion. The calculated activation barriers and reaction free energies for the insertion of olefins are shown in Table 5. The activation barrier for the insertion of ethylene in the system with ligand **1** ( $\beta$ -diketiminato) is lower than that of *cis*-2-butene (by 2.5 kcal/mol). One possible explanation is that *cis*-2-butene needs to overcome more steric hindrance than ethylene in the rotation process. The insertion of ethylene is calculated to be thermodynamically more favorable than the insertion of *cis*-2-butene.

These observations suggest that olefin oligomerization should be a more serious issue for hydroarylation of less-substituted olefins than more-substituted olefins.

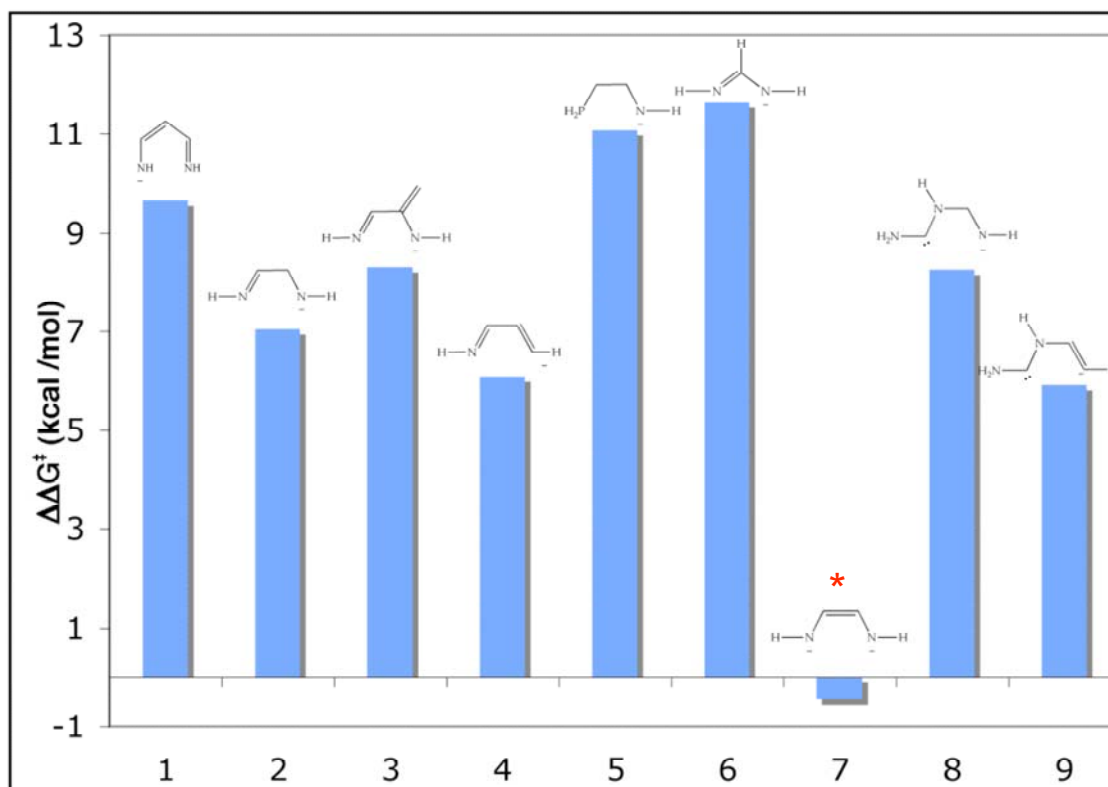
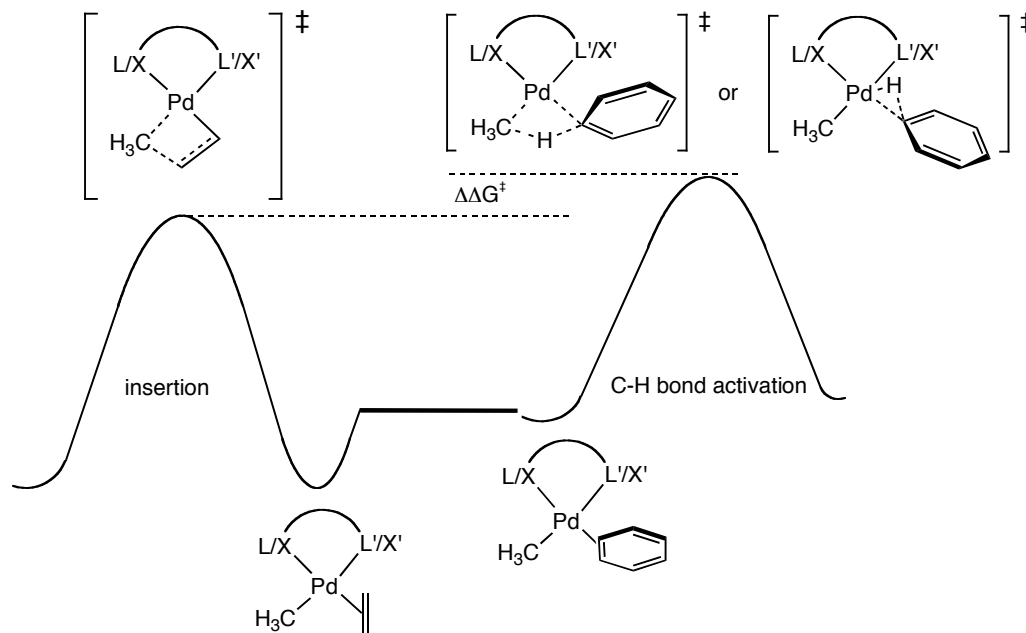
Much higher ethylene insertion barriers relative to the system with ligand **1** (at least 4.3 kcal/mol higher) are found for those with ligand **2** (iminoamide), **3** (iminopyrrolide), **4** (iminoaryl), and **7** (bisindolide), while all other ligands lead to insertion barriers comparable to the one with ligand **1** (difference within 3 kcal/mol). The high insertion barrier for the system with ligand **7** can be attributed to the dianionic nature of the ligand. The underlying reasons for those with ligand **2**, **3**, and **4**, however, are still unclear. It is noteworthy that all three ligands have an imine donor.

Barriers from 17 to 19 kcal/mol have been experimentally measured for the insertion of ethylene in a few  $[(\text{diimine})\text{Pd}(\text{alkyl})(\text{ethylene})]^+$  species.<sup>5</sup> DFT calculations on analogous systems give the insertion barriers  $\sim 20$  kcal/mol.<sup>6</sup> Comparing these data to our computational result clearly indicates that the anionic ligands disfavor the insertion of olefin relative to the neutral diimine-type ligands.

## 2.4 Competitive Benzene C-H Activation versus Ethylene Insertion

The relative barrier heights between benzene C-H bond activation and ethylene insertion are shown in Figure 2. Faster benzene C-H bond activation relative to the insertion of the disubstituted olefin (COD) has been experimentally observed for an analogous system supported by a  $\beta$ -diketiminate ligand. Our computation indicates that all ligands, with the exception of **5** (phosphineamide) and **6** (amidate), lead to smaller relative barriers than the system with ligand **1** ( $\beta$ -diketiminate). Therefore, benzene C-H

Figure 2.



\* The only system where oxidative addition is preferred over  $\sigma$ -bond metathesis.

bond activation by the systems with the ligands other than **1**, **5** and **6** is expected to be more favorable in its competition with the insertion of similar olefins (internal olefins) if we assume that the order of barrier heights observed for the insertion of ethylene can be extended to the insertion of internal olefins.

**7** (bisindolide) is the only ligand that gives a lower activation barrier of benzene C-H bond activation. Therefore, **7** is the most likely ligand among those investigated herein that will result in faster benzene C-H bond activation than the insertion of ethylene.

### 3. Conclusions

In summary, our computation suggests that bisindolide-type ligands (**7**) and carbenearyl-type ligands (**9**) might lead to faster benzene C-H bond activation as well as lower relative barrier heights of the C-H bond activation versus the insertion of olefins than those in monomethyl palladium(II) with  $\beta$ -diketiminate. The mechanism for the C-H bond activation, either oxidative addition or  $\sigma$ -bond metathesis, is found to be dependent on the ligand. The system with bisindolide (**7**) is the only one that results in a lower barrier of benzene C-H bond activation relative to the insertion of ethylene. Further investigations on the platinum analogues are underway to provide insights into the design of new catalysts of olefin hydroarylation.

### Computational Methodology

All the structures were fully optimized by using restricted hybrid density function theory B3LYP method as implemented in the Jaguar 6.5 program package.<sup>7</sup> The Pd was described by LACVP\*\*, a basis set consisting of the Wadt and Hay<sup>8</sup> relativistic effective



core potentials (RECPs) and valence double- $\zeta$  contraction functions. A modified variant of Pople's<sup>7</sup> all-electron basis set, 6-31G\*\*, where the six d functions have been reduced to five, was used for all other atoms.

All species were treated as singlets. Harmonic vibrational frequencies were calculated with the B3LYP method for the optimized geometries. Zero-point vibrational energy corrections and thermodynamic corrections were obtained by using unscaled frequencies. Free energies were calculated for each species at 298 K and 1 atmosphere in gas phase. All transition structures possess one and only one imaginary frequency and were further confirmed by following the corresponding normal mode toward each product and reactant.

## References

- (1) (a) Zhong, H. A.; Labinger, J. A.; Bercaw, J. E. *J. Am. Chem. Soc.* **2002**, *124*, 1378–1399. (b) Owen, J. S.; Labinger, J. A.; Bercaw, J. E. *J. Am. Chem. Soc.* **2006**, *128*, 2005–2016. (c) Chen, G. S.; Labinger, J. A.; Bercaw, J. E. *Proc. Natl. Acad. Sci. U. S. A.* **2007**, *104*, 6915–6920.
- (2) (a) Matsumoto, T.; Taube, D. J.; Periana, R. A.; Taube, H.; Yoshida, H. *J. Am. Chem. Soc.* **2000**, *122*, 7414–7415. (b) Matsumoto, T.; Periana, R. A.; Taube, D. J.; Yoshida, H. *J. Mol. Catal. A—Chem.* **2002**, *180*, 1–18. (c) Lail, M.; Arrowood, B. N.; Gunnoe, T. B. *J. Am. Chem. Soc.* **2003**, *125*, 7506–7507. (d) Foley, N. A.; Lail, M.; Lee, J. P.; Gunnoe, T. B.; Cundari, T. R.; Petersen, J. L. *J. Am. Chem. Soc.* **2007**, *129*, 6765–6781. (e) Foley, N. A.; Ke, Z. F.; Gunnoe, T. B.; Cundari, T. R.; Petersen, J. L. *Organometallics* **2008**, *27*, 3007–3017. (f) Karshedt, D.; McBee, J. L.; Bell, A. T.;

- Tilley, T. D. *Organometallics* **2006**, *25*, 1801–1811. (g) McKeown, B. A.; Foley, N. A.; Lee, J. P.; Gunnoe, T. B. *Organometallics* **2008**, *27*, 4031–4033. (h) Leudtke, A. T.; Goldberg, K. I. *Angew. Chem. Int. Ed.* **2008**, *120*, 7808–7810. (i) Oxgaard, J.; Muller, R. P.; Goddard, W. A.; Periana, R. A. *J. Am. Chem. Soc.* **2004**, *126*, 352–363. (j) Oxgaard, J.; Periana, R. A.; Goddard, W. A. *J. Am. Chem. Soc.* **2004**, *126*, 11658–11665.
- (3) Lin, B. -L. *Ph. D dissertation*, Chapter 4.
- (4) (a) Musaev, D. G.; Svensson, M.; Morokuma, S.; Stromberg, S.; Zetterberg, K.; Siegbahn, P. E. M. *Organometallics* **1997**, *16*, 1933–1945. (b) Deng, L.; Woo, T. K.; Cavallo, L.; Margl, P. M.; Ziegler, T. *J. Am. Chem. Soc.* **1997**, *119*, 6177–6186. (c) Albert, K.; Gisdakis, P.; Rösch, N. *Organometallics* **1998**, *17*, 1608–1616. (d) Michalak, A.; Ziegler, T. *J. Am. Chem. Soc.* **2001**, *123*, 12266–12278. (e) Lin, B.-L.; Liu, L.; Fu, Y.; Luo, S.-W.; Chen, Q.; Guo, Q.-X. *Organometallics* **2004**, *23*, 2114–2123.
- (5) Shultz, L. H.; Tempel, D. J.; Brookhart, M. *J. Am. Chem. Soc.* **2001**, *123*, 11539–11555.
- (6) Michalak, A.; Ziegler, T. *Organometallics* **2000**, *19*, 1850–1858.
- (7) Jaguar, version 6.5; Schrodinger, LLC, New York, **2005**.
- (8) Hay, P. J.; Wadt, W. R. *J. Chem. Phys.* **1985**, *82*, 299–310.
- (7) (a) Hariharan, P. C.; Pople, J. A. *Chem. Phys. Lett.* **1972**, *16*, 217–219. (b) Franel, M. M.; Pietro, W. J.; Hehre, W. J.; Binkley, J. S.; Gordon, M. S.; DeFrees, D. J.; Pople, J. A. *J. Chem. Phys.* **1982**, *77*, 3654–3665.

## Chapter 6. Mechanistic Investigations of Bipyrimidine-Promoted Palladium(II)-Catalyzed Allylic Acetoxylation of Olefins

### Abstract

Several pyridine-like ligands were found to improve Pd(OAc)<sub>2</sub>-catalyzed allylic oxidation of allylbenzene to cinnamyl acetate by *p*-benzoquinone in acetic acid. The best ligand examined, bipyrimidine, was used to identify the catalyst precursor for this system, (bipyrimidine)Pd(OAc)<sub>2</sub>, which was fully characterized. Mechanistic studies suggest the reaction takes place through disproportionation of (bipyrimidine)Pd(OAc)<sub>2</sub> to form a bipyrimidine-bridged dimer, which reacts with olefin to form a Pd<sup>II</sup>-olefin adduct, followed by allylic C-H activation to produce (η<sup>3</sup>-allyl)Pd<sup>II</sup> species. The (η<sup>3</sup>-allyl)Pd<sup>II</sup> intermediate undergoes a reversible acetate attack to generate a Pd<sup>0</sup>-(allyl acetate) adduct, which subsequently reacts with *p*-benzoquinone to release allyl acetate and regenerate (bipyrimidine)Pd(OAc)<sub>2</sub>. No KIE is observed for the competition experiment between allylbenzene-*d*<sub>0</sub> and allylbenzene-*d*<sub>5</sub>(CD<sub>2</sub>=CD-CD<sub>2</sub>-C<sub>6</sub>H<sub>5</sub>), suggesting that allylic C-H activation is not rate determining. Catalytic allylic acetoxylation of other terminal olefins as well as cyclohexene were also effected by (bipyrimidine)Pd(OAc)<sub>2</sub>.

## 1. Introduction

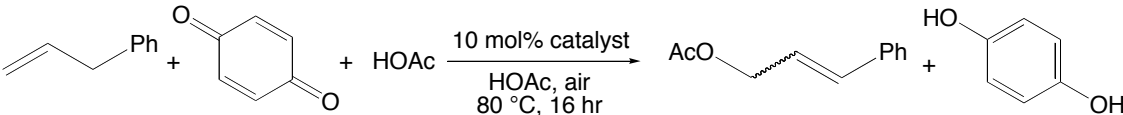
The selective oxidation of allylic C-H bonds offers a valuable approach to the construction of complex molecules.<sup>1</sup> While earlier catalysts based on copper or selenium suffer from problems such as limited substrate scope, low yields, and poor selectivities,<sup>2</sup> extensive work on systems based on Pd(II) has led to some remarkably selective allylic C-H activations and oxidations.<sup>3, 4</sup> The solvent often plays a key role in achieving selective oxidation to allyl acetates: in neat acetic acid, only symmetrical cyclic olefins are selectively oxidized with Pd(OAc)<sub>2</sub>,<sup>5</sup> whereas terminal olefins can be selectively oxidized in DMSO/acetic acid,<sup>6</sup> and yields can be further improved in dimethylacetamide (DMA).<sup>7</sup> The combination of Pd(II) with sulfoxide ligands also selectively oxidizes terminal olefins;<sup>8</sup> this reaction has been successfully applied for catalytic allylic aminations<sup>9</sup> and macrolactonizations.<sup>10</sup>

To date, no catalytic system has been reported to selectively oxidize both terminal and internal olefins to allyl acetates. Furthermore, in no case has the active catalytic species been characterized, which complicates the study and understanding of reaction mechanisms and impedes further development of new catalysts. Herein we disclose a well-defined new catalyst precursor, (bipyrimidine)Pd(OAc)<sub>2</sub>, that effects selective allylic acetoxylations of terminal olefins and cyclohexene in acetic acid, and offer evidences for its mechanism of operation.

## 2. Results and Discussion

The oxidation of allylbenzene by *p*-benzoquinone (BQ) in acetic acid at 80 °C, with Pd(OAc)<sub>2</sub> as the catalyst, leads to only a 13% yield of cinnamyl acetate (100% consumption of allylbenzene). Several other unidentified products, probably including the same Wacker-type products previously reported from reaction at 40 °C,<sup>6b</sup> are observed. The selectivity for cinnamyl acetate is significantly improved by the addition of pyridine-like nitrogen ligands (with the exception of 2, 2'-bipyridine, which shuts down the reaction) (Table 1). Among the ligands tested, bipyrimidine (BPM) is the best, leading to a 76% yield of cinnamyl acetate in 16 hours at 80 °C. However, further screening of the solvents and oxidants does not lead to any improved yield.

**Table 1.** Nitrogen ligand effects on Pd(OAc)<sub>2</sub>-catalyzed allylic acetoxylation of allylbenzene <sup>a</sup>

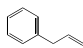
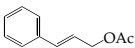
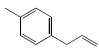
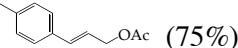
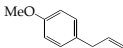
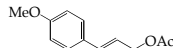
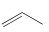
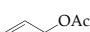
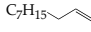
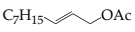
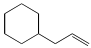
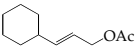

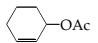


entry	catalyst	yield <sup>b,c</sup>
1	10 mol% Pd(OAc) <sub>2</sub>	13%
2	10 mol% Pd(OAc) <sub>2</sub> + 10 mol% 2,2'-bipyrimidine	76%
3	10 mol% Pd(OAc) <sub>2</sub> + 20 mol% pyridine	35%
4	10 mol% Pd(OAc) <sub>2</sub> + 10 mol% 1,10-phenanthroline	47%
5	10 mol% Pd(OAc) <sub>2</sub> + 10 mol% 2,2'-bipyridine	— <sup>d</sup>

<sup>a</sup> General experimental procedure: A mixture of catalyst, 0.7 mL glacial acetic acid, allylbenzene, 1 eq. BQ, and 20 µL nitrobenzene (internal standard for GC) is stirred and

heated in a sealed vial at 80 °C for 16 hours. <sup>b</sup> Sum of *cis* and *trans* isomers; GC yields. <sup>c</sup> Conversions of allylbenzene: entry 1–3, 100%; 4, 87%; 5, 3%. <sup>d</sup> No product detected

**Table 2.** (Bipyrimidine)Pd(OAc)<sub>2</sub>-catalyzed allylic acetoxylation of olefins<sup>a</sup>

Entry	Olefin	Temp. (°C)	Time (h)	Major Product (NMR Yield)	Overall Yield <sup>b</sup>
1		70	34	 (72%)	76%
2		70	33	 (75%)	78%
3		70	16	 (50%)	53%
4		70	24		45%
5		70	20	 (54%)	77%
6		70	20	 (65%)	77%
7		80	24	 (33%)	51%

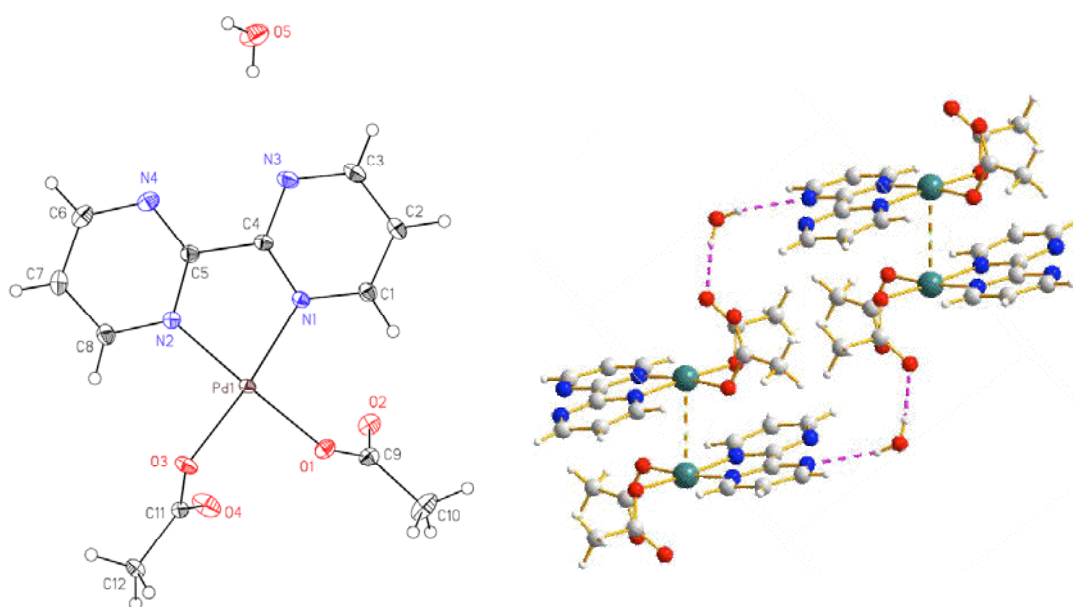
<sup>a</sup> Entry 1–6: 10 mol% catalyst loading and 2 eq. BQ; Entry 7: 5 mol% catalyst loading and 1.2 eq BQ; All reactions except 4 and 7 are near completion; <sup>b</sup> Product isolated as a mixture of isomers: Entries 1–3: *cis*- + *trans*- 1° allyl acetates; Entries 5–7: C=C bond migration results in minor products such as homoallyl acetates; Entries 5 and 6: small amounts of 2° allyl acetates observed.

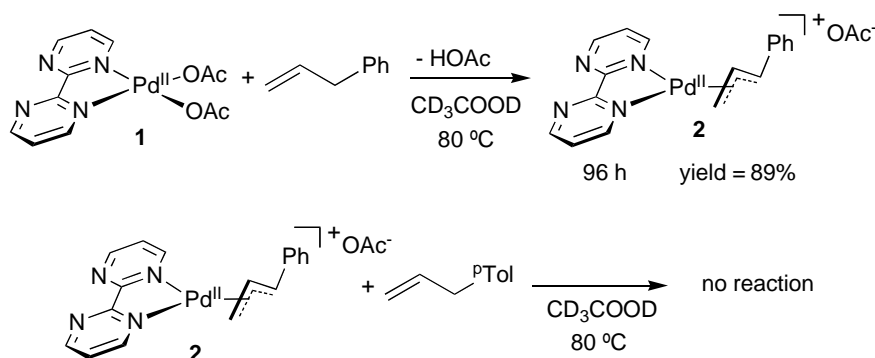
Studies of substrate scope (Table 2) indicate that both benzylic C-H and methoxy groups are compatible with the acetoxylation (Entries 2 and 3, Table 2). Unfortunately, the yield for olefins with alkyl groups at the allylic position (Entries 5 and 6, Table 2) suffers from olefin isomerization, giving byproducts such as homoallylic acetates. Cyclohexene is also an active substrate for the reaction, producing a mixture of

cyclohex-2-enyl acetate and cyclohex-3-enyl acetate (ca. 2.8:1) (Entry 7, Table 2). Interestingly, cyclohex-2-enyl acetate becomes the only allylic oxidation product if (1,10-phenanthroline)Pd(OAc)<sub>2</sub> or *bis*(oxazoline)Pd(OAc)<sub>2</sub><sup>11</sup> is used as the catalyst.

The reaction of bipyrimidine with Pd(OAc)<sub>2</sub> in CD<sub>3</sub>COOD forms (BPM)Pd(OAc)<sub>2</sub> (**1**) in quantitative yield after 30 minutes at room temperature, as monitored by <sup>1</sup>H NMR. A crystal structure for (BPM)Pd(OAc)<sub>2</sub>·H<sub>2</sub>O was obtained (Figure 1, CCDC634014). Heating (BPM)Pd(OAc)<sub>2</sub> with allylbenzene (10 eq) in CD<sub>3</sub>COOD at 80 °C for ~ 4 days affords [(BPM)Pd(η<sup>3</sup>-1-phenylallyl)]<sup>+</sup>(OAc)<sup>-</sup> (**2**), the product of allylic C-H activation, in ca. 89% yield (Scheme 1). Furthermore, the allylic C-H activation is irreversible, because neither olefin exchange nor deuterium incorporation into the allyl fragment is observed after heating **2** with *p*-allyltoluene in CD<sub>3</sub>COOD at 80 °C for 15 hours (Scheme 1). Similar irreversibility was also proposed for the sulfoxide-Pd(OAc)<sub>2</sub> system.<sup>8</sup>

**Figure 1.** X-ray crystallographic structure and the crystal packing of [(bipyrimidine)Pd(OAc)<sub>2</sub>·H<sub>2</sub>O] (CCDC634014)



**Scheme 1.**

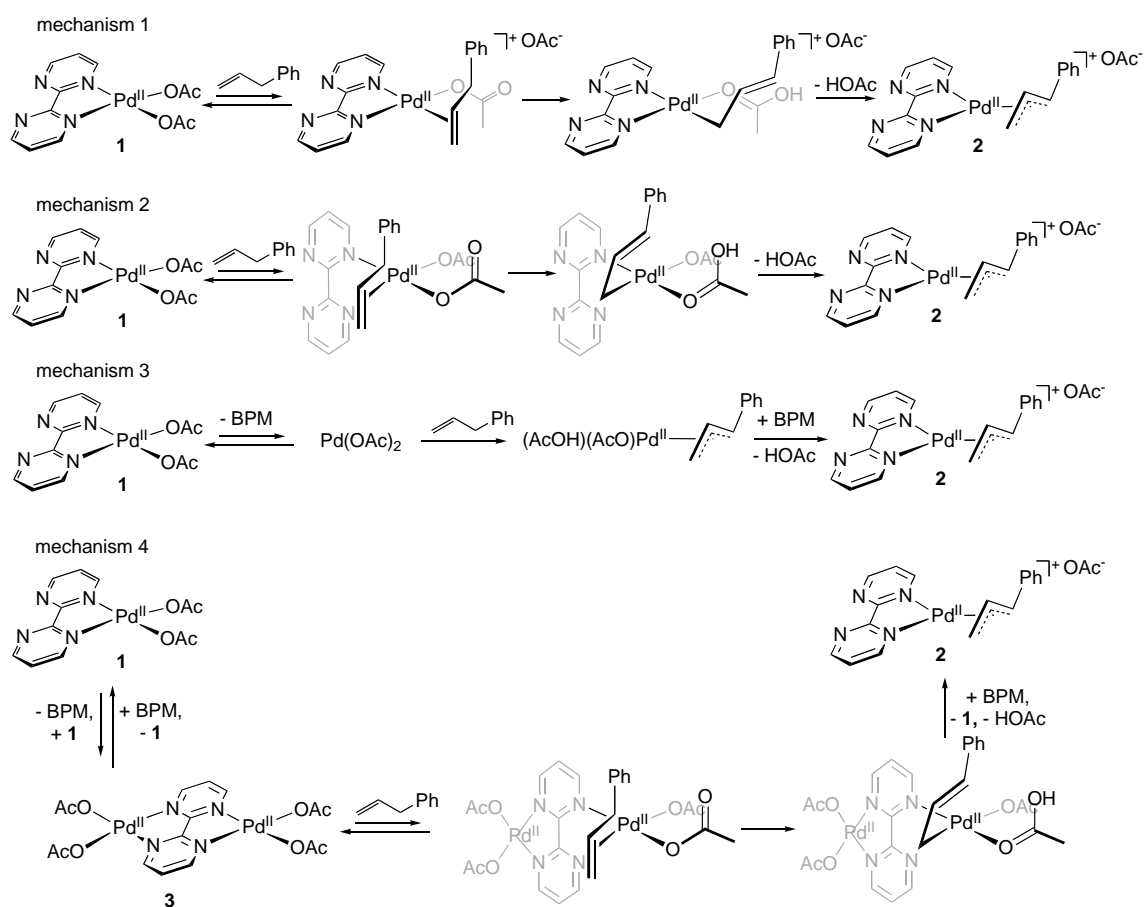
The reaction between allylbenzene and (BPM)Pd(OAc)<sub>2</sub> could occur via the displacement by the olefin of either an acetate or a coordinated BPM nitrogen to form a Pd(II)-olefin adduct, followed by allylic C-H activation to form **2** (mechanisms 1 and 2, Scheme 2). For either mechanism, addition of excess BPM should not have a significant effect on the reaction rate (a mixture of Pd(OAc)<sub>2</sub> and 1.15 eq. BPM in CD<sub>3</sub>COOD affords 1 eq. (BPM)Pd(OAc)<sub>2</sub> and 0.15 eq. free BPM (NMR)). However, no reaction is seen for allylbenzene or 1-decene when a slight excess ( $\leq 20$  mol% relative to Pd(OAc)<sub>2</sub>) of BPM is added (Scheme 3), clearly ruling out either mechanism for the acetoxylation.

Full dissociation of BPM from (BPM)Pd(OAc)<sub>2</sub>, forming Pd(OAc)<sub>2</sub> which then catalyzes the reaction, would be consistent with the inhibitory effect of excess BPM (mechanism 3, Scheme 2); but this is also unlikely to be the mechanism because Pd(OAc)<sub>2</sub> does not lead to selective allylic oxidation under current catalytic conditions (Entry 1, Table 1). The nonselective oxidation catalyzed by Pd(OAc)<sub>2</sub> must originate in the allylic C-H activation of allylbenzene by Pd(OAc)<sub>2</sub> rather than a subsequent step, because the solvolysis of  $[(\eta^3\text{-1-phenylallyl})\text{Pd}(\text{OAc})]_2$  in wet acetic acid at 75 °C

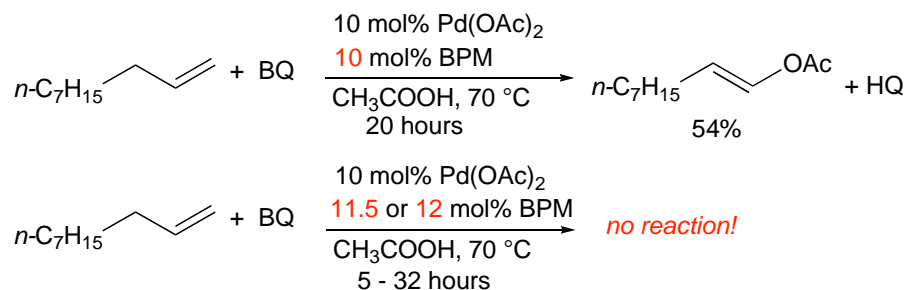


quantitatively forms allylic oxidation products (allylic acetates and cinnamaldehyde; the latter results from water as the nucleophile).<sup>12</sup>

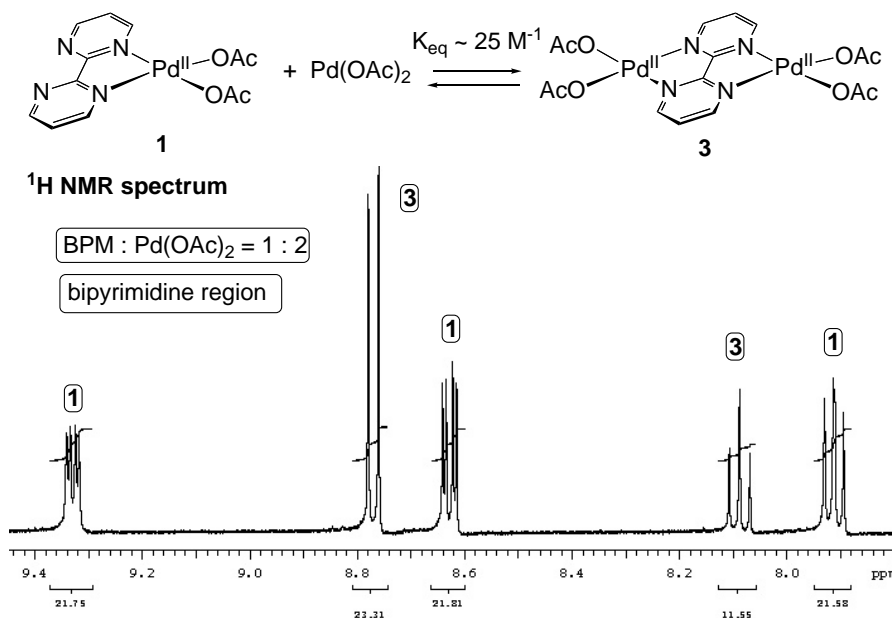
**Scheme 2.**



**Scheme 3.**



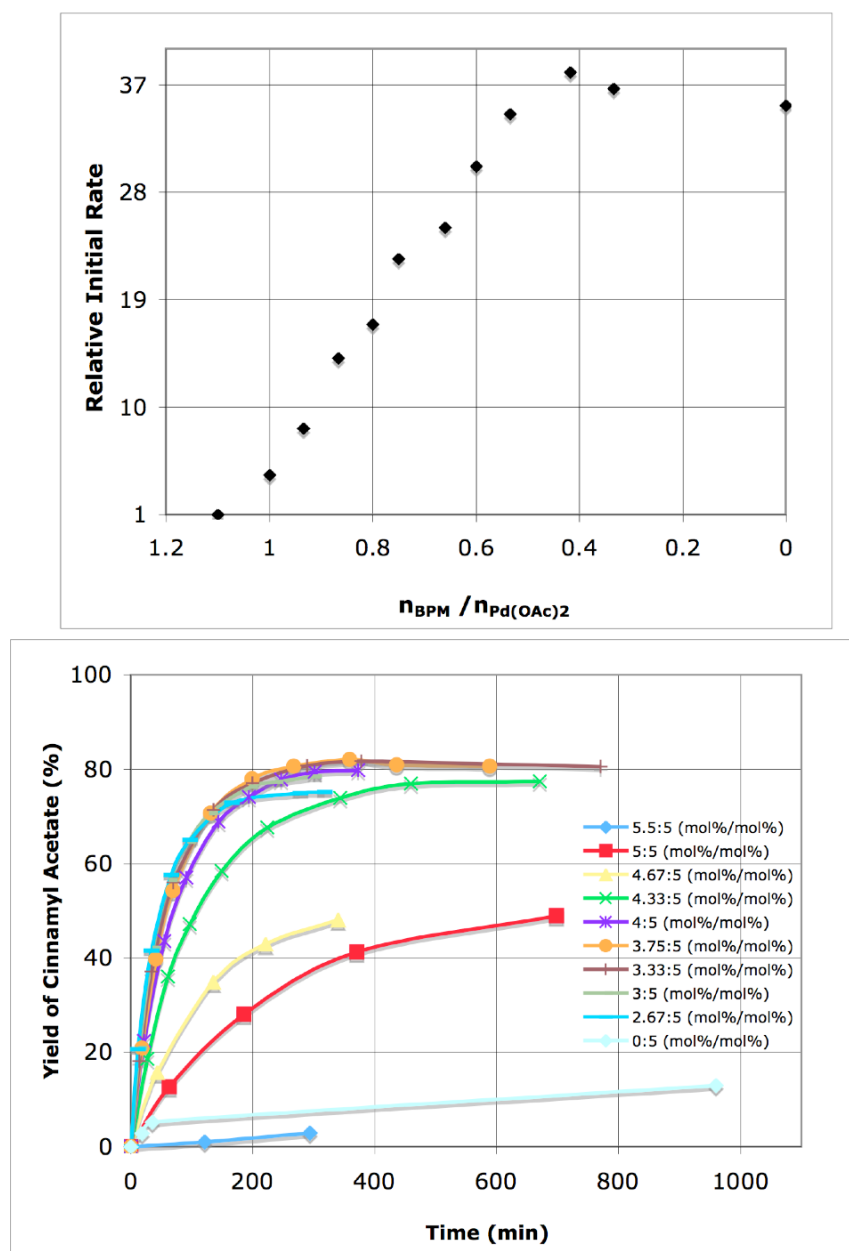
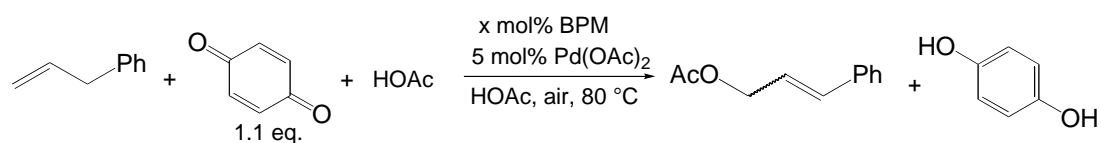
Scheme 4.



In a further experiment, a mixture of (BPM)Pd(OAc)<sub>2</sub> and Pd(OAc)<sub>2</sub> in CD<sub>3</sub>COOD (generated *in situ* by combining Pd(OAc)<sub>2</sub> and BPM in a 2:1 ratio) reacts to form a new species, characterized by <sup>1</sup>H NMR and MALDI as the BPM-bridged Pd(OAc)<sub>2</sub> dimer **3** (Scheme 4). The reaction does not reach 100% conversion, but equilibrates with  $K_{eq} \sim 25 \text{ M}^{-1}$ , as estimated by <sup>1</sup>H NMR. (The equilibrium constant is nearly temperature independent according to variable-temperature NMR from room temperature to 100 °C.) The resultant mixture reacts with allylbenzene under air *at room temperature* to form an  $\eta^3$ -allyl species, cinnamyl acetate, and palladium black.

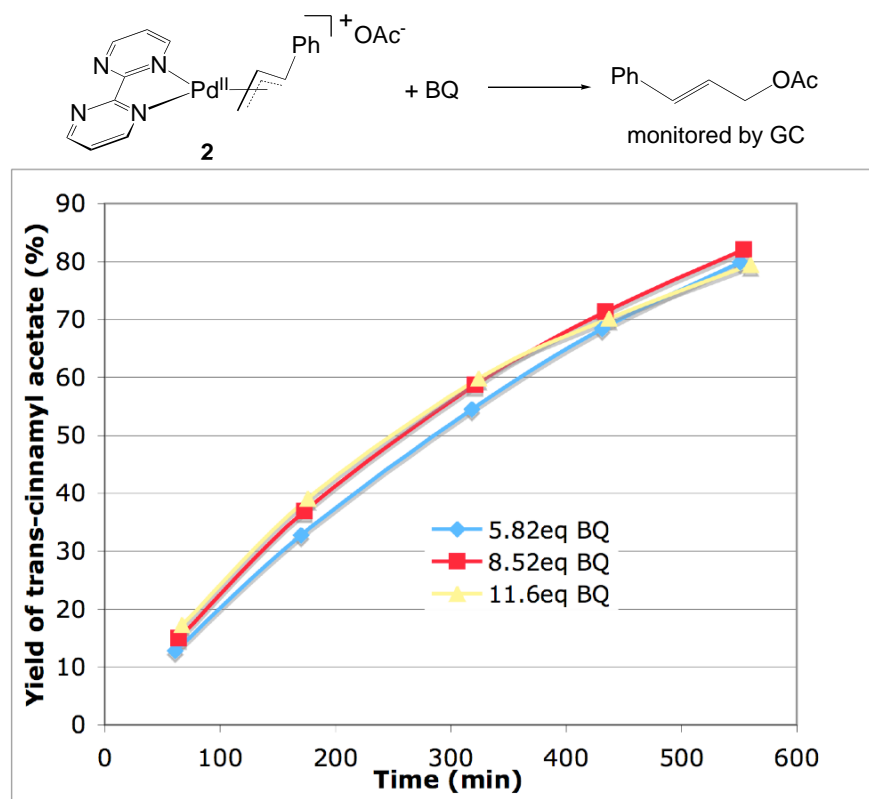
We propose that dimer **3** is the active species for the reaction with allylbenzene, because the Pd(OAc)<sub>2</sub>-only system results in less selective oxidation of allylbenzene, while heating is required for the reaction between (BPM)Pd(OAc)<sub>2</sub> and allylbenzene. According to our proposal, in the latter reaction small amounts of dimer and free BPM

**Figure 2.** Effect of BPM to Pd(OAc)<sub>2</sub> ratio on allylic oxidation of allylbenzene by benzoquinone, Pd(OAc)<sub>2</sub> fixed to be 5 mol%. Top: initial rates of the disappearance of allylbenzene relative to that of n(BPM)/n(Pd) = 1.1; bottom: appearance of cinnamyl acetate.



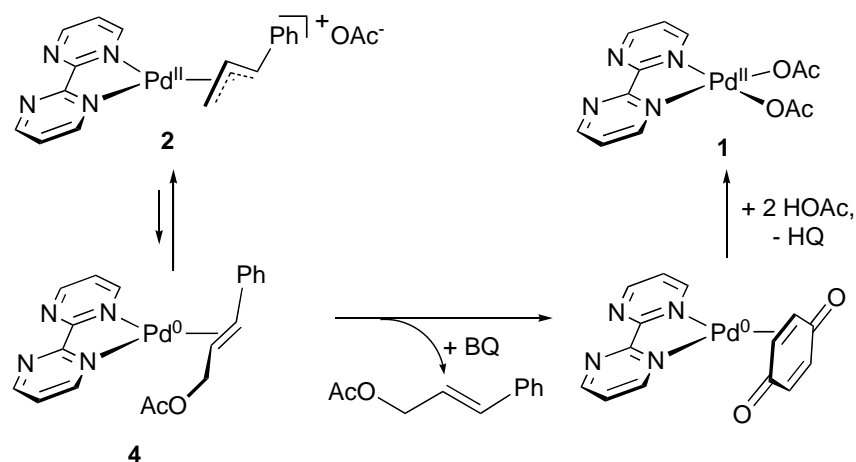
are formed via disproportionation of  $(\text{BPM})\text{Pd}(\text{OAc})_2$ , explaining the inhibition by excess BPM. The coordination of a second equivalent of  $\text{Pd}(\text{OAc})_2$  to BPM would be expected to weaken a Pd-N bond and thus facilitate the coordination of olefin; the Pd-olefin adduct subsequently undergoes allylic C-H activation to form **2** (mechanism 4, Scheme 2). This mechanism is further supported by the observation that the initial consumption rate of allylbenzene increases as the ratio of BPM to  $\text{Pd}(\text{OAc})_2$  decreases; the best overall yields ( $\sim 82\%$ ) were obtained by combining 3–4 mol% BPM with 5 mol%  $\text{Pd}(\text{OAc})_2$  (Figure 2).

**Figure 3.** Oxidation of  $(\eta^3\text{-allyl})\text{Pd}^{\text{II}}$  by benzoquinone is independent of the concentration of benzoquinone



Although **2** is stable in  $\text{CD}_3\text{COOD}$  at  $80\text{ }^\circ\text{C}$ , the addition of benzoquinone (BQ) releases cinnamyl acetate<sup>13</sup> and generates  $(\text{BPM})\text{Pd}(\text{OAc})_2$  and hydroquinone (HQ). It has been proposed that coordination of benzoquinone to  $\text{Pd}^{\text{II}}$  induces acetate attack,<sup>8, 14</sup> but we find that the rate of the reaction between **2** and benzoquinone in acetic acid is independent of the benzoquinone concentration when at least 5.8 equivalents are used (Figure 3), which argues against this mechanism.

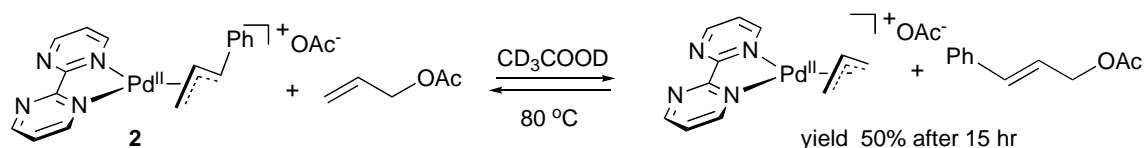
**Scheme 5.**



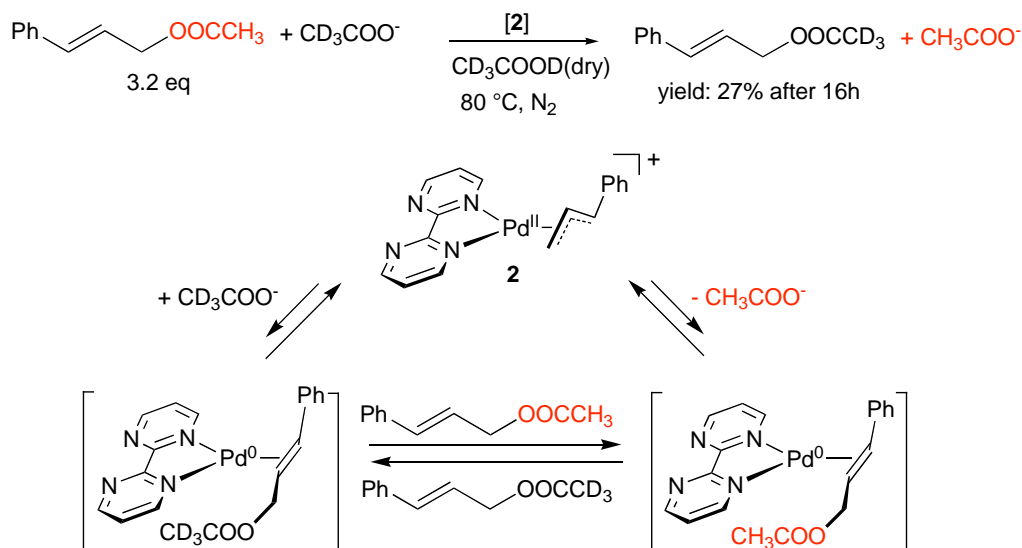
Instead, we believe that reversible attack of acetate at the  $\eta^3$ -allyl moiety<sup>15</sup> occurs in the absence of benzoquinone to form the (unobservable)  $\text{Pd}^0(\text{allyl acetate})$  species **4** (Scheme 5). Such a route is suggested by the reaction between allyl acetate and **2** in  $\text{CD}_3\text{COOD}$ , which generates cinnamyl acetate and  $[(\text{BPM})\text{Pd}(\eta^3\text{-propenyl})]^+(\text{OAc})^-$  (Scheme 6), and by the fact that **2** catalyzes exchange of labeled and unlabeled acetate between *trans*-cinnamyl acetate and  $\text{CD}_3\text{COOD}$  (Scheme 7).  $(\text{BPM})\text{Pd}^0(\text{cinnamyl acetate})$  complex **4** then reacts with BQ to release cinnamyl acetate and form  $(\text{BPM})\text{Pd}^0(\text{BQ})$ ,<sup>16</sup>

followed by a redox reaction with acetic acid to generate (BPM)Pd(OAc)<sub>2</sub> and hydroquinone (HQ) to complete the catalytic cycle (Scheme 5).

**Scheme 6.**



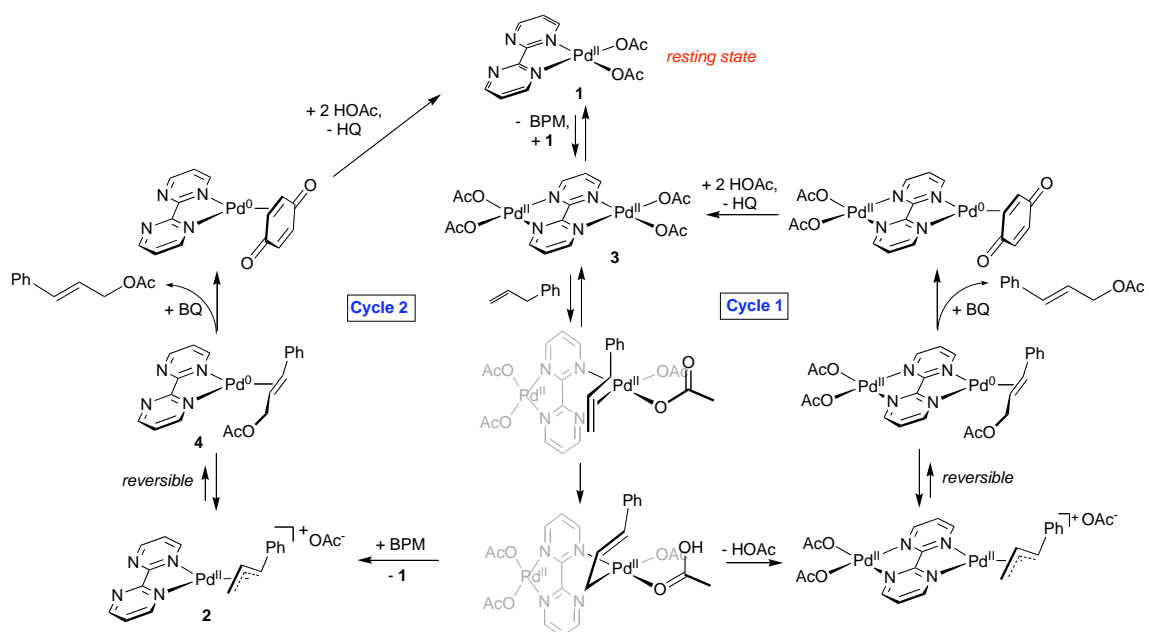
**Scheme 7.**



Scheme 8 shows a mechanism consistent with all current observations. Allylic C-H activation of allylbenzene by dimer **3** leads to a dimeric ( $\eta^3$ -allyl)Pd<sup>II</sup> complex, which can react either with benzoquinone to release cinnamyl acetate and regenerate the active dimer **3** (cycle 1), or with free BPM (generated from the disproportionation) to form the

monomeric ( $\eta^3$ -allyl)Pd<sup>II</sup> **2**, followed by reaction with benzoquinone to release cinnamyl acetate and regenerate (BPM)Pd(OAc)<sub>2</sub> (cycle 2). (We assume that the mechanistic inferences from the stoichiometric reactions described above, which would be rigorously applicable only to the monomeric intermediates in cycle 2, most probably would be valid for the analogous dimeric intermediates of cycle 1 as well.)

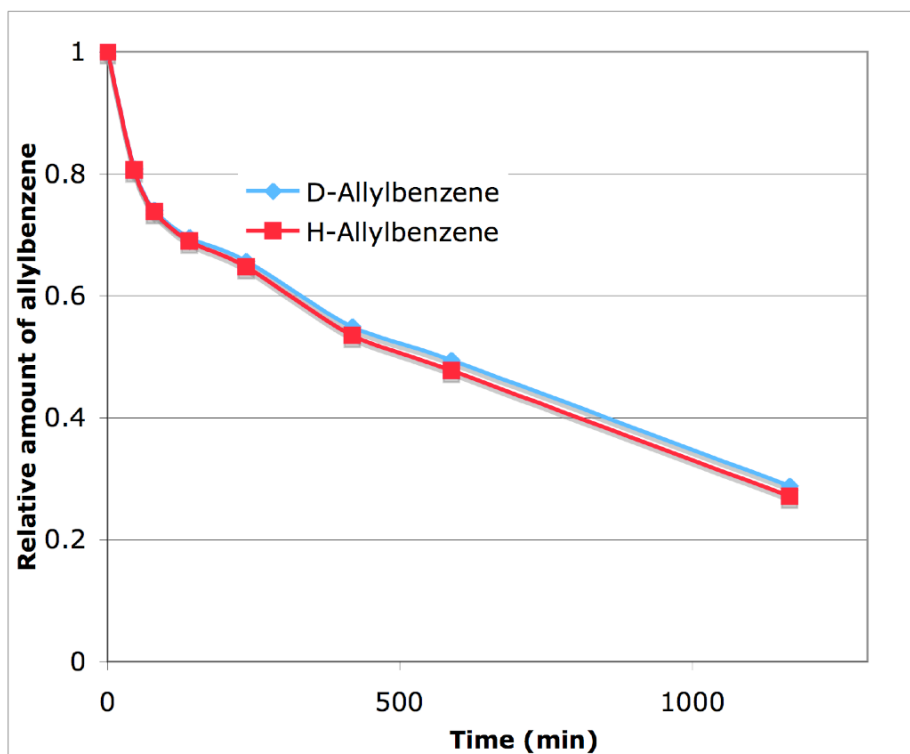
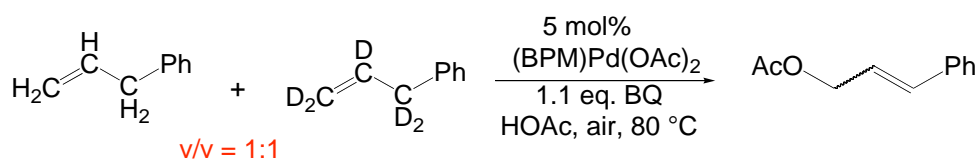
**Scheme 8.**



If cycle 2 is the dominant pathway, the rate-determining step for the whole catalytic cycle must occur before the formation of ( $\eta^3$ -allyl)Pd<sup>II</sup> because the only Pd species observed by <sup>1</sup>H NMR during the reaction is (BPM)Pd(OAc)<sub>2</sub>. In addition, the BPM inhibitory effect suggests a pre-equilibrium between (BPM)Pd(OAc)<sub>2</sub> and **3**. Therefore, either the olefin coordination or allylic C-H activation would be rate-determining. A

competition experiment using a 1:1 (v/v) ratio of allylbenzene- $d_0$  and allylbenzene- $d_5$  ( $\text{CD}_2=\text{CD}-\text{CD}_2-\text{C}_6\text{H}_5$ ) shows no kinetic isotope effect for the consumption rate of allylbenzene (Figure 4), suggesting olefin coordination rather than C-H activation is rate-determining.

**Figure 4.** No significant KIE is observed for competition reaction between allylbenzene- $d_0$  and allylbenzene- $d_5$



However, if cycle 1 is the dominant pathway, we cannot rule out the possibility that acetate attack on the dimeric  $(\eta^3\text{-allyl})\text{Pd}^{\text{II}}$  complex is rate-determining. In that case the



dimeric ( $\eta^3$ -allyl)Pd<sup>II</sup> complex would be the major species *within* the actual catalytic cycle, but it could still be unobservable if the equilibrium between **1** and **3** strongly favors the former. Since at present we do not know which cycle is dominant, we cannot conclusively identify the rate-determining step.

### 3. Conclusions

In summary, we have reported (BPM)Pd(OAc)<sub>2</sub> as a well-defined new catalyst for allylic C-H oxidation of olefins. Mechanistic studies have provided insight to understand the catalysis and led to further improvement of the reaction yield for the oxidation of allylbenzene. More studies are underway to explore the potential of the dimeric species and its derivatives in catalytic allylic C-H oxidations.

### Experimental Section

All starting materials are commercially available and used as received without any further purification. [ $(\eta^3$ -1-phenylallyl)PdCl]<sub>2</sub><sup>17</sup> and [ $(\eta^3$ -1-phenylallyl)Pd(OAc)]<sub>2</sub><sup>12</sup> were synthesized according to literature procedures. Allylbenzene-*d*<sub>5</sub> (C<sub>6</sub>H<sub>5</sub>CD<sub>2</sub>CD=CD<sub>2</sub>) was synthesized by a modified literature procedure<sup>18</sup> where allyl bromide-*d*<sub>5</sub> was used instead of allyl bromide-*d*<sub>0</sub>. Unless otherwise noted, all manipulations were carried out in air. <sup>1</sup>H and <sup>13</sup>C NMR spectra were recorded at room temperature on Varian Mercury 300 (<sup>1</sup>H, 299.8 MHz, <sup>13</sup>C, 125.9 MHz) spectrometers. NMR spectra were referenced to residual solvent peak (CDCl<sub>3</sub>, <sup>1</sup>H, 7.26 ppm, <sup>13</sup>C, 77.23 ppm; CD<sub>3</sub>COOD, <sup>1</sup>H, 2.04 ppm) and

reported in parts per million (ppm). Multiplicities were reported as follows: singlet (s), doublet (d), doublet of doublets (dd), doublet of triplets (dt), triplet (t), quartet (q), multiplet (m), and broad resonance (br). GC measurements were taken on an Agilent 6890 series GC instrument with an Agilent HP-5 column. The X-ray structure was obtained at Caltech X-ray Crystallography Laboratory. High-resolution mass spectra were obtained at Caltech Mass Spectrometry Laboratory. Reaction yields are corrected for the purities of the starting materials.

### **(Bipyrimidine)Pd(OAc)<sub>2</sub> (1)**

A solution of 25 mg Pd(OAc)<sub>2</sub> and 17.8 mg bipyrimidine (BPM) in 4.5 ml glacial acetic acid was stirred for 30 minutes, resulting in a clear yellow solution. After removing the solvent under vacuum (BPM)Pd(OAc)<sub>2</sub> (**1**) was obtained as a yellow powder, pure enough for NMR analyses. A yellow crystal of [(BPM)Pd(OAc)<sub>2</sub>·H<sub>2</sub>O] was obtained by slow evaporation of a chloroform solution of a 1:1:1 mixture of BPM, Pd(OAc)<sub>2</sub>, and acetic acid under air. (CCDC634014) <sup>1</sup>H NMR (CDCl<sub>3</sub>) δ 9.20 (dd, 2H, <sup>3</sup>J<sub>HH</sub> 4.8 Hz, <sup>4</sup>J<sub>HH</sub> 2.2 Hz), 8.68 (dd, 2H, <sup>3</sup>J<sub>HH</sub> 5.7 Hz, <sup>4</sup>J<sub>HH</sub> 2.2 Hz), 7.73 (dd, 2H, <sup>3</sup>J<sub>HH</sub> 5.7 Hz, 4.8 Hz), 2.13 (s, 6H); <sup>13</sup>C NMR (CDCl<sub>3</sub>) δ 178.9, 160.5, 157.6, 124.2, 23.3; HRMS (FAB+) *m/z* calcd for C<sub>10</sub>H<sub>9</sub>N<sub>4</sub>O<sub>2</sub>Pd<sup>+</sup> (M-OAc)<sup>+</sup> 322.9796, found 322.9774.

### **Oxidant Screening**

A few oxidants were screened for the reaction with allylbenzene. As shown in Table 3, increasing the loading of benzoquinone from 1 equivalent to 2 equivalents only slightly improves the reaction yield. The employment of phenylbenzoquinone leads to slower reactions with the selectivity of allylic oxidation similar to those of benzoquinone. Considering the higher cost of phenylbenzoquinone relative to benzoquinone, the latter

appears to be a better choice for the reactions. Several inorganic oxidants that can be recycled by dioxygen or air, such as  $\text{MnO}_2$  and  $\text{Cu}(\text{OAc})_2$ , also lead to catalyses. Unfortunately, the selectivity and the reaction rate are both worse than those of benzoquinone.

**Table 3.** Oxidant effects<sup>a</sup>

Oxidant	Yield <sup>c</sup>	Conversion <sup>c</sup>	Selectivity <sup>c</sup>
1 eq. BQ	70.5%	100%	70.5%
1.5 eq. BQ	71.1%	100%	71.1%
2 eq. BQ	72.5%	100%	72.5%
1 eq. PhBQ	66.2%	82.1%	80.6%
1.5 eq. PhBQ	68.9%	86.8%	79.4%
1 eq. $\text{MnO}_2$	41.0%	92.9%	44.1%
1 eq. $\text{MnO}_2^f$	0%	81.0%	0%
1 eq. $\text{CuCl}_2$	3.9%	23.7%	16.5%
1 eq. $\text{Cu}(\text{OAc})_2 \cdot \text{H}_2\text{O}$	34.8%	55.1%	63.2%
1 eq. $\text{Cu}(\text{OAc})_2 \cdot \text{H}_2\text{O}^f$	42.7%	74.1%	57.6%

a. General procedure: A mixture of 0.7 ml solution of  $(\text{BPM})\text{Pd}(\text{OAc})_2$  in  $\text{CH}_3\text{COOH}$  (10 mol%), 29.5  $\mu\text{l}$  allylbenzene, oxidant, and 20  $\mu\text{l}$  nitrobenzene (GC internal standard) is stirred and heated in a sealed vial at 80 °C for 16 hours. b. 24 hours at 80 °C without nitrobenzene. c. Conversions and yields are estimated according to the GC titration curve obtained from standard solutions. d. A mixture of 10 mol%  $(\text{BPM})\text{Pd}(\text{OAc})_2$ , 1.0 ml  $\text{CH}_3\text{COOH}$ , 50  $\mu\text{l}$  toluene and 29.5  $\mu\text{l}$  allylbenzene is stirred and heated under 1 atmosphere of  $\text{O}_2$  at 80 °C for 24 hours. e. Conversions and yields are estimated by NMR spectroscopy. f. A mixture of 0.6 ml solution of  $(\text{BPM})\text{Pd}(\text{OAc})_2$  in  $\text{CH}_3\text{COOH}$  (10 mol%), 0.6 ml  $\text{Ac}_2\text{O}$ , 29.5  $\mu\text{l}$  allylbenzene, oxidant, and 20  $\mu\text{l}$  nitrobenzene (GC internal standard) is stirred and heated in a sealed vial at 100 °C for 24 hours.

### Solvent Screening

The effect of various solvents on the oxidation of allylbenzene by benzoquinone catalyzed by 10 mol% (BPM)Pd(OAc)<sub>2</sub> at 80 °C has been investigated, as shown in Table 4. In general, an equal volume of acetic acid and cosolvent were mixed together with a known amount of nitrobenzene as the GC internal standard. After 24 hours, only the allylbenzene of the reaction with neat acetic acid or with water cosolvent has been fully consumed. The former gives a 70.3% yield of *trans*-cinnamyl acetate, which is better than

**Table 4.** Solvent effects at 80 °C<sup>a</sup>

Co-solvent	ε	Yield <sup>b</sup>	Conversion <sup>b</sup>	Selectivity <sup>b</sup>
Acetic Acid	6.2	70.3%	100%	70.3%
Benzene	2.3	67.3%	83.2%	80.9%
Toluene	2.4	62.6%	77.8%	80.5%
Ethyl Acetate	6.0	22.5%	26.9%	84.8%
DMA	37.8	11.9%	46.0%	25.9%
Acetic Anhydride	21.0	18.7%	29.5%	63.4%
DMSO	47	17.4%	58.2%	29.9%
<i>p</i> -Dioxane	2.21	31.2%	36.9%	84.6%
CHCl <sub>3</sub> <sup>c</sup>	4.81	64.8%	83.1%	78.0%
H <sub>2</sub> O	78.54	0%	100%	0%
EtOH	24.6	29.0%	88.3%	32.8%
CH <sub>3</sub> CN	37.5	19.9%	62.1%	32.0%
CH <sub>3</sub> NO <sub>2</sub>	39.4	21.1%	50.6%	41.7%

a. General procedure: A mixture of 0.6 ml solution of (BPM)Pd(OAc)<sub>2</sub> in CH<sub>3</sub>COOH (10 mol%), 0.6 ml co-solvent, 29.5 ul allylbenzene, 24.6 mg BQ, and 20 ul nitrobenzene (GC internal standard) is stirred and heated in a sealed vial at 80 °C for 24 hours. b. Conversions and yields are estimated according to the GC titration curve obtained from standard solutions. c. CHCl<sub>3</sub>, which contains EtOH as the stabilizer, is used as received.

all the reactions with cosolvent. However, high selectivity for the formation of cinnamyl acetate is observed for reactions with benzene, toluene, chloroform, ethyl acetate, and *p*-dioxane as the cosolvent, although less 40% of allylbenzene has been consumed for the latter three after 24 hours. Interestingly, all these solvents have dielectric constants less than that of acetic acid (6.2), which seems to suggest that allylic oxidation is favored by nonpolar solvents. Yields of cinnamyl acetate for reactions with polar solvents (acetic anhydride, EtOH, CH<sub>3</sub>CN, DMA, CH<sub>3</sub>NO<sub>2</sub>, DMSO, H<sub>2</sub>O) are mostly less than 40%. Reaction with water does not lead to any product of allylic oxidation. Wacker oxidation might be dominant, due to either nucleophile or solvent polarity change.

**Table 5.** Solvent effects at 100 °C<sup>a</sup>

Co-solvent	Yield <sup>b</sup>	Conversion <sup>b</sup>	Selectivity <sup>b</sup>
Acetic Acid	39.5%	100%	39.5%
Benzene	48.6%	100%	48.6%
Toluene	45.5%	100%	45.5%
Ethyl Acetate	43.6%	79.3%	55.0%
DMA	15.2%	71.5%	21.3%
Acetic Anhydride	41.9%	80.9%	51.8%

a. General procedure: A mixture of 0.6 ml solution of (BPM)Pd(OAc)<sub>2</sub> in CH<sub>3</sub>COOH (10 mol%), 0.6 ml co-solvent, 29.5 ul allylbenzene, 24.6 mg BQ, and 20 ul nitrobenzene (GC internal standard) is stirred and heated in a sealed vial at 100 °C for 24 hours. b. Conversions and yields are estimated according to the GC titration curve obtained from standard solutions.

Reactions with various cosolvents were also run at 100 °C for 24 hours. No reaction leads to a yield of cinnamyl acetate greater than 50% (Table 5).

### Effects of Acid and Base Additives

Addition of catalytic amounts of NaOAc leads to slower reactions and also reduces the selectivity of allylic oxidation. On the other hand, no allylic oxidation product was observed if  $\text{HBF}_4/\text{H}_2\text{O}$  is added to the reaction mixture. Olefin isomerization becomes the dominant reaction pathway.

**Table 6.** Acid-base effects<sup>a</sup>

Additive	Yield <sup>b</sup>	Conversion <sup>b</sup>	Selectivity <sup>b</sup>
no	70.3%	100%	70.3%
5 mol% NaOAc	58.0%	92.7%	62.6%
15 mol% NaOAc	58.0%	83.3%	69.6%
20 mol% NaOAc	48.2%	81.9%	58.9%
25 mol% NaOAc	52.5%	82.8%	63.4%
10 mol% $\text{HBF}_4/\text{H}_2\text{O}$	0%	70%	0%
20 mol% $\text{HBF}_4/\text{H}_2\text{O}$	0%	70%	0%

a. General procedure: A mixture of 1.2 ml solution of  $(\text{BPM})\text{Pd}(\text{OAc})_2$  in  $\text{CH}_3\text{COOH}$  (10 mol%), 29.5  $\mu\text{l}$  allylbenzene, 24.6 mg BQ, and the additive is stirred and heated at 80 °C in a sealed vial for 24 hours. b. Conversions and yields are estimated by NMR spectroscopy.

### General procedure for allylic oxidation (Entries 1, 2, 3, 5, and 6 of Table 2)

A solution of 25 mg  $\text{Pd}(\text{OAc})_2$  and 17.6 mg BPM in 4.5 ml glacial acetic acid was stirred for ~ 30 minutes, followed by sequential additions of 10 equivalents of olefin and 20 equivalents of benzoquinone. The mixture was heated at 70 °C with stirring, in a 20

ml glass vial sealed with a Teflon-lined cap and PTFE tape. After the reported time, the reaction mixture was cooled to room temperature in a water bath and neutralized with 50 ml of an aqueous solution of 6.2 g NaOH. The resultant mixture was extracted with 3x100 ml CH<sub>2</sub>Cl<sub>2</sub>. Organic portions were combined and dried over MgSO<sub>4</sub>. Volatiles were removed under vacuum. The resultant oil was further purified by flash silica gel column chromatography.

***trans*-Cinnamyl acetate (Entry 1, Table 2)**

Allylbenzene: 98% pure. Reaction time: 34 hours. Eluent: 1:10 (v/v) EtOAc/hexanes. The product was isolated as a mixture of *cis* and *trans* isomers. Mass: 146 mg; overall yield: 76%; NMR yield of the *trans* isomer: 72%. <sup>1</sup>H NMR (CDCl<sub>3</sub>) δ 7.20–7.45 (m, 5H), 6.60–6.71 (d, 1H, <sup>3</sup>J<sub>HH</sub> 15.9 Hz), 6.24–6.35 (dt, 1H, <sup>3</sup>J<sub>HH</sub> 15.9 Hz, 6.6 Hz), 4.71–4.76 (dd, 2H, <sup>3</sup>J<sub>HH</sub> 6.6 Hz, <sup>4</sup>J<sub>HH</sub> 1.3 Hz), 2.11 (s, 3H); <sup>13</sup>C NMR (CDCl<sub>3</sub>) δ 171.1, 136.4, 134.4, 128.9, 128.3, 126.9, 123.4, 65.3, 21.3; HRMS (FAB+) *m/z* calcd for C<sub>11</sub>H<sub>12</sub>O<sub>2</sub> 176.0837, found 176.0832.

***trans-p*-Methylcinnamyl acetate (entry 2, Table 2)**

*p*-Allyltoluene: 99% pure. Reaction time: 32 hours 46 minutes. Eluent: 1:10 (v/v) EtOAc/hexanes. The product was isolated as a mixture of *cis* and *trans* isomers. Mass: 165 mg; overall yield: 78%; NMR yield of the *trans* isomer: 75%. <sup>1</sup>H NMR (CDCl<sub>3</sub>) δ 7.26–7.32 (d, 2H, <sup>3</sup>J<sub>HH</sub> 8.1 Hz), 7.10–7.17 (d, 2H, <sup>3</sup>J<sub>HH</sub> 8.1 Hz), 6.58–6.68 (d, 1H, <sup>3</sup>J<sub>HH</sub> 15.9 Hz), 6.18–6.30 (dt, 1H, <sup>3</sup>J<sub>HH</sub> 15.9 Hz, 6.6 Hz), 4.68–4.76 (dd, 2H, <sup>3</sup>J<sub>HH</sub> 6.6 Hz, <sup>4</sup>J<sub>HH</sub> 1.3 Hz), 2.35 (s, 3H), 2.10 (s, 3H); <sup>13</sup>C NMR (CDCl<sub>3</sub>) δ 171.1, 138.2, 134.5, 133.6, 129.6, 126.8, 122.3, 65.5, 21.5, 21.3; HRMS (FAB+) *m/z* calcd for C<sub>12</sub>H<sub>14</sub>O<sub>2</sub> 190.0994, found 190.0995.

***trans-p*-Methoxycinnamyl acetate (Entry 3, Table 2)**

*p*-Methoxyallylbenzene: 98% pure. Reaction time: 16 hours. Eluent: 1.5:10 (v/v) EtOAc/hexanes. The product was isolated as a mixture of *cis* and *trans* isomers. Mass: 118 mg; overall yield: 53%; NMR yield of the *trans* isomer: 50%. <sup>1</sup>H NMR (CDCl<sub>3</sub>) δ 7.30–7.36 (d, 2H, <sup>3</sup>J<sub>HH</sub> 8.4 Hz), 6.82–6.89 (d, 2H, <sup>3</sup>J<sub>HH</sub> 8.4 Hz), 6.55–6.64 (d, 1H, <sup>3</sup>J<sub>HH</sub> 15.3 Hz), 6.10–6.21 (dt, 1H, <sup>3</sup>J<sub>HH</sub> 15.3 Hz, 6.6 Hz), 4.66–4.74 (dd, 2H, <sup>3</sup>J<sub>HH</sub> 6.6 Hz, <sup>4</sup>J<sub>HH</sub> 1.3 Hz), 3.80 (s, 3H), 2.09 (s, 3H); <sup>13</sup>C NMR (CDCl<sub>3</sub>) δ 171.2, 159.8, 134.3, 129.2, 128.1, 121.0, 114.2, 65.6, 55.5, 21.3; HRMS (FAB+) *m/z* calcd for C<sub>12</sub>H<sub>14</sub>O<sub>3</sub> 206.0943, found 206.0952.

**1-Acetoxy-*trans*-2-decene (Entry 5, Table 2)**

Reaction time: 20 hours. Eluent: 1:10 (v/v) EtOAc/hexanes. The product was isolated as a mixture of allylic acetates along with (1-acetoxy-)3-, 4- and 5-decenes. Both <sup>1</sup>H NMR and GC gave the estimated ratio of allylic acetates (sum of *trans*-primary allylic acetate, *cis*-primary allylic acetate, and secondary allylic acetate) to other isomers to be ~ 3.8. Only 1-acetoxy-*trans*-2-decene was fully characterized. Mass: 171 mg; overall yield: 78%; NMR yield of 1-acetoxy-*trans*-2-decene: 54%. <sup>1</sup>H NMR (CDCl<sub>3</sub>) δ 5.70–5.83 (m, 1H), 5.49–5.62 (m, 1H), 4.47–4.53 (dd, 2H, <sup>3</sup>J<sub>HH</sub> 6.6 Hz, <sup>4</sup>J<sub>HH</sub> 1 Hz), 2.06 (s, 3H), 1.92–2.08 (m, 2H), 1.27 (br s, 10H), 0.87 (t, 3H, <sup>3</sup>J<sub>HH</sub> 6.9 Hz); <sup>13</sup>C NMR (CDCl<sub>3</sub>) δ 171.1, 137.0, 123.9, 65.6, 32.5, 32.0, 29.6, 29.3, 29.1, 22.9, 21.3, 14.3; HRMS (FAB+) *m/z* calcd for C<sub>12</sub>H<sub>14</sub>O<sub>2</sub> 198.1620, found 198.1625.

**1-Acetoxy-3-cyclohexyl-*trans*-2-propene (Entry 6, Table 2)**

Allylcyclohexane: 96% pure. Reaction time: 20 hours. Eluent: 1:10 (v/v) EtOAc/hexanes. The product was isolated as a mixture of allylic acetates,



3-cyclohexylidenepropyl acetate and 3-cyclohexenylpropyl acetates. The ratio of allylic acetates (sum of *trans*-primary allylic acetate, *cis*-primary allylic acetate, and secondary allylic acetate) to other isomers was estimated to be  $\sim 6.2$  by  $^1\text{H}$  NMR and GC. Only 1-acetoxy-3-cyclohexyl-*trans*-2-propene was fully characterized. Mass: 150 mg, overall yield: 77%, NMR yield of 1-acetoxy-3-cyclohexyl-*trans*-2-propene: 65%.  $^1\text{H}$  NMR ( $\text{CDCl}_3$ )  $\delta$  5.66–5.75 (dd, 1H,  $^3J_{\text{HH}} \sim 15.6$  Hz, 6.3 Hz), 5.44–5.55 (dtd, 1H,  $^3J_{\text{HH}} 15.6$  Hz, 6.6 Hz,  $^4J_{\text{HH}} 1.1$  Hz), 4.46–4.52 (d, 2H,  $^3J_{\text{HH}} 6.6$  Hz), 2.05 (s, 3H), 1.84–2.05 (m, 1H), 0.94–1.79 (m, 10H);  $^{13}\text{C}$  NMR ( $\text{CDCl}_3$ )  $\delta$  171.1, 142.4, 121.5, 65.8, 40.6, 32.7, 26.3, 26.2, 21.3; HRMS (FAB+)  $m/z$  calcd for  $\text{C}_{11}\text{H}_{18}\text{O}_2$  182.1307, found 182.1313.

#### Allyl acetate (Entry 4, Table 2)

A 5 ml round-bottom flask was charged with 27.1 mg (BPM) $\text{Pd}(\text{OAc})_2$  (10 mol%), 153 mg BQ (2 eq), 20  $\mu\text{l}$  nitrobenzene, and 2.2 ml glacial acetic acid. 15.7 ml propylene (1 atm) was then condensed into the flask by liquid nitrogen after degassing. The mixture was stirred and heated at 70  $^\circ\text{C}$  for 24 hours. An aliquot of the reaction mixture was taken and filtered through a short pipette of silica gel with  $\text{Et}_2\text{O}$  as the eluent for GC analysis. The GC-peak area of allyl acetate relative to nitrobenzene was used to calculate the yield. Allyl acetate was the only allylic oxidation product observed by  $^1\text{H}$  NMR. GC Yield: 45%.

#### Cyclohexenyl acetates (Entry 7, Table 2)

The general procedure above was followed, except for the use of 20 equivalents of cyclohexene and 24 equivalents of benzoquinone, and heating at 80  $^\circ\text{C}$ . After 24 hours, the mixture was cooled to room temperature by water bath and neutralized by 6.2 g NaOH in 50 ml  $\text{H}_2\text{O}$ . The resultant mixture was extracted by 3x100 ml  $\text{CH}_2\text{Cl}_2$ . Organic

portions were combined and dried over  $\text{MgSO}_4$ . Volatiles were removed under vacuum. The resultant oil was further purified by reduced-pressure distillation. A  $\sim 2.8:1$  mixture of cyclohex-2-enyl acetate and cyclohex-3-enyl acetate was obtained. Mass: 160 mg; overall yield 51.3%. **Cyclohex-2-enyl acetate:**  $^1\text{H}$  NMR ( $\text{CDCl}_3$ )  $\delta$  5.87–5.98 (m, 1H), 5.63–5.73 (m, 1H), 5.18–5.27 (m, 1H), 2.03 (s, 3H), 1.53–2.45 (m, 6H);  $^{13}\text{C}$  NMR ( $\text{CDCl}_3$ )  $\delta$  171.0, 132.9, 125.9, 68.3, 28.5, 25.1, 21.6, 19.1; HRMS (FAB+)  $m/z$  calcd for  $\text{C}_8\text{H}_{12}\text{O}_2$  140.0837, found 140.0841. **Cyclohex-3-enyl acetate:**  $^1\text{H}$  NMR ( $\text{CDCl}_3$ )  $\delta$  5.62–5.67 (m, 1H), 5.51–5.60 (m, 1H), 4.93–5.03 (m, 1H), 2.03 (s, 3H), 1.53–2.45 (m, 6H);  $^{13}\text{C}$  NMR ( $\text{CDCl}_3$ )  $\delta$  171.0, 127.0, 123.9, 70.0, 30.9, 27.5, 23.5, 21.6.

**[(Bipyrimidine)Pd( $\eta^3$ -1-phenylallyl)] $^+(\text{OAc})^-$  (**2**)**

**Route 1:** A mixture of 8.6 mg (BPM)Pd(OAc) $_2$  and 29.5  $\mu\text{l}$  allylbenzene in 0.7 ml  $\text{CD}_3\text{COOD}$  was heated in a J-Young NMR tube under nitrogen at 80  $^\circ\text{C}$  for 96 hours. The yield of compound **2** based on Pd was 89%, as estimated by  $^1\text{H}$  NMR. **Route 2:** A 2:1 ratio of AgOAc (3.8 mg) and  $[(\eta^3\text{-1-phenylallyl})\text{PdCl}]_2$  (5.5 mg) was stirred in 1 ml acetone at room temperature for 30 minutes. After filtering off the precipitate, solvent was pumped away under vacuum. To the resultant yellow solid was added 3.6 mg BPM and 0.7 ml  $\text{CD}_3\text{COOD}$ .  $^1\text{H}$  NMR shows that  $[(\text{BPM})\text{Pd}(\eta^3\text{-1-phenylallyl})]^+(\text{OAc})^-$  was formed quantitatively. Unfortunately, compound **2** is not isolable due to rapid decomposition to Pd metal in the absence of acetic acid.  $^1\text{H}$  NMR ( $\text{CD}_3\text{COOD}$ )  $\delta$  9.24 (br s 4H), 7.78 (br s 2H), 7.46–7.82 (m, 5H), 6.59 (app dt, 1H,  $^3J_{\text{HH}}$  12.3 Hz, 7.2 Hz), 5.06 (d, 1H,  $^3J_{\text{HH}}$  12.3 Hz), 4.68 (d, 1H,  $^3J_{\text{HH}}$  7.2 Hz), 3.87 (d, 1H,  $^3J_{\text{HH}}$  12.3 Hz); HRMS (FAB+)  $m/z$  calcd for  $\text{C}_{17}\text{H}_{15}\text{N}_4\text{Pd}^+$  (M-OAc) $^+$  381.0332, found 381.0343.

**(Bipyrimidine)[Pd(OAc)<sub>2</sub>]<sub>2</sub> (3)**

3.6 mg BPM and 10 mg Pd(OAc)<sub>2</sub> (2 eq.) were mixed with 0.7 ml CD<sub>3</sub>COOD. A clear yellow solution was obtained after stirring for 2 hours. The solution contained an equilibrated mixture of Pd(OAc)<sub>2</sub>, (BPM)Pd(OAc)<sub>2</sub> (**1**), and (BPM)[Pd(OAc)<sub>2</sub>]<sub>2</sub> (**3**). The equilibrium constant was estimated to be  $\sim 25 \text{ M}^{-1}$  by <sup>1</sup>H NMR. NMR yield of compound **3** based on BPM: 35%. <sup>1</sup>H NMR (CD<sub>3</sub>COOD)  $\delta$  8.75 (d, 4H, <sup>3</sup>J<sub>HH</sub> 5.7 Hz), 7.78 (t, 2H, <sup>3</sup>J<sub>HH</sub> 5.7 Hz); MS (MALDI)  $m/z$  calcd for C<sub>16</sub>H<sub>18</sub>N<sub>4</sub>Pd<sub>2</sub><sup>+</sup> (M<sup>+</sup>) 605.919, found 605.7228.

**[(Bipyrimidine)Pd( $\eta^3$ -2-propenyl)]<sup>+</sup>(OAc)<sup>-</sup>**

To a solution of compound **1** in 0.7 ml CD<sub>3</sub>COOD was added 2.4  $\mu$ l allyl acetate (1 eq). After degassing, the solution was heated at 80 °C for 15 hours. According to the <sup>1</sup>H NMR spectrum,  $\sim 50\%$  of the starting material was converted to [(BPM)Pd( $\eta^3$ -2-propenyl)]<sup>+</sup>. <sup>1</sup>H NMR (CD<sub>3</sub>COOD)  $\delta$  9.32 (br s 4H), 7.99 (br s 2H), 6.03–6.19 (tt, 1H, <sup>3</sup>J<sub>HH</sub> 6.6 Hz, 12.6 Hz), 4.72–4.76 (dd, 2H, <sup>2</sup>J<sub>HH</sub> 1.3 Hz, <sup>3</sup>J<sub>HH</sub> 6.6 Hz), 3.60–3.72 (d, 2H, <sup>3</sup>J<sub>HH</sub> 12.6 Hz); HRMS (FAB+)  $m/z$  calcd for C<sub>11</sub>H<sub>11</sub>N<sub>4</sub>Pd<sup>+</sup> (M-OAc)<sup>+</sup> 305.0019, found 305.0044.

**Exchange between *trans*-cinnamyl acetate and CD<sub>3</sub>COOD**

A mixture of compound **2** and 10  $\mu$ l *trans*-cinnamyl acetate (3 eq.) in 0.7 ml CD<sub>3</sub>COOD was heated in a J-Young NMR tube under nitrogen at 80 °C. After 16 hours 5 minutes, 20% of the starting PhCH=CHCO<sub>2</sub>CH<sub>3</sub> was converted to PhCH=CHCO<sub>2</sub>CD<sub>3</sub>. No change of compound **2** was detected. Control experiments were carried out under similar conditions except that compound **2** was absent or replaced by an equimolar amount of NaOAc. In neither case was acetate scrambling detected by <sup>1</sup>H NMR.

### Competition between allylbenzene- $d_0$ and allylbenzene- $d_5$

A mixture of 4.3 mg (BPM)Pd(OAc)<sub>2</sub> (~ 5 mol%), 10  $\mu$ l nitrobenzene (internal standard), 15  $\mu$ l allylbenzene- $d_0$ , 15  $\mu$ l allylbenzene- $d_5$ , 25 mg BQ, and 0.35 ml CH<sub>3</sub>COOH was heated in a sealed vial with stirring at 80 °C. Aliquots (~ 5  $\mu$ l) were taken at certain times by microsyringe for GC analysis. The GC signals of allylbenzene- $d_0$  and allylbenzene- $d_5$  are fully separated, but those of the two isotopologs of trans-cinnamyl acetate are not.

### References

- (1) For examples see the following review: Eames, J.; Watkinson, M. *Angew. Chem.—Int. Ed.* **2001**, *40*, 3567–35571.
- (2) (a) Copper: Kharasch M. S.; Sosnovsky, G. *J. Am. Chem. Soc.* **1958**, *80*, 756. (b) Selenium: Umbreit M. A.; Sharpless, K. B. *J. Am. Chem. Soc.* **1977**, *99*, 5526–5528.
- (3) (a) Selective stoichiometric activation of allylic C-H bonds of olefins to form ( $\eta^3$ -allyl)Pd<sup>II</sup>: Trost, B. M.; Metzner, P. J. *J. Am. Chem. Soc.* **1980**, *102*, 3572–3577. (b) DMSO-promoted selective stoichiometric oxidation of 1-butene to but-2-enyl acetate: Kitching, W.; Rappoport, Z; Winstein, S.; Young, W. G. *J. Am. Chem. Soc.* **1966**, *88*, 2054–2055.
- (4) Pd-catalyzed selective oxidations of  $\alpha,\beta$ -enones (or ketals) to 1,4-enediones: Yu, J.-Q.; Corey E. J. *J. Am. Chem. Soc.* **2003**, *125*, 3232–3233.
- (5) (a) McMurry, J. E.; Kocovsky, P. *Tetrahedron Lett.* **1984**, *25*, 4187–4190. (b) Hansson, S.; Heumann, A.; Rein, T.; Akermark, B. *J. Org. Chem.* **1990**, *55*, 975–984. (c) Jia, C. G.; Müller, P.; Mimoun, H. *J. Mol. Catal. A—Chem.* **1995**, *101*, 127–136.

- (6) (a) Larock, R. C.; Hightower, T. R. *J. Org. Chem.* **1993**, *58*, 5298–5300. (b) Chen, M. S.; White, M. C. *J. Am. Chem. Soc.* **2004**, *126*, 1346–1347.
- (7) (a) Clark, D.; Hayden, P.; Smith, R. D. *Discuss. Faraday Soc.* **1968**, *46*, 98–109. (b) Mitsudome, T.; Umetani, T.; Nosaka, N.; Mori, K.; Mizugaki, T.; Ebitani, K.; Kaneda, K. *Angew. Chem.-Int. Edit.* **2006**, *45*, 481–485.
- (8) Chen, M. S.; Prabakaran, N.; Labenz, N. A.; White, M. C. *J. Am. Chem. Soc.* **2005**, *127*, 6970–6971.
- (9) Fraunhoffer, K. J.; White, M. C. *J. Am. Chem. Soc.* **2007**, *129*, 7274–7275.
- (10) Fraunhoffer, K. J.; Prabakaran, N.; Sirois, L. E.; White, M. C. *J. Am. Chem. Soc.* **2006**, *128*, 9032–9033.
- (11) Preliminary screening of the following enantiopure ligands at 60 °C did not, however, lead to significant enantioselectivity: (-)-sparteine, (4S)-Bz-Box, (4S)-<sup>t</sup>Bu-Box, and (S)-(-)-BINAP.
- (12) Kitching, W.; Sakakiyama, T.; Rappoport, Z.; Sleezer, P. D.; Winstein, S.; Young, W. G. *J. Am. Chem. Soc.* **1972**, *94*, 2329–2335.
- (13) A small amount of 1-phenylallyl acetate (~ 9%) is also formed during the reaction. More detailed mechanistic studies are underway to reconcile this observation with the proposed mechanism.
- (14) Bäckvall, J. E.; Nordberg, R. E.; Wilhelm, D. *J. Am. Chem. Soc.* **1985**, *107*, 6892–6898.
- (15) A similar equilibrium was also proposed for (PCy<sub>3</sub>)Pd(allyl)(OAc): Yamamoto, T.; Saito, O.; Yamamoto, A. *J. Am. Chem. Soc.* **1981**, *103*, 5600–5602.

- (16) (a) Mixing Pd(dba)<sub>2</sub>, BPM, and BQ in acetone forms (BPM)Pd(BQ): Klein, R. A.; Witte, P.; van Belzen, R.; Fraanje, J.; Goubitz, K.; Numan, M.; Schenk, H.; Ernsting, J. M.; Elsevier, C. J. *Eur. J. Inorg. Chem.* **1998**, 319–330. (b) BQ could be viewed as an electron-deficient olefin. For a detailed mechanistic study of olefin exchange on Pd<sup>0</sup>, see: Stahl, S. S.; Thorman, J. L.; de Silva, N.; Guzei, I. A.; Clark, R. W. *J. Am. Chem. Soc.* **2003**, *125*, 12–13.
- (17) Marion, N.; Navarro, O.; Mei, J.-G.; Stevens, E. D.; Scott, N. M.; Nolan, S. P. *J. Am. Chem. Soc.* **2006**, *128*, 4101–4111.
- (18) Ichihara, J. *Chem. Comm.* **1997**, 1921–1922.

## **Appendix A. Mechanistic Study of the One-Pot Synthesis of Methyl Acetate from a CH<sub>3</sub>OH/CH<sub>3</sub>CN Mixture with a Ru<sup>II</sup>-Sn<sup>II</sup> Bimetallic Complex as the Catalyst**

### **Abstract**

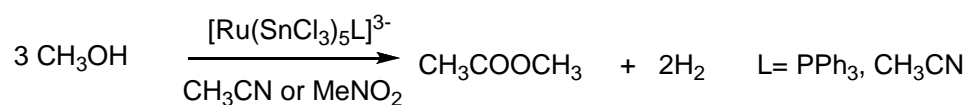
Mechanistic studies were performed for the one-pot synthesis of methyl acetate from a CH<sub>3</sub>OH/CH<sub>3</sub>CN mixture catalyzed by CpRu(PPh<sub>3</sub>)<sub>2</sub>(SnCl<sub>3</sub>). GC/MS analyses on two deuterium-labeled catalytic reactions indicate that the methyl acetate formed in the system developed by Gusevkava et al. is actually a product the hydrolysis of acetonitrile instead of the claimed transformation from methanol. The catalytic activity of SnCl<sub>2</sub>-only catalyst strongly suggests that those Ru-Sn bimetallic complexes simply serve as a source of SnCl<sub>2</sub>.

## 1. Introduction

Acetic acid is an important chemical commodity. Monsanto process is one of the major methods for the production of acetic acid. In this process, a  $\text{Rh}^{\text{I}}$  complex is employed as the catalyst with iodide as the additive for the carbonylation of methanol to form methyl acetate. Subsequent hydrolysis then transforms the methyl acetate to acetic acid. Because methanol is made from syngas ( $\text{CO}/\text{H}_2$ ), the only feedstock for this process is syngas.

In spite of the wide application of Monsanto process, it suffers from limitations such as the high cost of Rh catalyst and the extra cost to protect the production apparatus from the corrosive iodide additive. In the continuing effort to reduce the cost for the production process, a cheaper iridium-based catalyst has been developed by BP-Amoco. Nevertheless, practical catalytic systems in the absence of any corrosive additive are yet to emerge.

In 1990, Shinoda et al. reported that  $[\text{Ru}(\text{SnCl}_3)_5(\text{L})]^{3-}$  ( $\text{L} = \text{CH}_3\text{CN}$ ,  $\text{PPh}_3$ ) can catalyze the production of methyl acetate using methanol as the only starting material<sup>1</sup> (equation 1). In spite of the low turnover numbers reported (up to 15.7/100 h), these reactions still attract research attention due to the absence of corrosive additive. In a further study of several other Ru complexes by the same group, a catalytic activity following the order  $\text{RuCl}_2[\text{P}(\text{OMe})_3]_4 < \text{RuCl}(\text{SnCl}_3)[\text{P}(\text{OMe})_3]_4 < \text{Ru}(\text{SnCl}_3)_2[\text{P}(\text{OMe})_3]_4$  was observed, which suggests that the Ru-Sn functionality is crucial for the catalysis.<sup>2</sup>



equation (1)

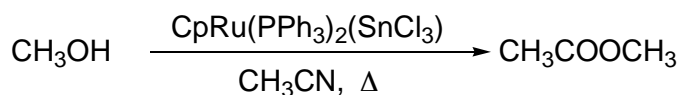


Based on similar Ru-Sn functional motifs, Gusevskaya et al. developed a series of  $\text{CpRu}(\text{PPh}_3)_2(\text{SnX}_3)$  complexes ( $\text{X}=\text{F}$ ,  $\text{Cl}$ , and  $\text{Br}$ ) that afford significantly improved catalytic efficiency (with TONs up to 120/40 h) for the transformation of methanol to methyl acetate in acetonitrile.<sup>3</sup> In these systems, a similar trend of catalytic activity was also observed between Ru-Sn bimetallic complexes and their monometallic Ru analogues.

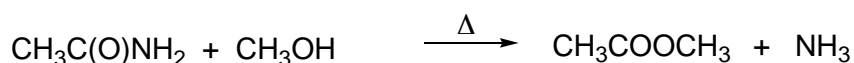
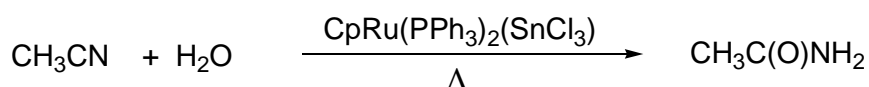
In order to further improve the catalytic efficiency, we decided to investigate the mechanism for Gusevkava's system. The most efficient catalyst reported so far,  $\text{CpRu}(\text{PPh}_3)_2(\text{SnCl}_3)$ , was chosen as the system for this investigation.<sup>4</sup> Methanol was claimed to be the only source for methyl acetate for this system. (Mechanism 1, Scheme 1) However, acetonitrile could also be the source because  $\text{Sn}(\text{II})$  has been long known to catalyze the hydrolysis of acetonitrile to acetic acid. (Mechanism 2, Scheme 1) Herein, we report evidence to support that it is the hydrolysis of acetonitrile instead of the conversion of methanol that leads to the formation of methyl acetate.

#### Scheme 1.

##### Mechanism 1:



##### Mechanism 2:



## 2. Result and Discussion

### 2.1 $\text{CpRu}(\text{PPh}_3)_2(\text{SnCl}_3)$

$\text{CpRu}(\text{PPh}_3)_2(\text{SnCl}_3)$  was synthesized according to a reported procedure.<sup>3</sup> Repeating Gusevkava et al.'s experiment did show the production of methyl acetate detectable by GC. However, the yield for the reaction is still too low to allow any reliable analysis of the reaction results. Therefore, further improvement of the catalytic activity is still needed before any meaningful mechanistic investigation.

### 2.2 $\text{SnCl}_2$ Additive

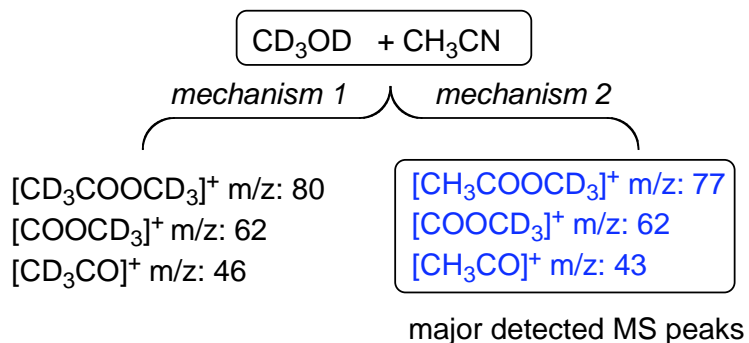
We noticed that Shinoda et al. reported earlier that a composite catalyst generated in situ from  $\text{RuCl}_3$  and  $\text{SnCl}_2$  catalyzes the production of methyl acetate from the mixture of methanol and acetonitrile.<sup>5</sup> According to their result, the addition of  $\text{SnCl}_2$  can significantly improve the turnover numbers. The optimal  $[\text{Sn}]/[\text{Ru}]$  ratio was found to be about 16. Inspired by this work, we decided to employ the same strategy to improve the yield of methyl acetate.

Fortunately, the addition of 16 equivalents of  $\text{SnCl}_2$  to the system with  $\text{CpRu}(\text{PPh}_3)_2(\text{SnCl}_3)$  did significantly improve the yield of methyl acetate to a level that can be readily detected by GC/MS instruments in the same period of time. Therefore, we used this composite catalytic system for further mechanistic investigations.

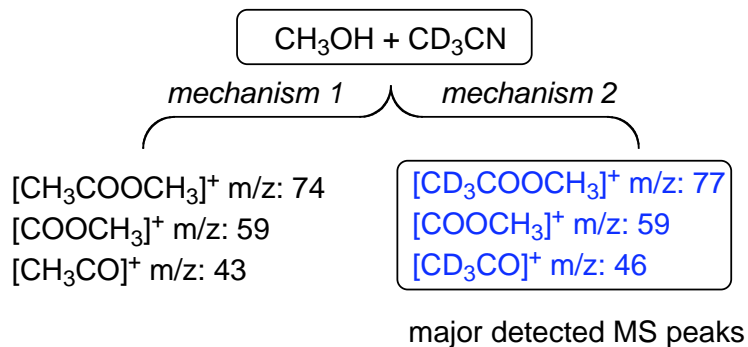
In order to identify the source of the acetate (methanol or acetonitrile), two isotope-labeling experiments ( $\text{CD}_3\text{OD}+\text{CH}_3\text{CN}/\text{CH}_3\text{OH}+\text{CD}_3\text{CN}$ ) were designed. As shown in Scheme 2, different isotopologues of methyl acetate,  $\text{CD}_3\text{COOCD}_3/\text{CH}_3\text{COOCH}_3$  versus  $\text{CH}_3\text{COOCD}_3/\text{CD}_3\text{COOCH}_3$ , which can be explicitly characterized by mass spectroscopy, are expected for mechanism 1 and mechanism 2, respectively.

## Scheme 2.

## Experiment 1:



## Experiment 2:



Mass spectra of methyl acetates from the two isotope-labeling experiments are shown in Figure 1 and Figure 3. These spectra clearly indicate that  $\text{CH}_3\text{COOCD}_3/\text{CD}_3\text{COOCH}_3$  instead of  $\text{CD}_3\text{COOCD}_3/\text{CH}_3\text{COOCH}_3$  are formed in these two experiments. Further inspections of the mass spectra of  $\text{CH}_3\text{CN}$  in experiment 1 and  $\text{CH}_3\text{OH}$  in experiment 2 indicate no D-incorporation for their major molecular cation signals, which suggests that no significant H/D exchange takes places during the reactions. Therefore, it can be concluded that the methyl acetate in this system comes from the hydrolysis of acetonitrile instead of the transformation of methanol as proposed by Gusevkava et al.

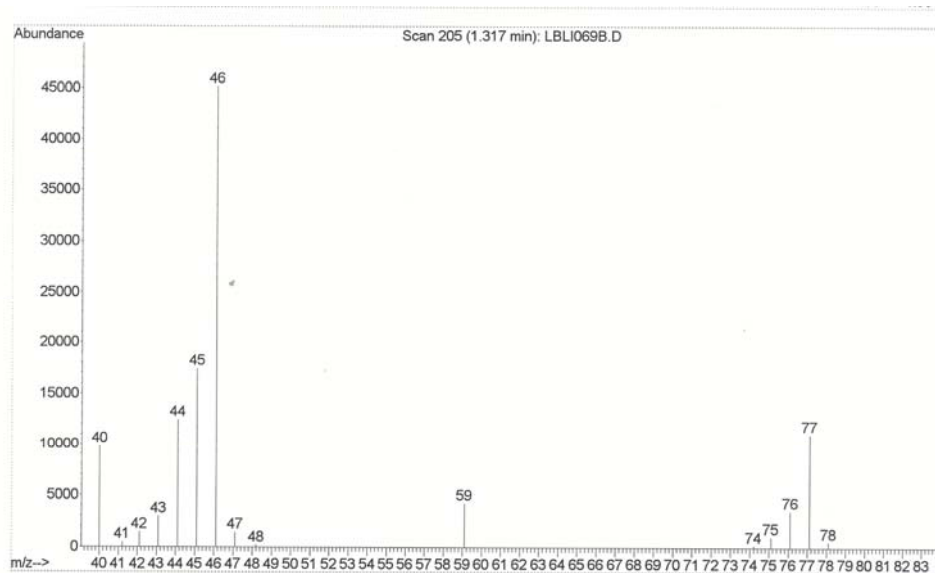
### 2.3 SnCl<sub>2</sub>-only catalyst

Finally, we found that the reaction with SnCl<sub>2</sub> only also results in the formation of a significant amount of methyl acetate. This result suggests that ruthenium is not necessary for the catalyses and the Ru-Sn bimetallic complexes reported in the literature might mainly act as a source of SnCl<sub>2</sub>.

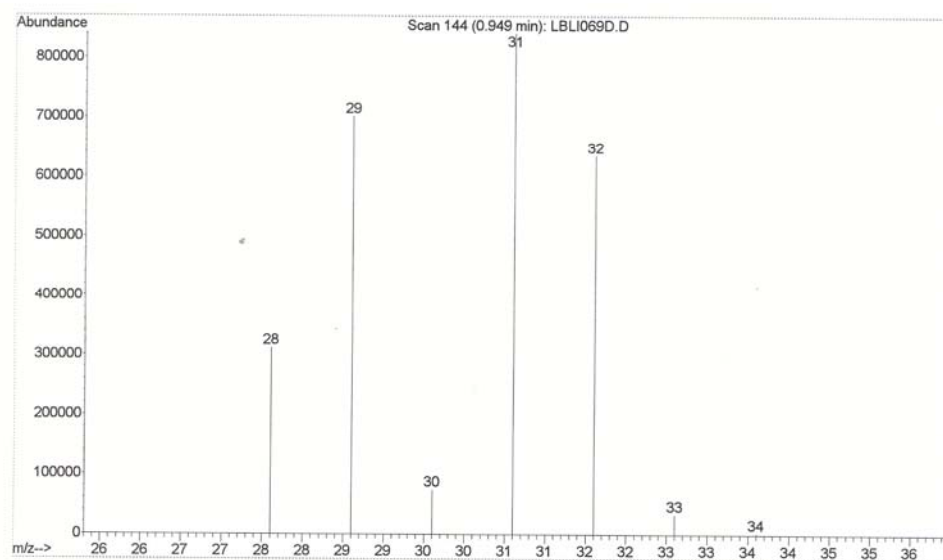
### 3. Conclusions

Our experiments strongly suggest that the methyl acetate produced by the system developed by Gusevkava et al. is more likely a result of the hydrolysis of acetonitrile instead of the proposed transformation of methanol. The catalytic activity of SnCl<sub>2</sub>-only catalyst further suggests that the Ru-Sn bimetallic complexes might be just a source to provide Sn reagent to catalyze the hydrolysis of acetonitrile. Finally, it should be pointed out that the possibility of methanol as the source of methyl acetate cannot be ruled out for the system developed by Shinodo et al. because the formation of methyl acetate was also reported for a MeOH/MeNO<sub>2</sub> system.

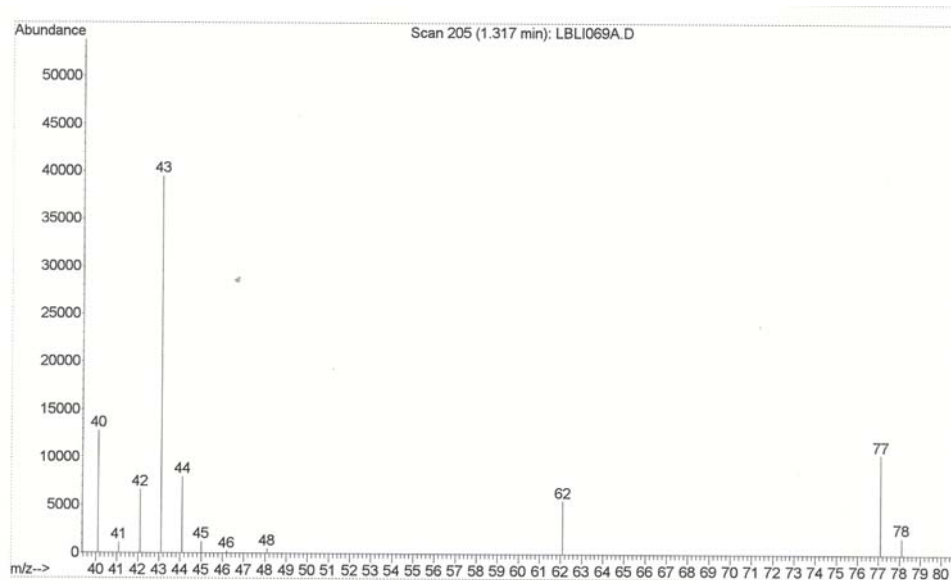
**Figure 1. Mass spectrum of the methyl acetate from the reaction of**  
 **$\text{CH}_3\text{OH} + \text{CD}_3\text{CN}$ ; m/z:  $[\text{CD}_3\text{COOCH}_3]^+$  77,  $[\text{COOCH}_3]^+$  59,  $[\text{CD}_3\text{C}(\text{O})]^+$  46**



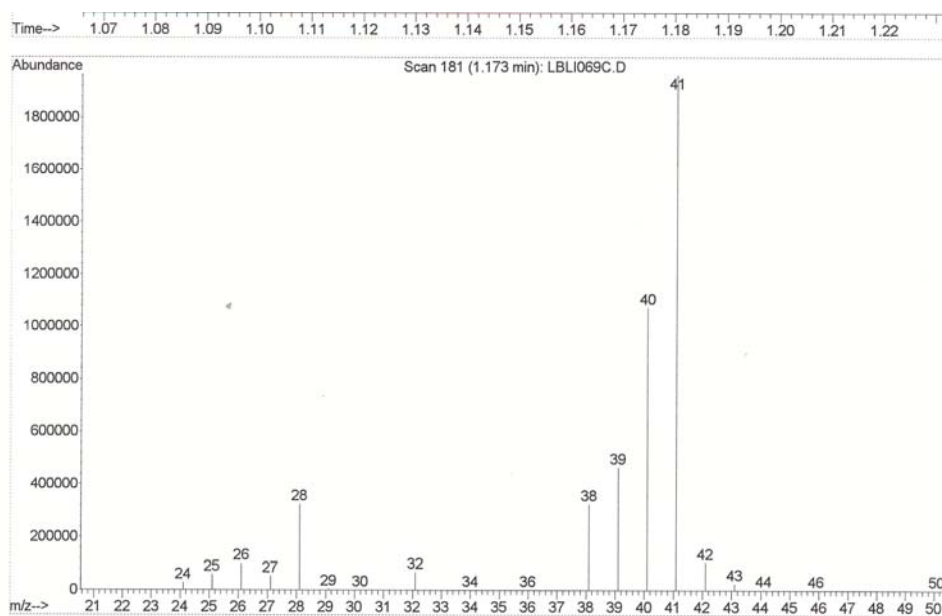
**Figure 2. Mass spectrum of methanol after the reaction indicates that there is no significant H/D exchange**



**Figure 3. Mass spectrum of the methyl acetate from the reaction of  $\text{CD}_3\text{OH} + \text{CH}_3\text{CN}$ ; m/z:  $[\text{CH}_3\text{COOCD}_3]^+ 77$ ,  $[\text{COOCD}_3]^+ 52$ ,  $[\text{CH}_3\text{C}(\text{O})]^+ 43$**



**Figure 4. Mass spectrum of acetonitrile after the reaction indicates that there is no significant H/D exchange**



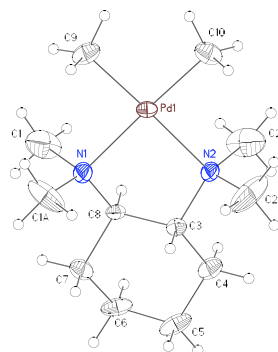
## Experimental Section

### General Information for the Catalytic Reactions

The catalytic reactions were carried out in a glass-tube-like 5 ml reactor equipped with a 90° angle HI-VAC vacuum valve. The solution of the catalyst in a methanol/acetonitrile mixture (v/v=1:1) was charged into the reactor and degassed by Schlenck techniques. After heating the solution in an oil bath at 140 °C for 40 hours, the reactor was taken out of the bath and cooled down to room temperature in a water bath. The product was then identified by GC/MS spectroscopy.

### Reference:

1. Shinoda, S.; Yamakawa, T. *J. Chem. Soc.—Chem. Commun.* **1990**, 1511–1512.
2. Yamakawa, T.; Hiroi, M.; Shinoda, S. *J. Chem. Soc. —Dalton Trans.* **1994**, 2265–2269.
3. Robles-Dutenhefner, P. A.; Moura, E. M.; Gama, G. J.; Siebald, H. G. L.; Gusevskaya, E. V. *J. Mol. Catal. A—Chem.* **2000**, *164*, 39–47.
4. Moura, E. M.; Siebald, H. G. L.; de Lima, G. M. *Polyhedron* **2002**, *21*, 2323–2331.
5. Yang, L. C.; Yamakawa, T.; Shinoda, S. *J. Mol. Catal. A—Chem.* **1998**, *130*, 249–253.

**Appendix B. X-Ray Crystallographic Data for Complex 2 (Chapter 2)****2**

**Note:** The crystallographic data have been deposited in the Cambridge Database (CCDC) and have been placed on hold pending further instructions from me. The deposition number is 263612. Ideally the CCDC would like the publication to contain a footnote of the type: "Crystallographic data have been deposited at the CCDC, 12 Union Road, Cambridge CB2 1EZ, UK, and copies can be obtained on request, free of charge, by quoting the publication citation and the deposition number 263612."



**Table B.1 Crystal data and structure refinement for 2 (CCDC 263612).**

Empirical formula	C <sub>12</sub> H <sub>28</sub> N <sub>2</sub> Pd
Formula weight	306.76
Crystallization solvent	Benzene
Crystal habit	Fragment
Crystal size	0.22 x 0.19 x 0.10 mm <sup>3</sup>
Crystal color	Colorless

**Data Collection**

Type of diffractometer	Bruker SMART 1000
Wavelength	0.71073 Å MoK $\alpha$
Data collection temperature	100(2) K
$\theta$ range for 6839 reflections used in lattice determination	2.32 to 37.02°
Unit cell dimensions	a = 8.7968(4) Å b = 14.4109(6) Å c = 10.9609(5) Å
Volume	1389.51(11) Å <sup>3</sup>
Z	4
Crystal system	Orthorhombic
Space group	Cmc2 <sub>1</sub>
Density (calculated)	1.466 Mg/m <sup>3</sup>
F(000)	640
Data collection program	Bruker SMART v5.630

$\theta$ range for data collection	2.71 to 42.65°
Completeness to $\theta = 42.65^\circ$	95.3 %
Index ranges	$-15 \leq h \leq 16$ , $-27 \leq k \leq 27$ , $-20 \leq l \leq 15$
Data collection scan type	$\omega$ scans at 5 $\phi$ settings
Data reduction program	Bruker SAINT v6.45A
Reflections collected	16623
Independent reflections	4181 [ $R_{\text{int}} = 0.0732$ ]
Absorption coefficient	1.311 mm <sup>-1</sup>
Absorption correction	None
Max. and min. transmission	0.8801 and 0.7613

### Structure Solution and Refinement

Structure solution program	Bruker XS v6.12
Primary solution method	Direct methods
Secondary solution method	Difference Fourier map
Hydrogen placement	Geometric positions
Structure refinement program	Bruker XL v6.12
Refinement method	Full matrix least-squares on $F^2$
Data / restraints / parameters	4181 / 1 / 101
Treatment of hydrogen atoms	Riding
Goodness-of-fit on $F^2$	1.379
Final R indices [ $I > 2\sigma(I)$ , 3385 reflections]	$R_1 = 0.0415$ , $wR_2 = 0.0743$
R indices (all data)	$R_1 = 0.0553$ , $wR_2 = 0.0769$
Type of weighting scheme used	Sigma

Weighting scheme used	$w=1/\sigma^2(F_o^2)$
Max shift/error	0.000
Average shift/error	0.000
Absolute structure parameter	0.05(5)
Largest diff. peak and hole	3.139 and -1.635 e.Å <sup>-3</sup>

### Special Refinement Details

The molecule occupies a special position in the unit cell, a mirror plane at  $x = 1$ . Several atoms (Pd1, N1, N2, C4, C7, C9, and C10) actually sit on the mirror; see Table B.2 for atoms with a  $x$ -coordinate identical to 1. The mirror creates the appropriate methyl groups associated with C1 (C1A) and C2 (C2A) to give a complete molecule; see Figure B.1. All other atoms lie above or below the mirror as appropriate for the pucker in the ring.

Peaks (and holes) on the final difference Fourier that are stronger than one electron lie within 0.8 Å of Pd.

Refinement of  $F^2$  against ALL reflections. The weighted R-factor ( $wR$ ) and goodness of fit ( $S$ ) are based on  $F^2$ , conventional R-factors ( $R$ ) are based on  $F$ , with  $F$  set to zero for negative  $F^2$ . The threshold expression of  $F^2 > 2\sigma(F^2)$  is used only for calculating R-factors(gt), etc., and is not relevant to the choice of reflections for refinement. R-factors based on  $F^2$  are statistically about twice as large as those based on  $F$ , and R-factors based on ALL data will be even larger.

All esds (except the esd in the dihedral angle between two l.s. planes) are estimated using the full covariance matrix. The cell esds are taken into account individually in the estimation of esds in distances, angles, and torsion angles; correlations



**Table B.2** Atomic coordinates (  $\times 10^4$ ) and equivalent isotropic displacement parameters ( $\text{\AA}^2 \times 10^3$ ) for **2** (CCDC 263612).  $U(\text{eq})$  is defined as the trace of the orthogonalized  $U^{ij}$  tensor.

	x	y	z	$U_{\text{eq}}$
Pd(1)	10000	7420(1)	7859(1)	18(1)
N(1)	10000	6502(4)	6263(4)	24(1)
N(2)	10000	8500(4)	6445(5)	21(1)
C(1)	8657(5)	5905(3)	6273(4)	57(1)
C(2)	8651(5)	9084(3)	6572(4)	67(2)
C(3)	10385(5)	8034(3)	5249(4)	18(1)
C(4)	10000	8639(3)	4128(4)	31(1)
C(5)	10425(5)	8153(3)	2932(10)	35(1)
C(6)	9528(5)	7244(3)	2872(15)	33(1)
C(7)	10000	6618(3)	3939(4)	29(1)
C(8)	9576(5)	7095(3)	5165(4)	18(1)
C(9)	10000	6387(5)	9119(6)	33(2)
C(10)	10000	8308(5)	9280(7)	33(2)

**Table B.3** Selected bond lengths [ $\text{\AA}$ ] and angles [ $^\circ$ ] for **2** (CCDC 263612)

Pd(1)-C(10)	2.016(7)	C(1)#1-N(1)-C(1)	107.8(5)
Pd(1)-C(9)	2.031(7)	C(2)#1-N(2)-C(2)	108.6(6)
Pd(1)-N(1)	2.192(5)		
Pd(1)-N(2)	2.196(6)		

Symmetry transformations used to generate equivalent atoms:

#1  $-x+2, y, z$

**Table B.4 Bond lengths [ $\text{\AA}$ ] and angles [ $^\circ$ ] for 2 (CCDC 263612)**


---

Pd(1)-C(10)	2.016(7)	C(10)-Pd(1)-C(9)	86.5(3)
Pd(1)-C(9)	2.031(7)	C(10)-Pd(1)-N(1)	177.7(3)
Pd(1)-N(1)	2.192(5)	C(9)-Pd(1)-N(1)	95.80(19)
Pd(1)-N(2)	2.196(6)	C(10)-Pd(1)-N(2)	95.45(17)
N(1)-C(1)#1	1.462(5)	C(9)-Pd(1)-N(2)	178.0(3)
N(1)-C(1)	1.462(5)	N(1)-Pd(1)-N(2)	82.2(2)
N(1)-C(8)	1.522(6)	C(1)#1-N(1)-C(1)	107.8(5)
N(2)-C(2)	1.462(5)	C(1)#1-N(1)-C(8)	122.3(4)
N(2)-C(2)#1	1.462(5)	C(1)-N(1)-C(8)	97.9(3)
N(2)-C(3)	1.512(7)	C(1)#1-N(1)-Pd(1)	110.5(3)
C(3)-C(8)	1.531(6)	C(1)-N(1)-Pd(1)	110.5(3)
C(3)-C(4)	1.544(5)	C(8)-N(1)-Pd(1)	107.0(3)
C(4)-C(5)	1.533(11)	C(2)#1-N(2)-C(2)	108.6(6)
C(5)-C(6)	1.530(6)	C(2)-N(2)-C(3)	121.4(4)
C(6)-C(7)	1.534(12)	C(2)#1-N(2)-C(3)	99.0(3)
C(7)-C(8)	1.555(5)	C(2)-N(2)-Pd(1)	109.9(3)
		C(2)#1-N(2)-Pd(1)	109.9(3)
		C(3)-N(2)-Pd(1)	107.3(3)
		N(2)-C(3)-C(8)	109.9(4)
		N(2)-C(3)-C(4)	113.0(4)
		C(8)-C(3)-C(4)	110.5(3)
		C(5)-C(4)-C(3)	111.6(4)
		C(6)-C(5)-C(4)	107.6(6)
		C(5)-C(6)-C(7)	109.3(7)
		C(6)-C(7)-C(8)	109.5(5)
		N(1)-C(8)-C(3)	109.5(4)
		N(1)-C(8)-C(7)	112.1(4)
		C(3)-C(8)-C(7)	109.3(3)

---

Symmetry transformations used to generate equivalent atoms:

#1 -x+2,y,z

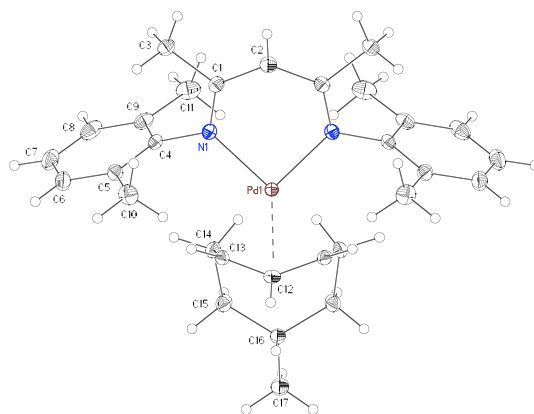
**Table B.5** Anisotropic displacement parameters ( $\text{\AA}^2 \times 10^4$ ) for **2** (CCDC 263612).

The anisotropic displacement factor exponent takes the form:  $-2\pi^2 [h^2 a^{*2} U^{11} + \dots + 2h k a^* b^* U^{12}]$ .

	$U^{11}$	$U^{22}$	$U^{33}$	$U^{23}$	$U^{13}$	$U^{12}$
Pd(1)	169(1)	235(1)	130(1)	10(5)	0	0
N(1)	340(20)	185(13)	200(20)	15(15)	0	0
N(2)	300(20)	172(15)	180(20)	29(12)	0	0
C(1)	470(20)	760(30)	480(20)	-280(20)	59(19)	-310(20)
C(2)	650(30)	750(30)	610(30)	320(20)	200(20)	460(20)
C(3)	170(20)	215(15)	150(19)	24(14)	-21(15)	10(12)
C(4)	380(20)	299(16)	236(19)	97(15)	0	0
C(5)	290(20)	520(20)	250(30)	220(40)	-50(40)	-55(17)
C(6)	304(19)	520(20)	145(16)	90(70)	-10(70)	-35(17)
C(7)	400(20)	304(16)	180(17)	-57(14)	0	0
C(8)	191(19)	224(16)	125(18)	3(15)	28(15)	-21(13)
C(9)	340(30)	390(30)	260(30)	130(20)	0	0
C(10)	320(30)	420(40)	250(30)	-90(20)	0	0



### Appendix C. X-Ray Crystallographic Data for Complex 3 (Chapter 4)



**3**

**Note:** The crystallographic data have been deposited in the Cambridge Database (CCDC) and have been placed on hold pending further instructions from me. The deposition number is 295981. Ideally the CCDC would like the publication to contain a footnote of the type: "Crystallographic data have been deposited at the CCDC, 12 Union Road, Cambridge CB2 1EZ, UK, and copies can be obtained on request, free of charge, by quoting the publication citation and the deposition number 295981."

**Table C.1 Crystal data and structure refinement for 3 (CCDC 295981)**

Empirical formula	C <sub>30</sub> H <sub>40</sub> N <sub>2</sub> Pd
Formula weight	535.04
Crystallization solvent	Dichloromethane/n-pentane
Crystal habit	Block
Crystal size	0.32 x 0.28 x 0.19 mm <sup>3</sup>
Crystal color	Yellow

**Data Collection**

Type of diffractometer	Bruker SMART 1000
Wavelength	0.71073 Å MoK $\alpha$
Data collection temperature	100(2) K
$\theta$ range for 24440 reflections used in lattice determination	2.18 to 49.62°
Unit cell dimensions	a = 15.0554(4) Å b = 7.2730(2) Å c = 11.8708(3) Å
Volume	1299.83(6) Å <sup>3</sup>
Z	2
Crystal system	Orthorhombic
Space group	Pmn2 <sub>1</sub>
Density (calculated)	1.367 Mg/m <sup>3</sup>
F(000)	560
Data collection program	Bruker SMART v5.630

$\theta$ range for data collection	2.18 to 45.01°
Completeness to $\theta = 45.01^\circ$	96.5 %
Index ranges	$-26 \leq h \leq 29$ , $-14 \leq k \leq 12$ , $-23 \leq l \leq 22$
Data collection scan type	$\omega$ scans at 7 $\phi$ settings
Data reduction program	Bruker SAINT v6.45A
Reflections collected	36614
Independent reflections	10105 [ $R_{\text{int}} = 0.0629$ ]
Absorption coefficient	0.734 mm <sup>-1</sup>
Absorption correction	None
Max. and min. transmission	0.8732 and 0.7991

### Structure Solution and Refinement

Structure solution program	Bruker XS v6.12
Primary solution method	Patterson method
Secondary solution method	Difference Fourier map
Hydrogen placement	Geometric positions
Structure refinement program	Bruker XL v6.12
Refinement method	Full matrix least-squares on $F^2$
Data / restraints / parameters	10105 / 1 / 160
Treatment of hydrogen atoms	Riding
Goodness-of-fit on $F^2$	1.370
Final R indices [ $I > 2\sigma(I)$ , 8998 reflections]	$R_1 = 0.0294$ , $wR_2 = 0.0589$
R indices (all data)	$R_1 = 0.0363$ , $wR_2 = 0.0601$

Type of weighting scheme used	Sigma
Weighting scheme used	$w=1/\sigma^2(Fo^2)$
Max shift/error	0.005
Average shift/error	0.000
Absolute structure determination	Anomalous differences
Absolute structure parameter	-0.008(14)
Largest diff. peak and hole	1.350 and -0.724 e.Å <sup>-3</sup>

### Special Refinement Details

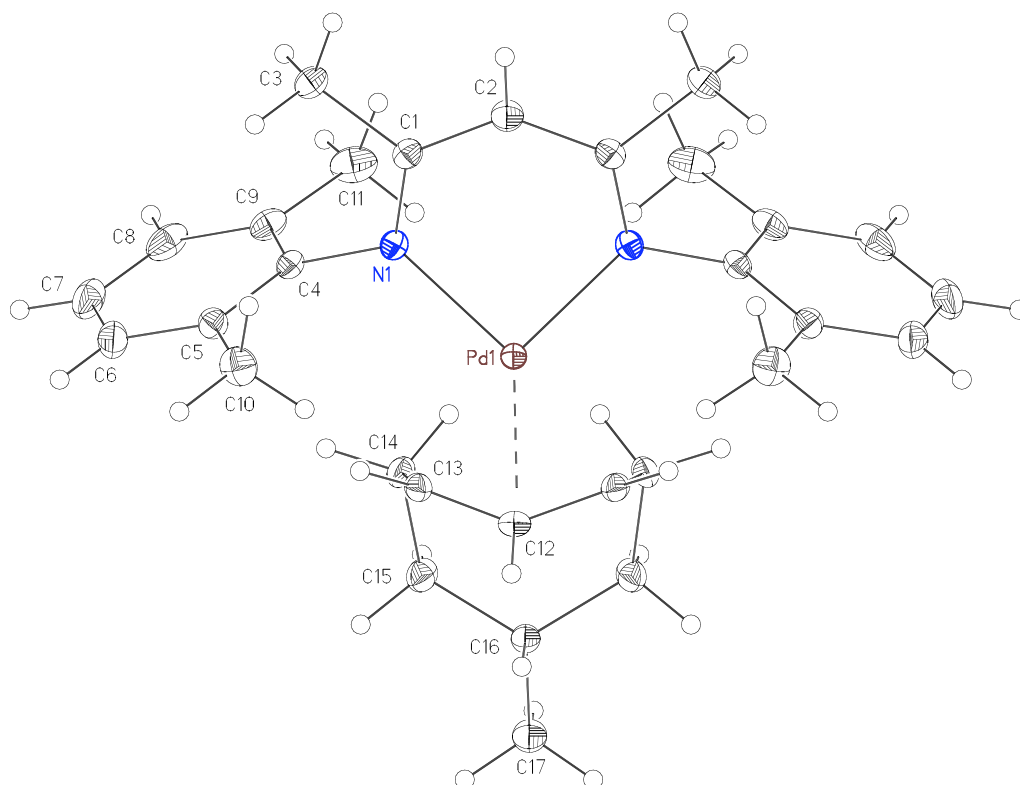
The molecule sits on a crystallographic mirror plane. Hydrogen atomic positions were evident in the difference Fourier map, and placed in geometrically calculated positions and treated as riding atoms during least-squares refinement. These calculated positions may vary slightly from the actual positions, particularly for hydrogens bonded to C12, C13, C14, C13A, and C14A.

Refinement of  $F^2$  against ALL reflections. The weighted R-factor ( $wR$ ) and goodness of fit ( $S$ ) are based on  $F^2$ , conventional R-factors ( $R$ ) are based on  $F$ , with  $F$  set to zero for negative  $F^2$ . The threshold expression of  $F^2 > 2\sigma(F^2)$  is used only for calculating R-factors(gt), etc., and is not relevant to the choice of reflections for refinement. R-factors based on  $F^2$  are statistically about twice as large as those based on  $F$ , and R-factors based on ALL data will be even larger.

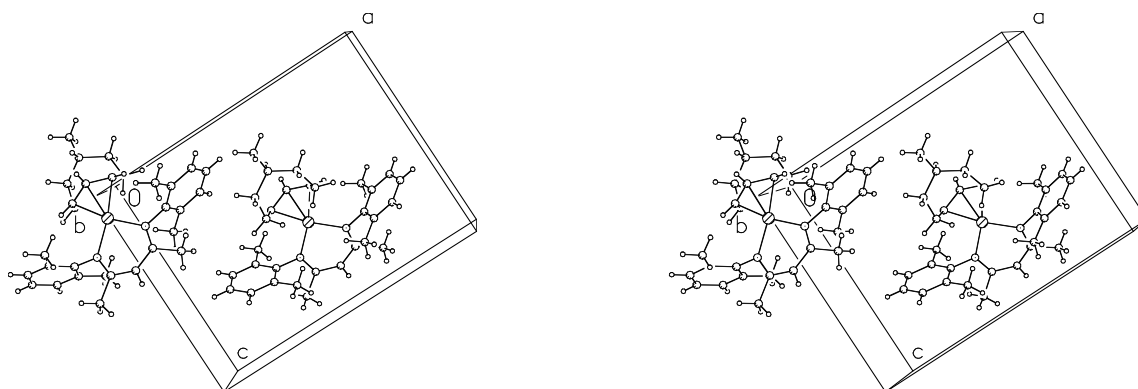
All esds (except the esd in the dihedral angle between two l.s. planes) are estimated using the full covariance matrix. The cell esds are taken into account individually in the estimation of esds in distances, angles, and torsion angles; correlations between esds in cell parameters are only used when they are defined by crystal symmetry. An

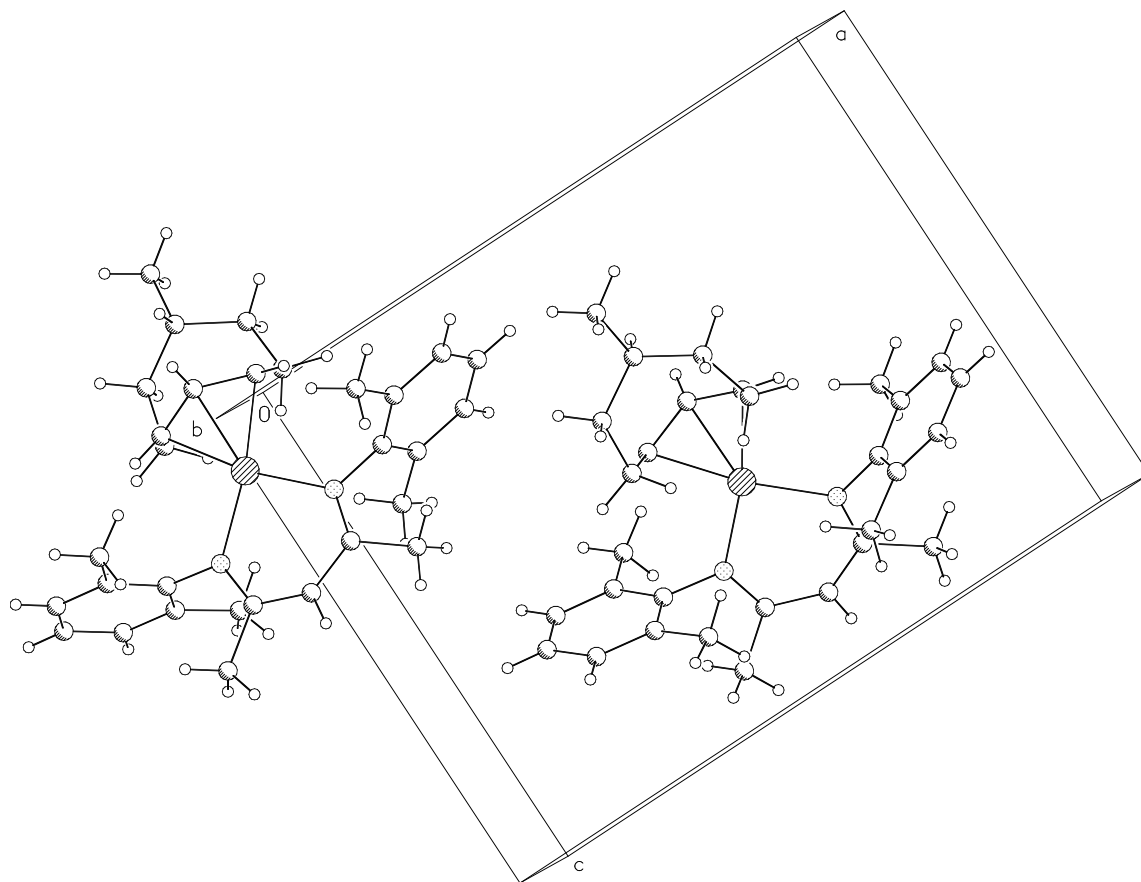
approximate (isotropic) treatment of cell esds is used for estimating esds involving l.s. planes.

**Figure C.1 Minimum overlap view of 3**



**Figure C.2 Crystal packing of 3**



**Figure C.1 Unit cell contents of 3**

**Table C.2 Atomic coordinates (  $\times 10^4$ ) and equivalent isotropic displacement parameters ( $\text{\AA}^2 \times 10^3$ ) for 3 (CCDC 295981).  $U(\text{eq})$  is defined as the trace of the orthogonalized  $U^{\text{ij}}$  tensor.**

	x	y	z	$U_{\text{eq}}$
Pd(1)	0	10589(1)	1080(1)	11(1)
N(1)	975(1)	11264(1)	2239(1)	13(1)
C(1)	839(1)	12182(2)	3189(1)	14(1)
C(2)	0	12730(2)	3584(1)	16(1)
C(3)	1627(1)	12642(2)	3935(1)	18(1)
C(4)	1852(1)	10562(2)	2039(1)	13(1)
C(5)	2466(1)	11605(2)	1417(1)	16(1)
C(6)	3315(1)	10884(2)	1250(1)	22(1)
C(7)	3556(1)	9185(2)	1689(1)	25(1)
C(8)	2935(1)	8154(2)	2291(1)	23(1)
C(9)	2079(1)	8819(2)	2470(1)	17(1)
C(10)	2207(1)	13446(2)	957(2)	22(1)
C(11)	1399(1)	7706(2)	3105(1)	25(1)
C(12)	0	10277(2)	-673(1)	15(1)
C(13)	816(1)	9552(2)	-286(1)	15(1)
C(14)	1012(1)	7520(2)	-113(1)	17(1)
C(15)	866(1)	6341(2)	-1184(1)	18(1)
C(16)	0	6614(2)	-1851(1)	14(1)
C(17)	0	5294(2)	-2860(2)	19(1)

**Table C.3** Selected bond lengths [ $\text{\AA}$ ] and angles [ $^\circ$ ] for **3** (CCDC 295981)

Pd(1)-N(1)	2.0708(10)	C(12)-Pd(1)-C(13)	38.70(4)
Pd(1)-N(1)#1	2.0708(10)	C(12)-Pd(1)-C(13)#1	38.70(4)
Pd(1)-C(12)	2.0932(16)	C(13)-Pd(1)-C(13)#1	69.03(4)
Pd(1)-C(13)	2.1696(11)	N(1)-Pd(1)-N(1)#1	90.23(5)
Pd(1)-C(13)#1	2.1696(11)	N(1)-Pd(1)-C(12)	133.35(3)
		N(1)#1-Pd(1)-C(12)	133.35(3)
		N(1)-Pd(1)-C(13)#1	168.65(4)
		N(1)-Pd(1)-C(13)	100.22(4)
		N(1)#1-Pd(1)-C(13)#1	100.22(4)

Symmetry transformations used to generate equivalent atoms:

#1 -x,y,z



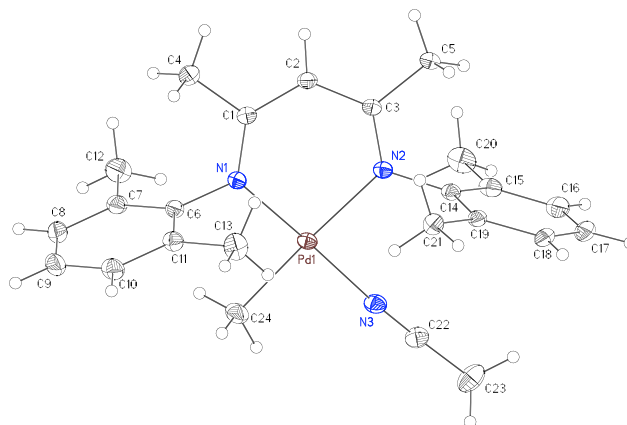
**Table C.4 Bond lengths [Å] and angles [°] for 3 (CCDC 295981)**

Pd(1)-N(1)	2.0708(10)	C(1)-N(1)-Pd(1)	125.14(7)
Pd(1)-N(1)#1	2.0708(10)	C(4)-N(1)-Pd(1)	117.23(7)
Pd(1)-C(12)	2.0932(16)	N(1)-C(1)-C(2)	124.40(11)
Pd(1)-C(13)	2.1696(11)	N(1)-C(1)-C(3)	119.16(10)
Pd(1)-C(13)#1	2.1696(11)	C(2)-C(1)-C(3)	116.41(11)
N(1)-C(1)	1.3257(15)	C(1)-C(2)-C(1)#1	128.02(15)
N(1)-C(4)	1.4367(14)	C(5)-C(4)-C(9)	121.14(10)
C(1)-C(2)	1.4057(13)	C(5)-C(4)-N(1)	120.01(10)
C(1)-C(3)	1.5170(16)	C(9)-C(4)-N(1)	118.85(10)
C(2)-C(1)#1	1.4057(13)	C(6)-C(5)-C(4)	118.28(11)
C(4)-C(5)	1.4046(16)	C(6)-C(5)-C(10)	121.52(11)
C(4)-C(9)	1.4089(16)	C(4)-C(5)-C(10)	120.21(10)
C(5)-C(6)	1.3957(15)	C(7)-C(6)-C(5)	121.35(12)
C(5)-C(10)	1.4980(18)	C(6)-C(7)-C(8)	119.71(12)
C(6)-C(7)	1.389(2)	C(9)-C(8)-C(7)	120.71(12)
C(7)-C(8)	1.395(2)	C(8)-C(9)-C(4)	118.79(12)
C(8)-C(9)	1.3926(18)	C(8)-C(9)-C(11)	121.21(12)
C(9)-C(11)	1.5074(19)	C(4)-C(9)-C(11)	120.00(11)
C(12)-C(13)	1.4144(14)	C(13)-C(12)-C(13)#1	120.72(15)
C(12)-C(13)#1	1.4144(14)	C(12)-C(13)-C(14)	125.04(11)
C(13)-C(14)	1.5213(17)	C(13)-C(14)-C(15)	113.57(10)
C(14)-C(15)	1.5493(17)	C(16)-C(15)-C(14)	118.09(10)
C(15)-C(16)	1.5380(14)	C(17)-C(16)-C(15)	108.71(9)
C(16)-C(17)	1.535(2)	C(17)-C(16)-C(15)#1	108.72(9)
C(16)-C(15)#1	1.5380(14)	C(15)-C(16)-C(15)#1	115.97(14)
C(12)-Pd(1)-C(13)	38.70(4)	Symmetry transformations used to generate equivalent atoms: #1 -x,y,z	
C(12)-Pd(1)-C(13)#1	38.70(4)		
C(13)-Pd(1)-C(13)#1	69.03(4)		
N(1)-Pd(1)-N(1)#1	90.23(5)		
N(1)-Pd(1)-C(12)	133.35(3)		
N(1)#1-Pd(1)-C(12)	133.35(3)		
N(1)-Pd(1)-C(13)#1	168.65(4)		
N(1)-Pd(1)-C(13)	100.22(4)		
N(1)#1-Pd(1)-C(13)#1	100.22(4)		
C(1)-N(1)-C(4)	117.46(9)		

**Table C.5** Anisotropic displacement parameters ( $\text{\AA}^2 \times 10^4$ ) for **3** (CCDC 295981).

The anisotropic displacement factor exponent takes the form:  $-2\pi^2 [h^2 a^{*2} U^{11} + \dots + 2h k a^* b^* U^{12}]$ .

	$U^{11}$	$U^{22}$	$U^{33}$	$U^{23}$	$U^{13}$	$U^{12}$
Pd(1)	106(1)	113(1)	105(1)	3(1)	0	0
N(1)	125(3)	119(4)	138(4)	-2(3)	-9(3)	2(3)
C(1)	149(4)	122(4)	149(4)	1(3)	-16(3)	-17(3)
C(2)	174(6)	153(7)	161(6)	-37(5)	0	0
C(3)	184(4)	173(5)	170(5)	-23(4)	-33(4)	-19(4)
C(4)	128(4)	119(4)	133(4)	-11(3)	-22(3)	2(3)
C(5)	147(4)	163(4)	159(4)	-17(4)	-1(3)	-18(4)
C(6)	145(4)	288(6)	230(9)	-71(5)	0(4)	-9(4)
C(7)	170(5)	323(7)	265(6)	-106(5)	-53(5)	81(5)
C(8)	267(5)	196(5)	226(5)	-51(5)	-98(5)	99(5)
C(9)	217(5)	139(4)	164(5)	-1(4)	-53(4)	22(4)
C(10)	236(4)	174(4)	248(9)	35(5)	18(5)	-37(4)
C(11)	364(7)	167(5)	212(6)	52(4)	-27(5)	-8(5)
C(12)	179(6)	153(6)	105(5)	5(4)	0	0
C(13)	130(4)	182(5)	133(4)	-19(4)	10(3)	-35(4)
C(14)	127(4)	215(5)	156(4)	-29(4)	-27(3)	40(4)
C(15)	155(4)	204(5)	187(5)	-41(4)	-20(4)	47(4)
C(16)	139(5)	145(6)	134(6)	-12(5)	0	0
C(17)	195(7)	184(7)	179(7)	-45(5)	0	0

**Appendix D. X-Ray Crystallographic Data for Complex 6 (Chapter 4)****3**

**Note:** The crystallographic data have been deposited in the Cambridge Database (CCDC) and have been placed on hold pending further instructions from me. The deposition number is 296075. Ideally the CCDC would like the publication to contain a footnote of the type: "Crystallographic data have been deposited at the CCDC, 12 Union Road, Cambridge CB2 1EZ, UK, and copies can be obtained on request, free of charge, by quoting the publication citation and the deposition number 296075."

**Table D.1 Crystal data and structure refinement for 6 (CCDC 296075)**

Empirical formula	C <sub>24</sub> H <sub>31</sub> N <sub>3</sub> Pd
Formula weight	467.92
Crystallization solvent	Dichloromethane/n-pentane
Crystal habit	Block
Crystal size	0.30 x 0.26 x 0.26 mm <sup>3</sup>
Crystal color	Pale yellow

**Data Collection**

Type of diffractometer	Bruker SMART 1000	
Wavelength	0.71073 Å MoK $\alpha$	
Data collection temperature	100(2) K	
$\theta$ range for 26590 reflections used		
in lattice determination	2.72 to 49.62°	
Unit cell dimensions	$a = 7.9947(2)$ Å	$\alpha = 72.0190(10)^\circ$
	$b = 11.0299(3)$ Å	$\beta = 86.2190(10)^\circ$
	$c = 14.0889(4)$ Å	$\gamma = 69.5370(10)^\circ$
Volume	1105.90(5) Å <sup>3</sup>	
Z	2	
Crystal system	Triclinic	
Space group	P-1	
Density (calculated)	1.405 Mg/m <sup>3</sup>	
F(000)	484	
Data collection program	Bruker SMART v5.630	

$\theta$ range for data collection	1.52 to 49.65°
Completeness to $\theta = 49.65^\circ$	83.5 %
Index ranges	$-15 \leq h \leq 16$ , $-22 \leq k \leq 22$ , $-29 \leq l \leq 25$
Data collection scan type	$\omega$ scans at 7 $\phi$ settings
Data reduction program	Bruker SAINT v6.45A
Reflections collected	44455
Independent reflections	19083 [ $R_{\text{int}} = 0.0610$ ]
Absorption coefficient	0.853 mm <sup>-1</sup>
Absorption correction	None
Max. and min. transmission	0.8088 and 0.7840

### Structure Solution and Refinement

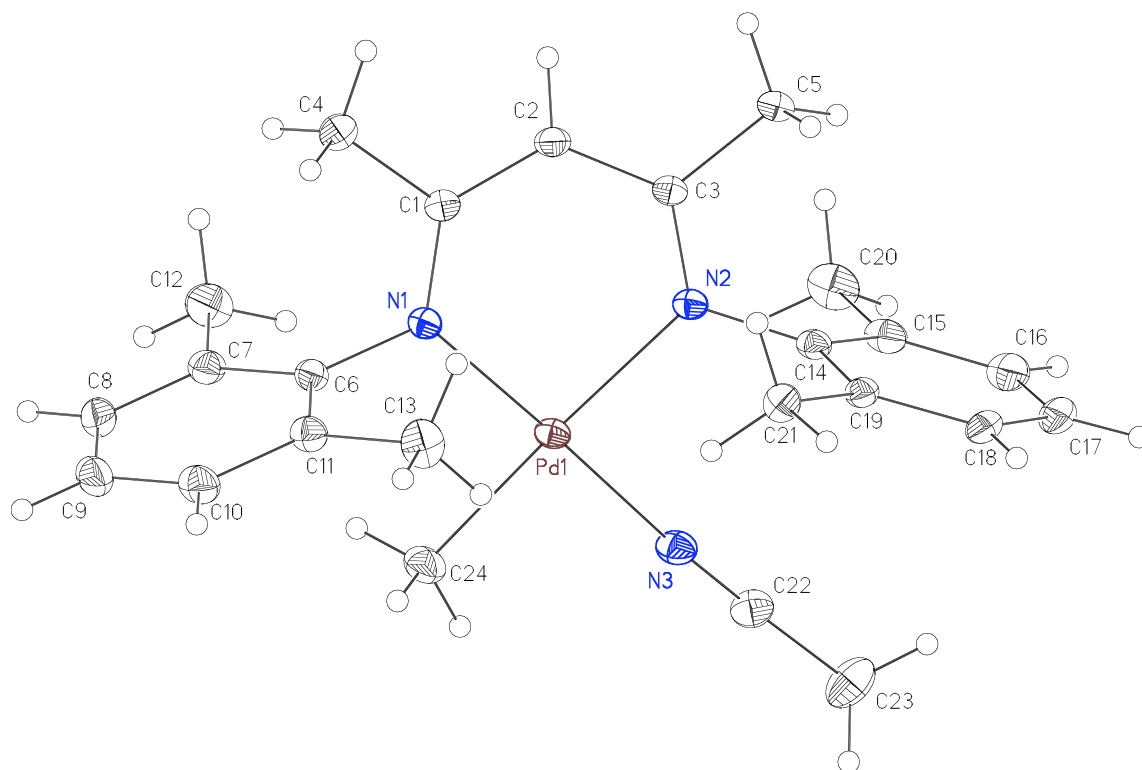
Structure solution program	Bruker XS v6.12
Primary solution method	Patterson method
Secondary solution method	Difference Fourier map
Hydrogen placement	Geometric positions
Structure refinement program	Bruker XL v6.12
Refinement method	Full matrix least-squares on $F^2$
Data / restraints / parameters	19083 / 0 / 261
Treatment of hydrogen atoms	Riding
Goodness-of-fit on $F^2$	1.202
Final R indices [ $I > 2\sigma(I)$ , 15817 reflections]	$R1 = 0.0301$ , $wR2 = 0.0673$

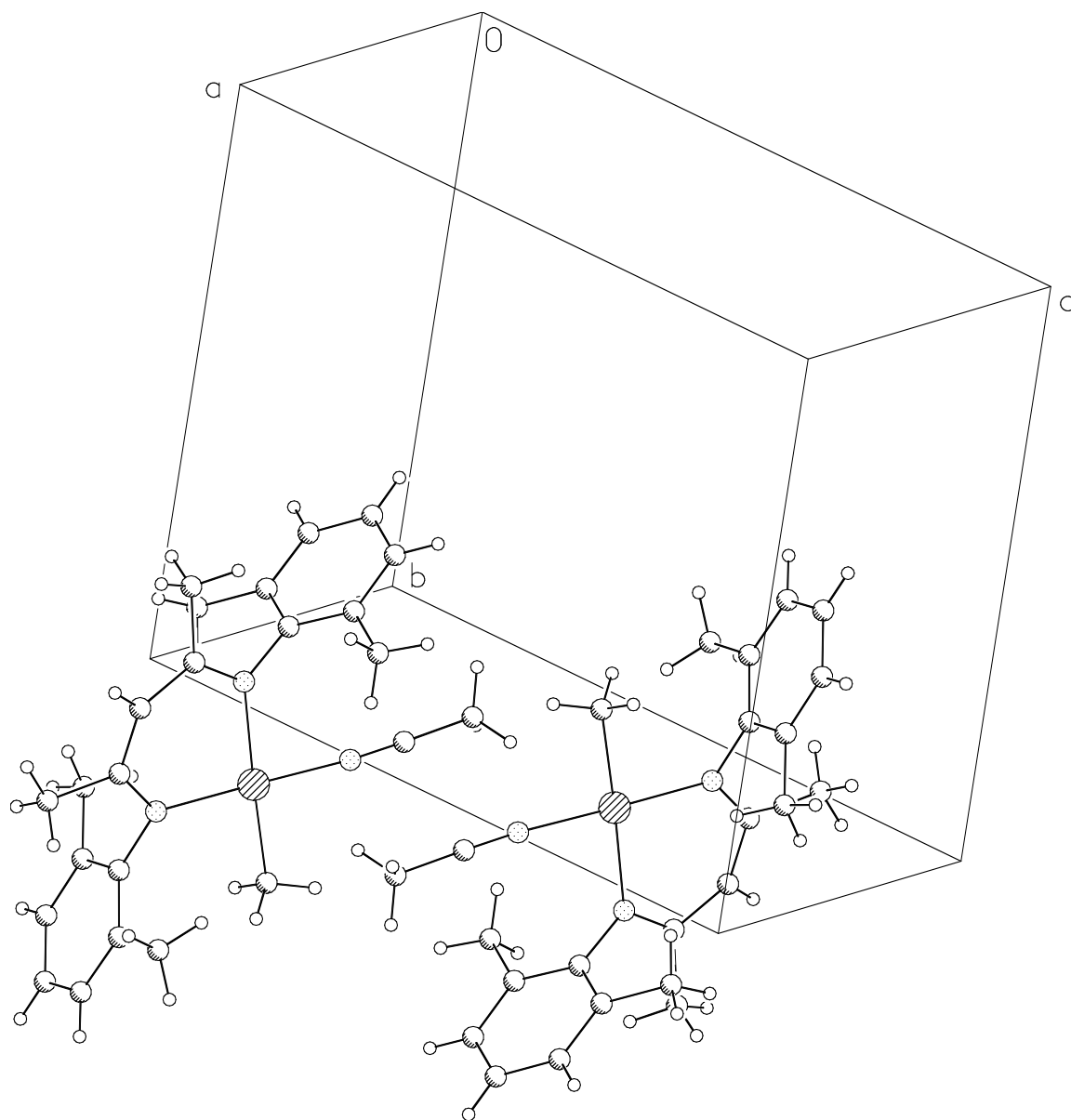
R indices (all data)	$R1 = 0.0409, wR2 = 0.0701$
Type of weighting scheme used	Sigma
Weighting scheme used	$w=1/\sigma^2(Fo^2)$
Max shift/error	0.003
Average shift/error	0.000
Largest diff. peak and hole	1.677 and -0.800 e.Å <sup>-3</sup>

### Special Refinement Details

Refinement of  $F^2$  against ALL reflections. The weighted R-factor ( $wR$ ) and goodness of fit ( $S$ ) are based on  $F^2$ , conventional R-factors ( $R$ ) are based on  $F$ , with  $F$  set to zero for negative  $F^2$ . The threshold expression of  $F^2 > 2\sigma(F^2)$  is used only for calculating R-factors(gt), etc., and is not relevant to the choice of reflections for refinement. R-factors based on  $F^2$  are statistically about twice as large as those based on  $F$ , and R-factors based on ALL data will be even larger.

All esds (except the esd in the dihedral angle between two l.s. planes) are estimated using the full covariance matrix. The cell esds are taken into account individually in the estimation of esds in distances, angles, and torsion angles; correlations between esds in cell parameters are only used when they are defined by crystal symmetry. An approximate (isotropic) treatment of cell esds is used for estimating esds involving l.s. planes.



**Figure D.3 Unit cell contents of 6**



**Table D.2 Atomic coordinates (  $\times 10^4$ ) and equivalent isotropic displacement parameters ( $\text{\AA}^2 \times 10^3$ ) for **6** (CCDC 296075).  $U(\text{eq})$  is defined as the trace of the orthogonalized  $U^{\text{ij}}$  tensor.**

	x	y	z	$U_{\text{eq}}$
Pd(1)	7947(1)	9405(1)	7206(1)	13(1)
N(1)	6030(1)	8793(1)	8008(1)	13(1)
N(2)	6434(1)	11458(1)	7054(1)	13(1)
N(3)	9910(1)	9956(1)	6432(1)	18(1)
C(1)	4376(1)	9624(1)	8077(1)	14(1)
C(2)	3739(1)	11044(1)	7666(1)	15(1)
C(3)	4741(1)	11900(1)	7274(1)	14(1)
C(4)	3049(1)	9034(1)	8681(1)	20(1)
C(5)	3791(1)	13397(1)	7162(1)	19(1)
C(6)	6490(1)	7410(1)	8641(1)	14(1)
C(7)	6108(1)	6446(1)	8323(1)	17(1)
C(8)	6558(1)	5119(1)	8974(1)	22(1)
C(9)	7396(1)	4750(1)	9905(1)	23(1)
C(10)	7783(1)	5714(1)	10204(1)	21(1)
C(11)	7333(1)	7052(1)	9581(1)	16(1)
C(12)	5223(2)	6815(1)	7312(1)	26(1)
C(13)	7763(2)	8094(1)	9907(1)	24(1)
C(14)	7329(1)	12424(1)	6802(1)	14(1)
C(15)	7391(1)	13164(1)	5797(1)	18(1)
C(16)	8221(1)	14141(1)	5584(1)	23(1)
C(17)	8975(1)	14370(1)	6341(1)	23(1)
C(18)	8953(1)	13597(1)	7331(1)	19(1)
C(19)	8143(1)	12615(1)	7569(1)	14(1)
C(20)	6544(2)	12936(1)	4977(1)	26(1)
C(21)	8091(1)	11787(1)	8638(1)	17(1)
C(22)	10984(1)	10341(1)	6001(1)	19(1)
C(23)	12303(2)	10874(1)	5444(1)	28(1)
C(24)	9516(1)	7434(1)	7334(1)	22(1)

**Table D.3** Selected bond lengths [ $\text{\AA}$ ] and angles [ $^\circ$ ] for **6** (CCDC 296075)

Pd(1)-N(3)	2.0135(9)	N(3)-Pd(1)-N(1)	178.19(3)
Pd(1)-N(1)	2.0262(8)	N(3)-Pd(1)-C(24)	87.01(4)
Pd(1)-C(24)	2.0526(9)	N(1)-Pd(1)-C(24)	91.41(4)
Pd(1)-N(2)	2.1113(7)	N(3)-Pd(1)-N(2)	90.54(3)
		N(1)-Pd(1)-N(2)	91.03(3)
		C(24)-Pd(1)-N(2)	177.45(4)

**Table D.4 Bond lengths [ $\text{\AA}$ ] and angles [ $^\circ$ ] for **6** (CCDC 296075)**

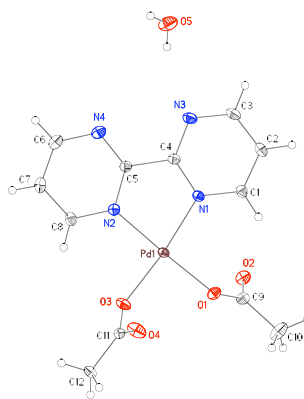
Pd(1)-N(3)	2.0135(9)	N(1)-Pd(1)-N(2)	91.03(3)
Pd(1)-N(1)	2.0262(8)	C(24)-Pd(1)-N(2)	177.45(4)
Pd(1)-C(24)	2.0526(9)	C(1)-N(1)-C(6)	116.01(7)
Pd(1)-N(2)	2.1113(7)	C(1)-N(1)-Pd(1)	124.39(6)
N(1)-C(1)	1.3372(11)	C(6)-N(1)-Pd(1)	119.23(5)
N(1)-C(6)	1.4381(11)	C(3)-N(2)-C(14)	116.66(7)
N(2)-C(3)	1.3203(11)	C(3)-N(2)-Pd(1)	124.45(6)
N(2)-C(14)	1.4278(12)	C(14)-N(2)-Pd(1)	118.53(5)
N(3)-C(22)	1.1457(13)	C(22)-N(3)-Pd(1)	176.10(8)
C(1)-C(2)	1.4031(12)	N(1)-C(1)-C(2)	125.72(8)
C(1)-C(4)	1.5154(13)	N(1)-C(1)-C(4)	119.28(7)
C(2)-C(3)	1.4100(13)	C(2)-C(1)-C(4)	114.95(7)
C(3)-C(5)	1.5186(12)	C(1)-C(2)-C(3)	127.84(8)
C(6)-C(7)	1.4023(13)	N(2)-C(3)-C(2)	123.68(8)
C(6)-C(11)	1.4051(12)	N(2)-C(3)-C(5)	120.14(8)
C(7)-C(8)	1.3993(14)	C(2)-C(3)-C(5)	116.10(8)
C(7)-C(12)	1.5057(14)	C(7)-C(6)-C(11)	121.00(8)
C(8)-C(9)	1.3901(16)	C(7)-C(6)-N(1)	120.62(8)
C(9)-C(10)	1.3877(16)	C(11)-C(6)-N(1)	118.38(8)
C(10)-C(11)	1.3961(12)	C(8)-C(7)-C(6)	118.28(9)
C(11)-C(13)	1.5075(14)	C(8)-C(7)-C(12)	120.28(9)
C(14)-C(19)	1.4021(13)	C(6)-C(7)-C(12)	121.44(8)
C(14)-C(15)	1.4069(11)	C(9)-C(8)-C(7)	121.31(10)
C(15)-C(16)	1.4021(15)	C(10)-C(9)-C(8)	119.66(9)
C(15)-C(20)	1.5030(15)	C(9)-C(10)-C(11)	120.74(9)
C(16)-C(17)	1.3868(18)	C(10)-C(11)-C(6)	118.99(9)
C(17)-C(18)	1.3944(14)	C(10)-C(11)-C(13)	120.58(9)
C(18)-C(19)	1.3937(13)	C(6)-C(11)-C(13)	120.43(8)
C(19)-C(21)	1.5078(12)	C(19)-C(14)-C(15)	120.93(8)
C(22)-C(23)	1.4533(15)	C(19)-C(14)-N(2)	118.97(7)
		C(15)-C(14)-N(2)	120.11(8)
N(3)-Pd(1)-N(1)	178.19(3)	C(16)-C(15)-C(14)	118.32(9)
N(3)-Pd(1)-C(24)	87.01(4)	C(16)-C(15)-C(20)	121.01(9)
N(1)-Pd(1)-C(24)	91.41(4)	C(14)-C(15)-C(20)	120.65(9)
N(3)-Pd(1)-N(2)	90.54(3)	C(17)-C(16)-C(15)	121.08(9)

C(16)-C(17)-C(18)	119.88(9)
C(19)-C(18)-C(17)	120.53(10)
C(18)-C(19)-C(14)	119.18(8)
C(18)-C(19)-C(21)	120.96(8)
C(14)-C(19)-C(21)	119.84(8)
N(3)-C(22)-C(23)	178.08(11)

**Table D.5** Anisotropic displacement parameters ( $\text{\AA}^2 \times 10^4$ ) for **6** (CCDC 296075).

The anisotropic displacement factor exponent takes the form:  $-2\pi^2 [h^2 a^{*2} U^{11} + \dots + 2 h k a^* b^* U^{12}]$ .

	U <sup>11</sup>	U <sup>22</sup>	U <sup>33</sup>	U <sup>23</sup>	U <sup>13</sup>	U <sup>12</sup>
Pd(1)	117(1)	137(1)	106(1)	-38(1)	7(1)	-21(1)
N(1)	125(2)	128(2)	131(3)	-35(2)	3(2)	-32(2)
N(2)	116(2)	140(2)	124(2)	-33(2)	1(2)	-30(2)
N(3)	151(3)	185(3)	165(3)	-57(2)	30(2)	-30(2)
C(1)	125(3)	158(3)	136(3)	-47(2)	4(2)	-44(2)
C(2)	110(3)	159(3)	171(3)	-47(2)	1(2)	-30(2)
C(3)	117(3)	140(3)	134(3)	-36(2)	-13(2)	-25(2)
C(4)	165(3)	198(4)	236(4)	-55(3)	51(3)	-70(3)
C(5)	125(3)	146(3)	252(4)	-39(3)	2(3)	-18(2)
C(6)	132(3)	135(3)	144(3)	-39(2)	2(2)	-38(2)
C(7)	148(3)	172(3)	213(4)	-84(3)	3(3)	-45(2)
C(8)	197(4)	165(3)	299(5)	-84(3)	48(3)	-71(3)
C(9)	214(4)	156(3)	262(4)	-13(3)	54(3)	-51(3)
C(10)	198(4)	196(4)	170(4)	4(3)	6(3)	-45(3)
C(11)	166(3)	172(3)	138(3)	-30(2)	-3(2)	-49(2)
C(12)	251(5)	260(4)	285(5)	-141(4)	-61(4)	-60(4)
C(13)	309(5)	244(4)	175(4)	-63(3)	-54(3)	-105(4)
C(14)	116(3)	140(3)	126(3)	-19(2)	16(2)	-26(2)
C(15)	160(3)	191(3)	126(3)	-2(2)	21(2)	-20(3)
C(16)	184(4)	223(4)	192(4)	24(3)	59(3)	-54(3)
C(17)	159(3)	208(4)	281(5)	1(3)	57(3)	-81(3)
C(18)	126(3)	196(3)	233(4)	-36(3)	22(3)	-69(3)
C(19)	114(3)	146(3)	144(3)	-21(2)	14(2)	-39(2)
C(20)	289(5)	292(5)	129(4)	-31(3)	-14(3)	-56(4)
C(21)	188(3)	194(3)	131(3)	-22(2)	-8(2)	-77(3)
C(22)	179(4)	236(4)	161(3)	-75(3)	40(3)	-66(3)
C(23)	279(5)	419(6)	212(4)	-121(4)	96(4)	-207(5)
C(24)	193(4)	176(4)	258(4)	-66(3)	66(3)	-22(3)

**Appendix E. X-Ray Crystallographic Data for Complex 1·H<sub>2</sub>O (Chapter 6)****1·H<sub>2</sub>O**

**Note:** The crystallographic data have been deposited in the Cambridge Database (CCDC) and have been placed on hold pending further instructions from me. The deposition number is 634014. Ideally the CCDC would like the publication to contain a footnote of the type: "Crystallographic data have been deposited at the CCDC, 12 Union Road, Cambridge CB2 1EZ, UK, and copies can be obtained on request, free of charge, by quoting the publication citation and the deposition number 634014."

**Table E.1 Crystal data and structure refinement for 1·H<sub>2</sub>O (CCDC634014)**

Empirical formula	C <sub>12</sub> H <sub>12</sub> N <sub>4</sub> O <sub>4</sub> Pd • H <sub>2</sub> O		
Formula weight	400.67		
Crystallization solvent	Dichloromethane		
Crystal habit	Block		
Crystal size	0.36 x 0.31 x 0.27 mm <sup>3</sup>		
Crystal color	Yellow		
Data Collection			
Type of diffractometer	Bruker SMART 1000		
Wavelength	0.71073 Å MoKα		
Data collection temperature	100(2) K		
θ range for 17214 reflections used			
in lattice determination	2.47 to 44.89°		
Unit cell dimensions	a = 9.6974(3) Å		
	b = 14.9781(4) Å	β= 98.7400(10)°	
	c = 10.0106(3) Å		
Volume	1437.14(7) Å <sup>3</sup>		
Z	4		
Crystal system	Monoclinic		
Space group	P2 <sub>1</sub> /n		
Density (calculated)	1.852 Mg/m <sup>3</sup>		
F(000)	800		
Data collection program	Bruker SMART v5.630		

$\theta$ range for data collection	2.47 to 44.89°
Completeness to $\theta = 44.89^\circ$	77.7 %
Index ranges	$-18 \leq h \leq 17$ , $-29 \leq k \leq 29$ , $-17 \leq l \leq 17$
Data collection scan type	$\omega$ scans at 7 $\phi$ settings
Data reduction program	Bruker SAINT v6.45A
Reflections collected	28065
Independent reflections	9164 [ $R_{\text{int}} = 0.0588$ ]
Absorption coefficient	1.321 mm <sup>-1</sup>
Absorption correction	None
Max. and min. transmission	0.7168 and 0.6477

### Structure Solution and Refinement

Structure solution program	Bruker XS v6.12
Primary solution method	Direct methods
Secondary solution method	Difference Fourier map
Hydrogen placement	Difference Fourier map
Structure refinement program	Bruker XL v6.12
Refinement method	Full matrix least-squares on $F^2$
Data / restraints / parameters	9164 / 0 / 255
Treatment of hydrogen atoms	Unrestrained
Goodness-of-fit on $F^2$	1.485
Final R indices [ $I > 2\sigma(I)$ , 7498 reflections]	$R1 = 0.0305$ , $wR2 = 0.0664$
R indices (all data)	$R1 = 0.0393$ , $wR2 = 0.0678$

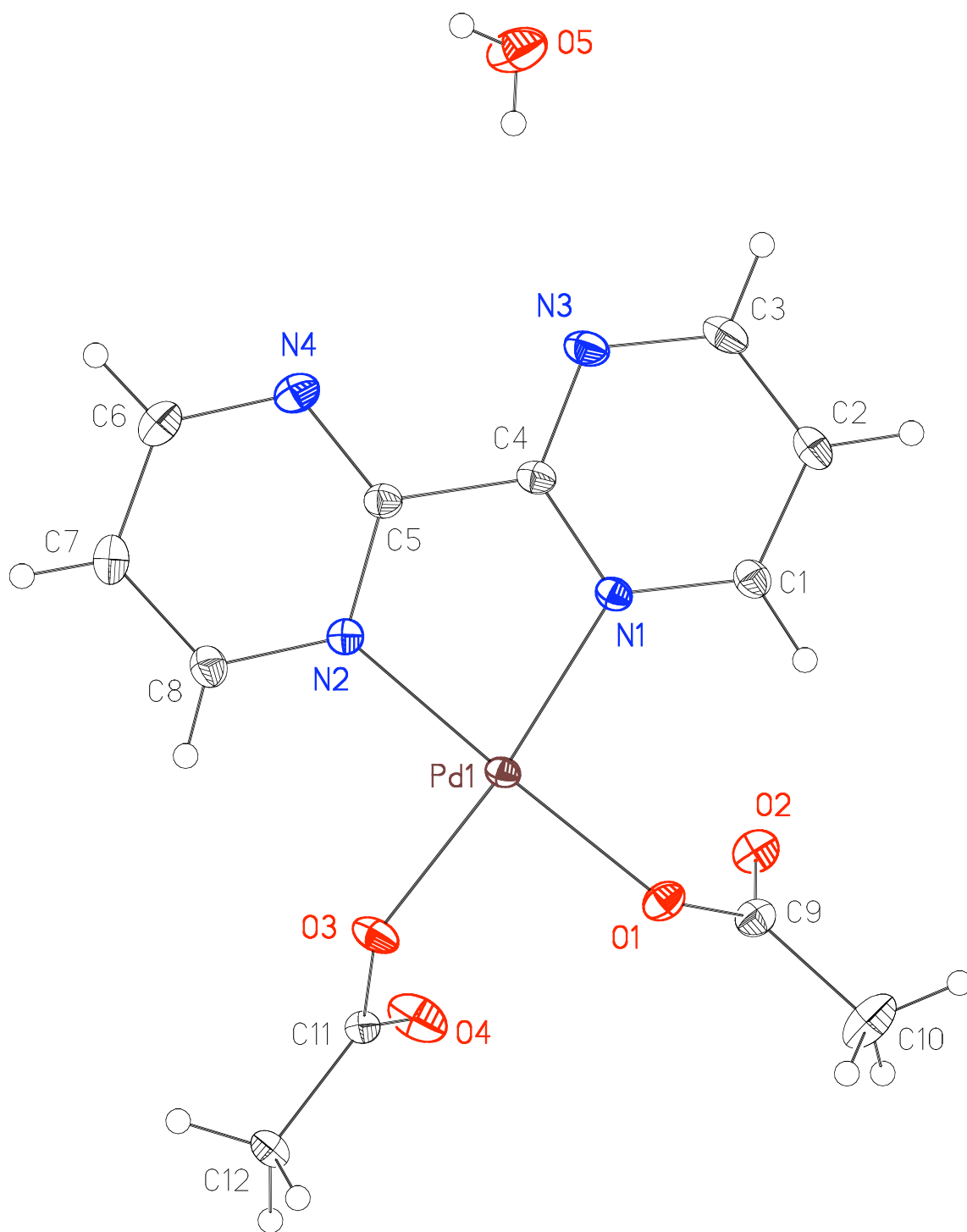


Type of weighting scheme used	Sigma
Weighting scheme used	$w=1/\sigma^2(Fo^2)$
Max shift/error	0.004
Average shift/error	0.000
Largest diff. peak and hole	1.503 and -1.576 e.Å <sup>-3</sup>

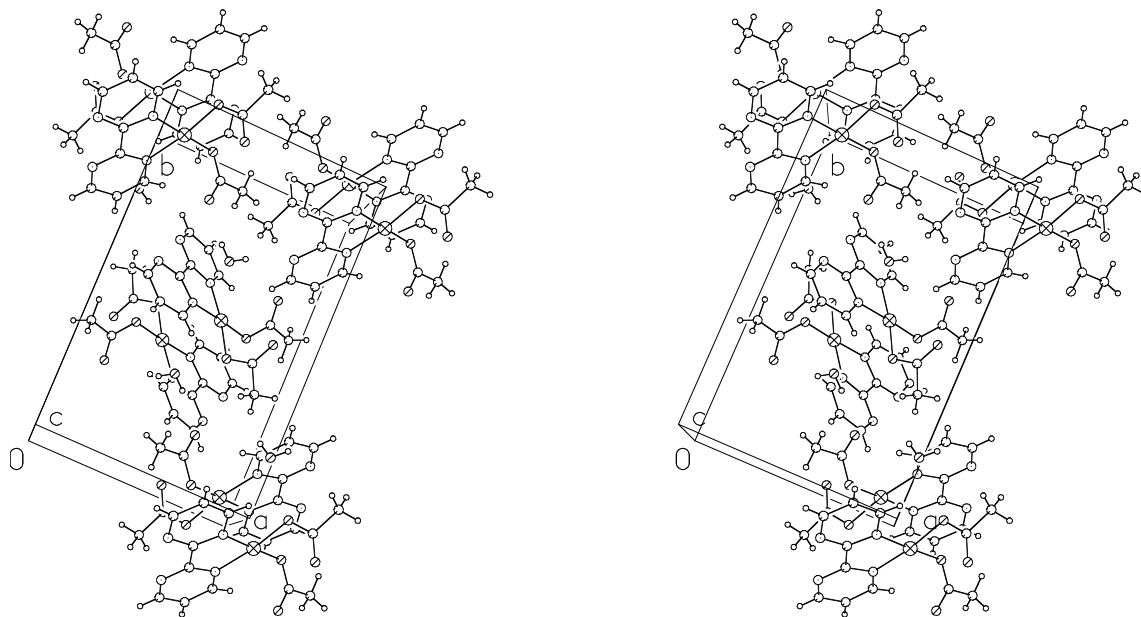
### Special Refinement Details

Refinement of  $F^2$  against ALL reflections. The weighted R-factor ( $wR$ ) and goodness of fit ( $S$ ) are based on  $F^2$ , conventional R-factors ( $R$ ) are based on  $F$ , with  $F$  set to zero for negative  $F^2$ . The threshold expression of  $F^2 > 2\sigma(F^2)$  is used only for calculating R-factors(gt), etc., and is not relevant to the choice of reflections for refinement. R-factors based on  $F^2$  are statistically about twice as large as those based on  $F$ , and R-factors based on ALL data will be even larger.

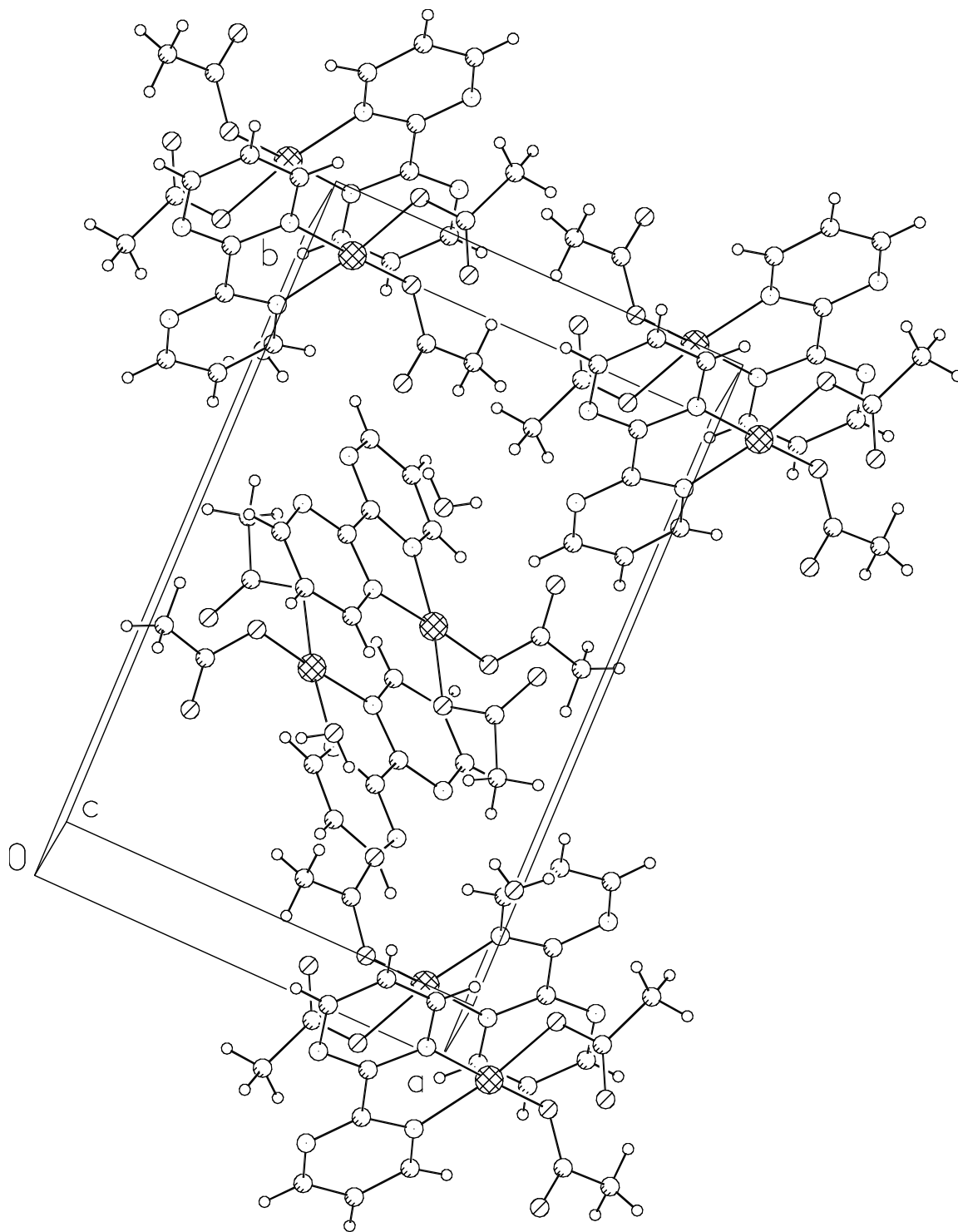
All esds (except the esd in the dihedral angle between two l.s. planes) are estimated using the full covariance matrix. The cell esds are taken into account individually in the estimation of esds in distances, angles, and torsion angles; correlations between esds in cell parameters are only used when they are defined by crystal symmetry. An approximate (isotropic) treatment of cell esds is used for estimating esds involving l.s. planes.

**Figure E.1 Minimum overlap view of 1·H<sub>2</sub>O**

**Figure E.2** Crystal packing of  $1 \cdot \text{H}_2\text{O}$



**Figure E.3** Unit cell contents of  $1 \cdot \text{H}_2\text{O}$



**Table E.2 Atomic coordinates (  $\times 10^4$ ) and equivalent isotropic displacement parameters ( $\text{\AA}^2 \times 10^3$ ) for  $1 \cdot \text{H}_2\text{O}$  (CCDC634014).  $U(\text{eq})$  is defined as the trace of the orthogonalized  $U_{ij}$  tensor.**

	x	y	z	$U_{\text{eq}}$
Pd(1)	3946(1)	4468(1)	8878(1)	10(1)
O(1)	2450(1)	4539(1)	10063(1)	14(1)
O(2)	1779(1)	3145(1)	9486(1)	17(1)
O(3)	3080(1)	5540(1)	7890(1)	16(1)
O(4)	1412(1)	4708(1)	6699(1)	23(1)
O(5)	9853(1)	1781(1)	9727(2)	28(1)
N(1)	5055(1)	3468(1)	9870(1)	11(1)
N(2)	5546(1)	4434(1)	7824(1)	12(1)
N(3)	7157(1)	2643(1)	9910(1)	16(1)
N(4)	7742(1)	3732(1)	7775(1)	17(1)
C(1)	4772(1)	3027(1)	10963(1)	14(1)
C(2)	5664(1)	2371(1)	11558(1)	16(1)
C(3)	6851(1)	2197(1)	10991(1)	17(1)
C(4)	6252(1)	3268(1)	9403(1)	12(1)
C(5)	6549(1)	3827(1)	8251(1)	13(1)
C(6)	7967(2)	4312(1)	6801(2)	18(1)
C(7)	6995(2)	4953(1)	6291(1)	18(1)
C(8)	5763(1)	4998(1)	6833(1)	15(1)
C(9)	1631(1)	3859(1)	10074(1)	14(1)
C(10)	484(2)	3966(1)	10923(2)	26(1)
C(11)	1951(1)	5432(1)	7018(1)	12(1)
C(12)	1360(1)	6299(1)	6402(2)	16(1)

**Table E.3** Selected bond lengths [ $\text{\AA}$ ] and angles [ $^\circ$ ] for  $1 \cdot \text{H}_2\text{O}$  (CCDC634014)

Pd(1)-O(3)	2.0024(9)	O(3)-Pd(1)-N(2)	93.45(4)
Pd(1)-N(2)	2.0054(11)	O(3)-Pd(1)-O(1)	87.93(4)
Pd(1)-O(1)	2.0112(10)	N(2)-Pd(1)-O(1)	175.36(4)
Pd(1)-N(1)	2.0155(10)	O(3)-Pd(1)-N(1)	172.58(4)
		N(2)-Pd(1)-N(1)	80.91(4)
		O(1)-Pd(1)-N(1)	97.32(4)

**Table E.4 Bond lengths [ $\text{\AA}$ ] and angles [ $^\circ$ ] for  $1 \cdot \text{H}_2\text{O}$  (CCDC634014)**

Pd(1)-O(3)	2.0024(9)	C(12)-H(12A)	0.93(2)
Pd(1)-N(2)	2.0054(11)	C(12)-H(12B)	0.97(2)
Pd(1)-O(1)	2.0112(10)	C(12)-H(12C)	0.98(2)
Pd(1)-N(1)	2.0155(10)		
Pd(1)-Pd(1)#1	3.22051(18)	O(3)-Pd(1)-N(2)	93.45(4)
O(1)-C(9)	1.2924(15)	O(3)-Pd(1)-O(1)	87.93(4)
O(2)-C(9)	1.2392(15)	N(2)-Pd(1)-O(1)	175.36(4)
O(3)-C(11)	1.3027(15)	O(3)-Pd(1)-N(1)	172.58(4)
O(4)-C(11)	1.2249(15)	N(2)-Pd(1)-N(1)	80.91(4)
O(5)-H(5A)	0.79(2)	O(1)-Pd(1)-N(1)	97.32(4)
O(5)-H(5B)	0.70(2)	O(3)-Pd(1)-Pd(1)#1	96.99(3)
N(1)-C(1)	1.3423(16)	N(2)-Pd(1)-Pd(1)#1	85.39(3)
N(1)-C(4)	1.3491(16)	O(1)-Pd(1)-Pd(1)#1	90.05(3)
N(2)-C(8)	1.3443(16)	N(1)-Pd(1)-Pd(1)#1	77.83(3)
N(2)-C(5)	1.3525(15)	C(9)-O(1)-Pd(1)	117.55(8)
N(3)-C(4)	1.3293(15)	C(11)-O(3)-Pd(1)	118.54(7)
N(3)-C(3)	1.3437(18)	H(5A)-O(5)-H(5B)	106(2)
N(4)-C(5)	1.3244(16)	C(1)-N(1)-C(4)	117.82(10)
N(4)-C(6)	1.3476(19)	C(1)-N(1)-Pd(1)	127.39(8)
C(1)-C(2)	1.3826(17)	C(4)-N(1)-Pd(1)	114.68(8)
C(1)-H(1)	0.936(18)	C(8)-N(2)-C(5)	118.01(11)
C(2)-C(3)	1.383(2)	C(8)-N(2)-Pd(1)	126.38(9)
C(2)-H(2)	0.957(18)	C(5)-N(2)-Pd(1)	115.35(8)
C(3)-H(3)	0.933(19)	C(4)-N(3)-C(3)	116.38(11)
C(4)-C(5)	1.4880(17)	C(5)-N(4)-C(6)	115.95(12)
C(6)-C(7)	1.388(2)	N(1)-C(1)-C(2)	120.57(12)
C(6)-H(6)	0.90(2)	N(1)-C(1)-H(1)	117.2(11)
C(7)-C(8)	1.3866(19)	C(2)-C(1)-H(1)	122.2(11)
C(7)-H(7)	0.87(2)	C(1)-C(2)-C(3)	117.57(12)
C(8)-H(8)	0.89(2)	C(1)-C(2)-H(2)	123.2(11)
C(9)-C(10)	1.507(2)	C(3)-C(2)-H(2)	119.2(11)
C(10)-H(10A)	0.99(3)	N(3)-C(3)-C(2)	122.40(11)
C(10)-H(10B)	0.85(3)	N(3)-C(3)-H(3)	117.1(12)
C(10)-H(10C)	0.94(3)	C(2)-C(3)-H(3)	120.5(12)
C(11)-C(12)	1.5125(17)	N(3)-C(4)-N(1)	125.22(12)

N(3)-C(4)-C(5)	119.83(11)
N(1)-C(4)-C(5)	114.93(10)
N(4)-C(5)-N(2)	125.75(12)
N(4)-C(5)-C(4)	120.08(11)
N(2)-C(5)-C(4)	114.09(10)
N(4)-C(6)-C(7)	122.46(13)
N(4)-C(6)-H(6)	120.8(13)
C(7)-C(6)-H(6)	116.7(13)
C(8)-C(7)-C(6)	117.84(13)
C(8)-C(7)-H(7)	122.0(14)
C(6)-C(7)-H(7)	120.1(14)
N(2)-C(8)-C(7)	119.96(12)
N(2)-C(8)-H(8)	116.9(14)
C(7)-C(8)-H(8)	123.1(13)
O(2)-C(9)-O(1)	124.08(12)
O(2)-C(9)-C(10)	120.56(12)
O(1)-C(9)-C(10)	115.30(12)
C(9)-C(10)-H(10A)	110.1(16)
C(9)-C(10)-H(10B)	109.4(18)
H(10A)-C(10)-H(10B)	113(3)
C(9)-C(10)-H(10C)	115.0(16)
H(10A)-C(10)-H(10C)	111(2)
H(10B)-C(10)-H(10C)	97(2)
O(4)-C(11)-O(3)	124.53(11)
O(4)-C(11)-C(12)	122.25(12)
O(3)-C(11)-C(12)	113.22(10)
C(11)-C(12)-H(12A)	111.4(15)
C(11)-C(12)-H(12B)	114.8(13)
H(12A)-C(12)-H(12B)	108(2)
C(11)-C(12)-H(12C)	111.1(12)
H(12A)-C(12)-H(12C)	106.2(18)
H(12B)-C(12)-H(12C)	104.5(17)

---

Symmetry transformations used to

generate equivalent atoms: #1 -x+1,-

y+1,-z+2



**Table E.5** Anisotropic displacement parameters ( $\text{\AA}^2 \times 10^4$ ) for  $1 \cdot \text{H}_2\text{O}$  (CCDC634014). The anisotropic displacement factor exponent takes the form: -

$$2\pi^2 [h^2 a^{*2} U^{11} + \dots + 2 h k a^* b^* U^{12}].$$

	U <sup>11</sup>	U <sup>22</sup>	U <sup>33</sup>	U <sup>23</sup>	U <sup>13</sup>	U <sup>12</sup>
Pd(1)	88(1)	85(1)	110(1)	-1(1)	-5(1)	2(1)
O(1)	131(4)	137(3)	169(5)	-36(3)	41(3)	-10(3)
O(2)	155(4)	159(3)	183(5)	-46(3)	26(3)	-21(3)
O(3)	141(4)	102(3)	215(5)	28(3)	-41(3)	3(3)
O(4)	244(5)	130(3)	269(6)	-23(4)	-81(4)	-14(3)
O(5)	194(5)	143(4)	530(8)	-15(5)	120(5)	-1(4)
N(1)	108(4)	100(3)	115(5)	0(3)	-3(3)	2(3)
N(2)	114(4)	110(3)	119(5)	-9(3)	12(3)	-7(3)
N(3)	135(5)	117(3)	223(6)	21(4)	3(3)	19(3)
N(4)	149(5)	171(4)	191(6)	-25(4)	45(3)	16(4)
C(1)	141(5)	137(4)	123(6)	8(4)	-1(3)	-5(4)
C(2)	185(6)	131(4)	135(6)	24(4)	-19(4)	-11(4)
C(3)	156(5)	119(4)	210(7)	32(4)	-33(4)	8(4)
C(4)	117(5)	106(4)	146(6)	-3(4)	2(3)	8(3)
C(5)	121(5)	113(4)	142(6)	-6(4)	15(3)	5(3)
C(6)	165(6)	207(5)	193(7)	-30(5)	65(4)	-15(4)
C(7)	212(6)	189(5)	147(6)	13(5)	53(4)	-33(4)
C(8)	162(5)	155(4)	127(6)	12(4)	9(4)	-11(4)
C(9)	118(5)	168(4)	128(6)	-23(4)	7(3)	-7(4)
C(10)	203(7)	287(7)	307(9)	-103(6)	126(5)	-60(6)
C(11)	110(5)	120(4)	123(5)	4(4)	22(3)	14(3)
C(12)	169(6)	152(4)	171(6)	55(4)	13(4)	34(4)

**Table E.6 Hydrogen coordinates (  $\times 10^4$ ) and isotropic displacement parameters ( $\text{\AA}^2 \times 10^3$ ) for 1·H<sub>2</sub>O (CCDC634014)**

	x	y	z	U <sub>iso</sub>
H(1)	3952(19)	3182(13)	11295(18)	16(4)
H(2)	5491(19)	2033(13)	12327(18)	17(4)
H(3)	7479(19)	1757(14)	11355(19)	20(5)
H(6)	8780(20)	4307(13)	6460(20)	21(5)
H(5A)	10460(20)	2135(16)	9730(20)	37(6)
H(5B)	9230(20)	2023(16)	9570(20)	31(6)
H(7)	7150(20)	5298(16)	5630(20)	25(5)
H(8)	5100(20)	5393(14)	6570(20)	22(5)
H(10A)	430(30)	4592(18)	11210(30)	44(7)
H(10B)	-280(30)	3780(20)	10490(30)	61(9)
H(10C)	530(30)	3570(20)	11660(30)	56(8)
H(12A)	1940(20)	6551(16)	5850(20)	40(7)
H(12B)	1170(20)	6747(16)	7050(20)	35(6)
H(12C)	470(20)	6203(14)	5827(19)	21(5)

**Table E.7 Hydrogen bonds for 1·H<sub>2</sub>O (CCDC634014) [Å and °]**

D-H...A	d(D-H)	d(H...A)	d(D...A)	<(DHA)
O(5)-H(5A)...O(2)#2	0.79(2)	2.02(2)	2.8035(15)	170(2)
O(5)-H(5B)...N(3)	0.70(2)	2.28(2)	2.9472(16)	158(2)

Symmetry transformations used to generate equivalent atoms:

#1 -x+1,-y+1,-z+2

#2 x+1,y,z